Applications of Raman Spectroscopy to Solid State Chemistry

by

Myrl Wendy Venter

Submitted in partial fulfillment of the

requirements for the degree of

Philosophiæ Doctor

in the Faculty of Science

University of Pretoria, PRETORIA

June 1989

Promoter: Prof. A.M. Heyns

Summary

Two investigations of solid state chemistry problems, using various aspects of Raman spectroscopy, are described. The first includes high pressure studies of pyridine and $ZnCl_2py_2$. Both of these studies gave phases which have not previously been described. Single crystal polarization studies on $CdCl_2py_2$ and $CuCl_2py_2$ gave unambiguous assignments of the lattice vibrations in the polymeric octahedral complexes, which were subsequently used to show that the higher pressure phase of $ZnCl_2py_2$ belongs to the polymeric octahedral class of structures.

The second investigation showed that the decomposition of ammonium metavanadate under ambient pressures to vanadium pentoxide proceeds via the intermediate ammonium hexavanadate. An important contribution was also made in terms of the elucidation of the vibrational spectra of these compounds using techniques such as deuteration, high pressures and temperatures.

Samevatting

Twee ondersoeke na vastetoestandchemie probleme, met behulp van verskeie aspekte van Raman spektroskopie, word beskryf. Die eerste sluit hoë druk studies van pyridien en $ZnCl_2py_2$ in. Beide studies het fases gelewer wat nog nie vantevore beskryf is nie. Enkelkristal polarisasie studies van $CdCl_2py_2$ en $CuCl_2py_2$ het gelei tot die ondubbelsinnige toekenning van die roostertrillings in polimeriese oktahedriese komplekse, wat daarna gebruik is om aan te toon dat die hoër druk fases van $ZnCl_2py_2$ aan die polimeriese oktahedriese klas van strukture behoort.

Die tweede ondersoek het getoon dat die ontbinding van ammonium metavanadaat by atmosferiese druk na vanadiumpentoksied, geskied deur middel van 'n intermediêre produk, ammonium heksavanadaat. 'n Belangrike bydra is ook gemaak in die verklaring van die vibrasiespektra van hierdie verbindings, deur die gebruik van tegnieke soos deuterering, hoë druk en temperature.

Acknowledgements

I wish to express my thanks to my promoter, Prof. A.M. Heyns, for his support through some difficult times during my studies. He has always been a pillar of support and encouragement. His inspiration and ideas have been a tremendous help in deciding the most difficult question of all, i.e. "What next?".

I thank also Prof. K.-J. Range from the Universität Regensburg, for most useful discussions. His cooperation, particularly in the work relating to the decomposition of ammonium metavanadate is greatly appreciated.

Of course, the person most deserving of thanks is the unfortunate typist, in this case my husband. I wish therefore to express my deep appreciation to my husband for the many laborious hours of typing and proofreading this thesis. Naturally, any errors that remain must be blamed on the author.

Financial support was received form the University of South Africa, the Council for Scientific and Industrial Research, and the University of Pretoria.

Contents

Chapter 1

INTRODUCTION

The work described in this thesis was conducted as part of a research program using Raman spectroscopy as a tool in studying various problems encountered in solid state chemistry.

The thesis consists of two parts. The first concerns a study of pyridine and some of its metal complexes, while the second describes a study of the decomposition reaction of ammonium metavanadate.

1.1 PYRIDINE

Pyridine is a well-known corrosion inhibitor[7,33,108]. However, the behaviour of pyridine in such systems is poorly understood. Any increased understanding of the behaviour of pyridine and its complexes under high pressure, may therefore contribute to a better understanding of these systems.

Furthermore, until this study, no phase diagram has been available for pyridine. And while some low temperature i.r. studies of pyridine have

appeared in the literature[16,56], its behaviour under pressure is not fully understood.

Chapter 2 describes a study of pyridine under pressures up to 45 kbar. Two new phases were identified, one at 11 kbar and another at 25 kbar. The Raman spectra of these phases resemble the vibrational spectra of the phases obtained for benzene[2,27], whose phase diagram has already been published[3,92].

Pyridine is a polar molecule with a dipole moment of 2,20D and can thus be expected to be highly associated in solution[106]. When pyridine is used as a corrosion inhibitor, some association of pyridine with the metal surface takes place [7,33,108]. It was also decided to study metal pyridine complexes. MCl_2py_2 complexes are the simplest of the divalent metal complexes and are thus used in this study. In the 1^{st} row transition elements, the d^4 - d^{10} M^{II} ions all form MCl_2py_2 complexes which have either polymeric octahedral or distorted polymeric octahedral structures except for $ZnCl_2py_2$, which is tetrahedral, and $CoCl_2py_2$, which has both tetrahedral and polymeric octahedral complexes. Of the two anomalies, the $ZnCl_2py_2$ complex is more amenable to a Raman study than the highly coloured $CoCl_2py_2$ complexes. $ZnCl_2py_2$ therefore seemed the most interesting complex for a detailed pressure study. Some other complexes were also included for comparison purposes (Chapter 3).

The behaviour of any compound under pressure is defined by certain rules (see Appendix A). According to these rules $ZnCl_2py_2$ under pressure would be expected to assume the polymeric octahedral structure, since both $CdCl_2py_2$ and $HgCl_2py_2$, which also have d^{10} electronic occupation, have the polymeric octahedral structure.

At high pressures $ZnCl_2py_2$ has a Raman spectrum analogous to those obtained for the polymeric octahedral complexes. No evidence could be found for the decomposition of $ZnCl_2py_2$ at high pressures.

It has been found that the behaviour of the $ZnCl_2py_2$ complex also relates to the extensive hydrogen bonding found in the complex.

In order to be sure that $ZnCl_2py_2$ does in fact have the polymeric octahedral structure, it was necessary to obtain good vibrational spectra with an unambiguous assignment of the lattice vibrations. There is however a great deal of confusion in the literature surrounding the assignment of vibrational bands of the MCl_2py_2 polymeric octahedral chain complexes[35]. This prompted a single crystal polarization Raman study (Chapter 4) of representatives of each of the two classes, namely distorted polymeric octahedral (as in $CuCl_2py_2$) and polymeric octahedral (as in $CdCl_2py_2$).

The fact that the polymeric octahedral complexes have a chain-like structure is the reason for the confusion in the literature. Calculation of the normal vibrations based on the choice of a particular "structural unit" has led to a number of conflicting results. The results of these particular Raman experiments are best described by an approach already published[1].

1.2 AMMONIUM METAVANADATE

The most widely used method of obtaining the important V_2O_5 catalyst is by the thermal decomposition of ammonium metavanadate. This method of obtaining V_2O_5 has been used for a number of years. However, the mechanism of the reaction remains controversial.

In order to optimize the reaction (in industrial terms), it is important that the mechanism be well understood so that the most viable experimental conditions can be established.

This study has established that the most important and perhaps only intermediate in this reaction is the ammonium hexavanadate $(NH_4)_6V_6O_{16}$. The formation of this intermediate depends greatly on the experimental conditions used, resulting in a large range of temperatures possible for the formation of the ammonium hexavanadate.

The spectroscopic study carried out has revealed that hydrogen bonding plays a particularly important role in the reaction mechanism. Bifurcated hydrogen bonds between the NH_4^+ groups and oxygen atoms are prevalent in the O-V-O chains in ammonium metavanadate. This hydrogen bonding is discussed at length in both Chapter 5 and Appendix B.

In studying the reaction method by vibrational means, it is important to have good reference spectra of both the starting material as well as the product, with clear assignments in all cases. There have been some reports where assignments of these spectra are given[67,68], but in these cases the O-V-O chain structure has been ignored. This study has used the method developed by Adams and Newton[1] to determine the number and type of normal vibrations in these chain structures.

Chapter 2

PYRIDINE

2.1 INTRODUCTION

The Raman spectra of solid pyridine and pyridine-d_5 (the deuterated compound) obtained by the application of pressure in a diamond anvil cell at ambient temperatures have been studied. Although a number of experimental and theoretical studies on the vibrational spectra of pyridine and deuterated pyridine have already appeared in the literature, these have dealt mainly with the liquid and vapour phases of pyridine. Very few studies on the vibrational spectra of the solid phase have been published[16,56].

Two crystalline modifications of pyridine have been characterized by X-ray methods[11]. These modifications, Pmmm(D_{2h}^1) and Pnnn(D_{2h}^2) do not show great structural differences and the conditions for the conversion of the one into the other were not established. A "glassy" state of pyridine was obtained when the vapour was deposited onto a cold CsI window, it changed to a crystal form upon warming, and in solid pyridine-d_5 a phase

transition was observed that could not be detected in pyridine itself[62]. The multiplicity of several of the vibrational bands was explained in terms of close-lying overtones and combination bands[16], however, a subsequent crystal structure analysis of single crystals of pyridine revealed that it has an unexpectedly complicated crystal structure with sixteen molecules per unit cell[62], thus explaining the multiplicity of the infrared bands. The Raman spectra of the internal vibrations of pyridine and pyridine-d_5 are comparatively speaking much less complicated than the infrared ones and closely resemble those of the liquid samples of pyridine.

The solidification of liquid pyridine upon cooling therefore yields samples which are either "glassy" or crystalline, and the latter phase most probably has a complex crystal structure. No reports could be found in the literature on solid pyridine obtained by the solidification of liquid samples with pressure prior to this work and therefore a study of the high-pressure Raman spectra of pyridine and pyridine-d_5 was undertaken with the following aims in mind. Since the phase diagram of pyridine has not yet been published, it would be informative to ascertain at what pressure pyridine solidifies; whether the structure of this phase is in agreement with that obtained for single crystals[62], and also whether any further phases can be identified.

Since the high-pressure results described here have been published[46] two articles have appeared in which the ν_1(ring stretch) and ν_{12}(ring bend) vibrational modes of liquid pyridine were studied under compression. These workers confirmed a freezing point for pyridine at $\approx$ 11 kbar [106,107]. Their high pressure studies of pyridine dissolved in various solvents showed that even at low concentrations of pyridine in aqueous solutions, pyridine

is largely associated in dimeric units which involve self-association via the ring hydrogens.

In a high-pressure study like the present one, the intermolecular interactions in solid pyridine deserve particular attention. In other words, whether the interactions originate largely in hydrogen bonding, in π–π bonding involving the aromatic rings, or in C-H—π interactions. In order to study this, a careful analysis of the ring, in-phase and out-of-phase vibrations of pyridine will be required.

The polymorphism of solid pyridine is expected to resemble that of various planar aromatic molecules like benzene. Studies on solid benzene have revealed the presence of various solid phases at high pressures[2,92], and the crystal structures of the first two of these have been obtained[22,73] while structures have been postulated for the remaining phases[92]. Raman spectra of benzene I and benzene II have been reported at pressures up to 40 kbar and temperatures down to 77 K[2,27,92]. Another Raman study between the temperatures 4.2 K and 273 K included benzene-d_5 crystals[49]. It will thus be useful to compare the polymorphism of pyridine with that of solid benzene which has been very carefully studied.

Solid pyridine is a molecular crystal, and is likely to be very compressible. An increase in pressure on molecular crystals inducing a phase change is characterized in the vibrational spectra by severe changes in peak position, disappearance of peaks and new peak formation. The lattice modes, which are largely controlled by intermolecular forces, should change significantly upon compression of the samples since the intermolecular distances are likely to be greatly affected. The low-frequency vibrational spectra of solid pyridine have not been thoroughly studied before.

Pyridine is a very important liquid in coordination chemistry and numerous reports on the vibrational spectra of pyridine complexes appear regularly in the literature. Studies of pyridine on metal surfaces using Surface Enhanced Raman Spectroscopy (SERS) under various conditions are also prolific see for example [17,23]. It is therefore necessary to learn more about the vibrational spectra of solid pyridine, this applies to both the internal and external modes. The vibrational spectra of pyridine in the vapour phase, liquid pyridine, solid pyridine and pyridine bonded in metal complexes and also in adduct compounds can then all be compared with pyridine adsorbed on surfaces.

2.2 CRYSTAL STRUCTURE AND SELECTION RULES

2.2.1 Pyridine

According to its crystal structure[36], pyridine belongs to the orthorhombic space group $Pna2_1$, (C_{2v}^9) with a = 1752.4, b = 896.9, and c = 1135.2 pm at 153 K and Z = 16. There are four independent molecules and the formerly two-fold N-C-H axis of the molecules are arranged in layers perpendicular to the c-axis and separated by c/4. The internal bond angles and distances do not differ significantly from those in a "free" pyridine molecule of C_{2v}-symmetry. This significantly complicated structure can be approximated by the centrosymmetric space group Pccn (D_{2h}^{10}) with the same axial lengths if all independent atoms are shifted $\approx$ 50 pm up and down b for all molecules in the unit cell with $0 < x < 2$ and $0.5 < x < 1$ respectively [62].

The pyridine molecule has C_{2v}-symmetry (see figure 2.1) and consists of 11 atoms, therefore $(3n-6)$ i.e. 27 modes of vibration are expected. There are also three translations (along the x,y and z axes), and three rotations: (a) about the y-axis through the centre of the molecule, (b) about the z-axis and (c) about the x-axis in the plane of the molecule. The molecular vibrations of pyridine are given by $\Gamma_{vib} = 10A_1 + 3A_2 + 9B_1 + 5B_2$ where $\Gamma_{rot} = A_2 + B_1 + B_2$ and $\Gamma_{trans} = A_1 + B_1 + B_2$.

Figure 2.1:

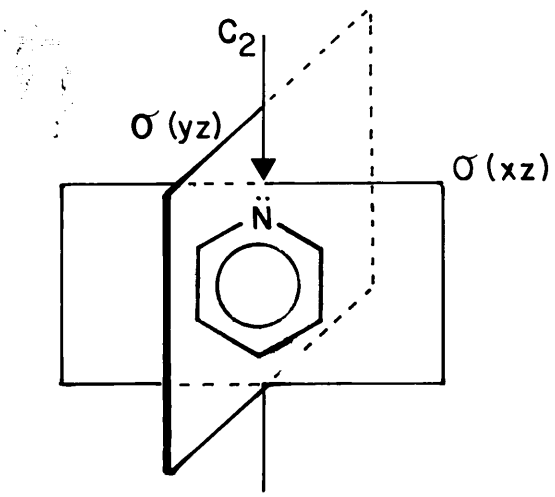

All the bands are Raman active and the low symmetry of the pyridine molecule could be expected to cause a considerable amount of mixing of the rotational and translational modes to take place.

Note: $\Gamma_{vib} = 10A_1 + 3A_2 + 5B_1 + 9B_2$ if yz instead of xz defines the plane of the molecule.

Under C_{2v}^9-symmetry each of the above 27 internal modes of pyridine should split into $A_1 + A_2 + B_1 + B_1$ components. It must further be kept in mind that there are four independent groups in the unit cell, giving rise to four times as many modes. All of the correlation field components are Raman-active, but neglecting these latter components, each mode corresponding to the "free" pyridine should have a multiplicity of at least

four corresponding to the different molecules. The rotational modes are given by $12A_1 + 12A_2 + 12B_1 + 12B_2$, and $11A_1 + 12A_2 + 11B_1 + 11B_2$ translational vibrations are predicted. All of these modes are Raman-active and consequently, under C_{2v}^9-symmetry, a very complicated Raman spectrum for pyridine can be expected.

Although the bond angles and bond lengths in solid pyridine do not differ significantly in the four groups and for that matter also from the ones reported for pyridine vapour[74], the orientations of the pyridine molecules in the crystal lattice are widely different and at least two of these groups are orientated in a completely different manner[62]. As far as the internal pyridine modes are concerned, single crystal Raman measurements or spectra recorded at very low temperatures could be required to resolve the full multiplicity of these bands. However, in the present measurements it can be expected that at least the lattice modes will reflect the complexity of the crystal structure at ambient temperatures. If the approximate structure of Pccn(D_{2h}^{10}) as mentioned on the previous page is used, where Z = 8 [62] then each vibrational mode of the "free" pyridine molecule should split into $2(A_g + B_{1g} + B_{2g} + B_{3g})$ Raman-active components, the coefficient of 2 denoting the two possible independent groups in the crystal. The Raman-active translational and rotational modes should each correspond to the representation $\Gamma = 6A_g + 6B_{1g} + 6B_{2g} + 6B_{3g}$ under Pccn (D_{2h}^{10}), in other words, a total number of 48 Raman-active lattice modes could be expected to occur under this symmetry. Once again, a rather complex Raman spectrum is predicted for the Pccn-space group.

2.2.2 Other planar aromatic molecules

The other well-known planar molecule, benzene, belongs to the orthorhombic space group Pbca (D_{2h}^{15}) in Phase I[48]. Benzene II which is stable at pressures greater than about 11 kbar, belongs to the monoclinic space group $P2_1/c$ (C_{2h}^{5})[27,73]. The phase diagram of benzene, which can be regarded as a representative example of such a molecule, is shown in figure 2.2[3]. More recent studies[92] on the polymorphism of benzene confirmed the phase transitions occuring at 14 and 40 kbar (both first-order ones) and revealed a second-order transition at 110 kbar. Two monoclinic structures have been proposed for the phases above 15 kbar in addition to the one known already[3]. It is interesting to note that 4-cyanopyridine also belongs to the space group Pccn (D_{2h}^{10})[54], but with Z = 4 as opposed to pyridine which has sixteen molecules per unit cell. The reason for the complex crystal structure of pyridine is not clear, particularly in view of the fact that the monoclinic space group $P2_1/a$ is generally favoured by planar molecules because the screw axis facilitates efficient packing of the molecules in the crystal[94]. Compounds such as 3,5-dichloropyridine in Phase I belong to the monoclinic space group $P2_1/m$ (C_{2h}^{2}), with Z = 2[79].

The full spectra of pyridine in the vapour, liquid and crystalline phases are summarized in tables 2.1 and 2.2. DiLella and Stidham[24] carefully studied the Raman spectra of pyridine and all of its deuterated analogues and the assignment of bands in tables 2.1 and 2.2 is based on these results.

DiLella and Stidham[24] used polarization studies and comparisons with vapour phase i.r. data in order to assign the A_1 fundamentals. Three of the A_1 fundamentals, ie. ν_{6a}, ν_1 and ν_{8a} were assigned using polarization

Table 2.1: OBSERVED FREQUENCIES FOR THE INTERNAL VIBRATIONS OF PYRIDINE IN THE GASEOUS, LIQUID AND SOLID STATES

Mode	Spec.	Description	Vapour IR	Liquid Raman	Liquid IR	Crystalline Pyridine Phase I, 10.5 kbar	$1/\nu \cdot d\nu/dp$ $\times 10^4$ $kbar^{-1}$	Crystalline Pyridine Phase II, 26.5kbar	$1/\nu \cdot d\nu/d$ $\times 10^4$ $kbar^{-1}$
ν_1	A_1	C-C Ring stretch	991.4	991 vs	991 ms	998 vs	3.7	1004 vs	2.7
ν_2	A_1	C-H stretch	3094.2	3057 vs	3053 wm,sh	3070 vs	2.8	3082 vs	2.3
ν_3	B_2	In-plane H bend	1227	1227 w,sh	-	1233 w,m	3.4	1238 w,m	2.6
ν_4	B_1	Out-of plane ring bend	744	709 vw	703 vs	-	-	-	-
ν_5	B_1	Out-of plane H bend	1007	942 vw	941 w	1010[1] vw	4.3	1016 w	3.9
ν_{6a}	A_1	In-plane ring bend	601.4	604 wm	603 ms	609 vw,br	-	611 w,br	-
ν_{6b}	B_2	In-plane ring bend	652	653 m	654 w	653 w,m	-	656 m	-
ν_{7a}	A_1	Out-of plane H bend	-	3042	-	3061 should	1.5	3068 m,should	1.6
ν_{7b}	B_2	Out-of plane H bend	3042.4	-	-	3042 w	2.8	3054 w	-
ν_{8a}	A_1	C-C ring stretch	1583.9	1582 ms	1581 s	1588 m,sh	1.9	1594 m,sh	1.8
ν_{8b}	B_2	C-C ring stretch	1580.5	1574 w,sh	1574 m,sh	1577 m,sh	2.3	1583 m,sh	2.0
ν_{9a}	A_1	In-plane H bend	1218.0	1217 ms	1217 ms	1233 w,m	3.9	1238[4] w	-
ν_{9b}	B_2	In-plane H bend	-	1227 m,sh	-	1213 w,m	3.3	1217 w,br	2.3
ν_{10a}	A_2	Out-of plane H bend	880	884 w	884 w	899 vw,br	6.0	909 vw,br	4.1
ν_{10b}	B_1	Out-of plane H bend	936.6	750 vw	747 s	∿960 vvw,br	2.7	∿962 vvw,br	-
ν_{11}	B_1	Out-of plane H bend	700.3	709 vw	703 vs	-	-	-	-
ν_{12}	A_1	In-plane ring bend	1031.7	1031 vs	1030 ms	1038 vs	3.4	1042 vs	2.3
ν_{13}	A_1	C-H stretch	3072.8	3057	3057	3093 w,should	0.7	3097 ms,should	1.6
ν_{14}	B_2	C-C ring stretch	1362.3	1355 vw	1355 w	-	-	-	-
ν_{15}	B_2	In-plane H bend	1143.3	1147 wm	1146 ms	1150 w,br	5.0	1153 w,br	2.0
ν_{16a}	A_2	Out-of plane ring bend	373	380 vw	-	384 w,br	2.6	383 vw	4.7
ν_{16b}	B_1	Out-of plane ring bend	403.3	407 w	406 ms	417[3] w	8.6	421[3] w,br	1.9
ν_{17a}	A_2	Out-of plane H bend	980	-	-	986 vw	-	989 vvw	-
ν	B	Out-of plane H bend	-	1007 vw, sh	-	1010 w	5.4	1016 w	4.1

Table 2.2: OBSERVED FREQUENCIES FOR THE INTERNAL VIBRATIONS OF PYRIDINE-d_5 IN THE GASEOUS, LIQUID AND SOLID STATES

Mode	Spec.	Description	Vapour IR	Liquid Raman	Liquid IR	Crystalline Pyridine-d_5 Phase I,11 kbar	$1/\nu \cdot d\nu/dp$ $kbar^{-1}$ $x10^4$	Crystalline Pyridine-d_5 Phase II,25 kbar	$1/\nu \cdot d\nu/d$ $kbar^{-1}$ $x10^4$
ν_1	A_1	C-C Ring stretch	963.7	963 vs	963 ms	971 vs/978 w	3.2	976vs,985 vs	4.0
ν_2	A_1	C-H stretch	2276.7	2294 vs	-	230 vs	3.9	2318s[1]	3.5
ν_3	B_2	In-plane H bend	1046.3	1041 vw	1041 vw	-	-	-	-
ν_4	B_1	Out-of plane ring bend	630.8	-	633 sh,vw	-	-	-	-
ν_5	B_1	Out-of plane H bend	828.3	824 wm	824 s	843[1]	6.1	847[2] w	6.0
ν_{6a}	A_1	In-plane ring bend	579.2	582 w	581 ms	586 w,br	-	589 vvw,br	-
ν_{6b}	B_2	In-plane ring bend	625.7	625 m	624 wm	625	6.9	628[1,2]	2.6
ν_{7a}	A_1	Out-of plane H bend	-	-	-	-	-	-	-
ν_{7b}	B_2	Out-of plane H bend	2256.6	-	-	2260 w,sp	2.4	2267[2] w	4.7
ν_{8a}	A_1	C-C Ring stretch	1554.1	1551 m	1550 s,sh	1559 w	1.8	1565 w	2.2
ν_{8b}	B_2	C-C Ring stretch	1549.9	1537 m	1537 vs	1544 m[1]	1.7	1547[1]	2.6
ν_{9a}	A_1	In-plane H bend	882.5	887 m	888 m	893/900 w,sp	5.4	899 w/907 w	4.5
ν_{9b}	B_2	In-plane H bend	-	-	-	-	-	-	-
ν_{10a}	A_2	Out-of plane H bend	690	690 wm	690 w	700 w,br	-	693 /703 w,br	-
ν_{10b}	B_1	Out-of plane H bend	765.3	769 w	768 wm	778 w[1]	-	775 vw,br	-
ν_{11}	B_1	Out-of plane H bend	525.8	538 vw	536 vs	-	-	-	-
ν_{12}	A_1	In-plane ring bend	1014.8	1009 s	1009 w	1015 w/1006 m	3.3	1010[1] m	3.0
ν_{13}	A_1	C-H stretch	2268.6	2271 s	2268 w,sh	2284 w	4.2	2300 w[2],	1.5
ν_{14}	B_2	C-C ring stretch	1226.4	1230 sh,vw	1228 wm	-	-	-	-
ν_{15}	B_2	In-plane H bend	856.1	867 sh,vw	863 vvw	870 vvw	-	878 vvw	-
ν_{16a}	A_2	Out-of plane ring bend	318.0	328 vw	-	-	-	-	-
ν_{16b}	B_1	Out-of plane ring bend	367.6	370 vw	368 ms	-	-	-	-

Mode	Spec.	Description	Vapour IR	Liquid Raman	Liquid IR	Crystalline Pyridine Phase I,10.5 kbar	$1/\nu \cdot d\nu/dp$ $x10^4$ $kbar^{-1}$	Crystalline Pyridine Phase II,26.5kbar	$1/\nu \cdot d\nu/$ $x10^4$ $kbar^{-1}$
ν_{18a}	A_1	In-plane H bend	1071.9	1069 m	1069 ms	1068 vw	-	1067 vw,br	-
ν_{18b}	B_2	In-plane H bend	1079	1069 wm	1069 ms	1068 vw	-	1067 vw,br	-
ν_{19a}	A_1	C-C ring stretch	1483.4	1483 wm	1483 ms	-	-	-	-
ν_{19b}	B_2	C-C ring stretch	1441.9	1438 vw	1437 s	-	-	-	-
ν_{20a}	A_1	C-H stretch	3030.1	3057	-	3061 w,should	2.0	3068 m,should	1.7
ν_{20b}	B_2	C-H stretch	3086.9	3079	-	3081 w,should	3.1	3097[5] m,should	2.4
$2x\nu_{8a}$	A_1		-	3156 w,sh	3156	3160 w	1.3	3180 w,br	-
$2x\nu_{8b}$	A_1		3150 vw	3146 m	3145 w	3151 w,m	2.4	3162 m	1.2
$2x\nu_{19a}$	A_1		2968	2955 m	2955 w	2963[1] br,w	2.7	2970 w	1.6
$\nu_{19b}+\nu_{8b}$	A_1		-	-	3001 m	2997[1] br,w	3.1	3005 w,br	1.4
$2x\nu_{6a}$	A_1		-	-	1205 vw,sh	1218 w,m	7.2	1225 vvw,br	3.8
$2x\nu_{8a}$	A_1		-	3175 w,sh	-	3184 w,br	3.5	-	-
$\nu_{6a}+\nu_1$	A_1		1599 vw, sh	1598 wm	1598 wm	1607[1]	2.0	1614 w,br	-

1 At 11,0 kbar

2 At 14,5 kbar

3 Could be split

4 Asymmetric

5 ν_{20b} and ν_{13} have merged

6 At 18,0 kbar

Figure 2.2:

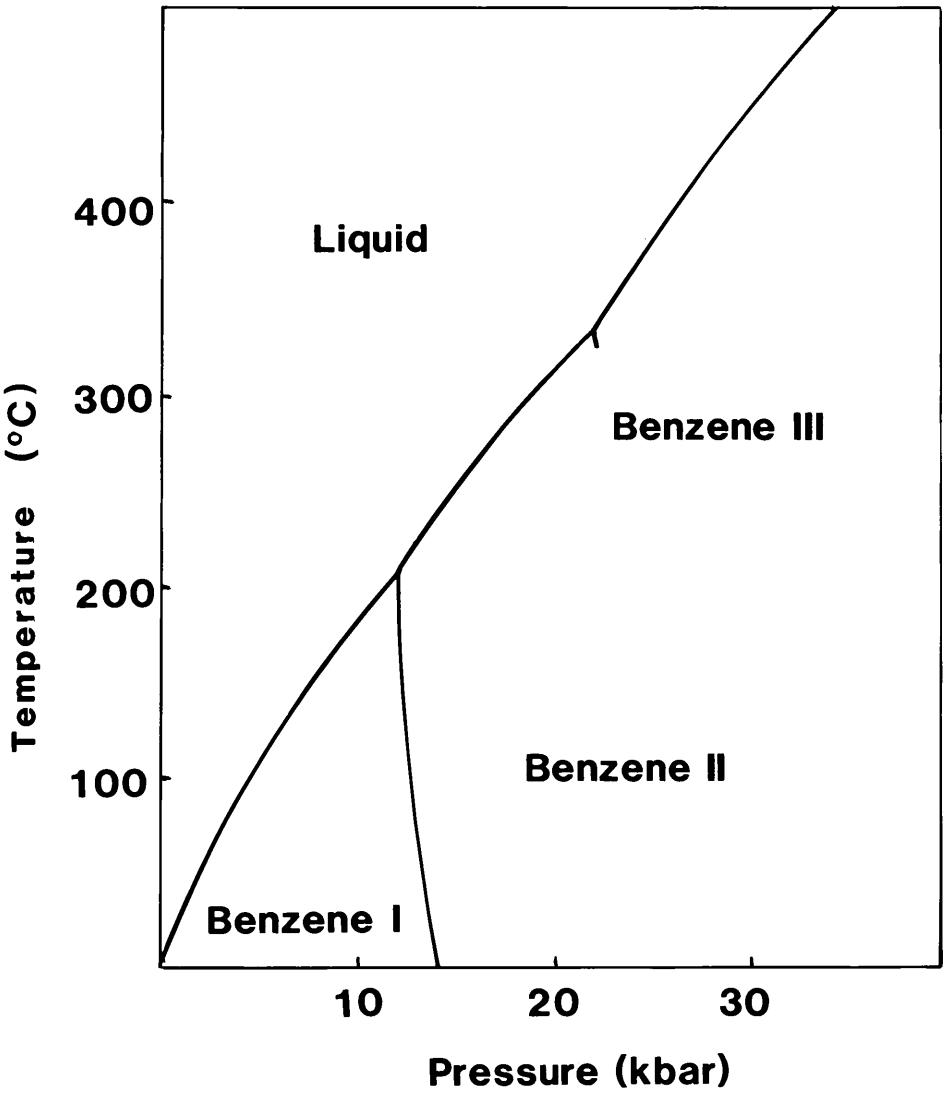

studies as well as comparing the spectra to those of the hydrogen-bonded water complexes of both pyridine and its isotopic species.

The B_1 species were selected on the basis that the C_{2v} isotopic pyridines should have C-type bands. The B_i fundamentals should thus all have sharp central Q-branches. The harmonic calculation of the thermodynamic functions were also in agreement with the experimental selections of some of these fundamentals.

In the case of A_2 vibrations, the frequencies for pyridine and pyridine-d_4 must occur as identical sets of three series for the C_{2v} molecules, as the symmetry restrictions prevent participation of nuclei on the C_2 axis in A_2 vibrations. Depolarization studies of these two molecules revealed three A_2 species at 980, 884 and 380 cm^{-1}.

Some of the B_2 vibrations were assigned on vapour phase band contours. The remaining B_2 fundamentals were chosen from the unassigned depolarized Raman bands. Some of these assignments were confirmed by using the overtone region. It was possible to verify these results in the pressure studies since $\frac{d\nu}{dp}$ values of the combination modes are much higher than the fundamentals. The bond stretching modes are also generally more pressure sensitive than the bending modes.

2.3 RESULTS

2.3.1 Solidification of Pyridine, Phase I

Solidification of both pyridine and pyridine-d_5 occurs at $\approx$ 10 kbar on compression of a liquid sample. The Raman spectra of solid pyridine and

pyridine-d_5 do not display a multiplicity of bands, as would be expected under a space group symmetry of $Pna2_1$ (C_{2v}^9) with Z = 16. In fact, these spectra closely resemble the corresponding ones in the liquid phase, excepting of course the occurrence of lattice modes, and a general upward shift in most of the internal modes in the solid samples. In some of the Raman bands in solid pyridine-d_5 either a splitting of the bands occurred or asymmetries developed.

At 11 kbar, splitting of the $\nu_1(A_1)$ C-C stretching mode into components at 971 and 988 cm^{-1} is prominent, but the multiple bands have a much lower intensity. The ν_{12} vibration displayed asymmetry with a shoulder at 1015 cm^{-1}. However, the multiplets expected under Pna2 (C_{2v}^9) symmetry were not observed. It has already been mentioned that the Raman spectrum of solid pyridine recorded at low temperatures at ambient pressures also did not show a multiplicity of bands[16], in direct contrast to the infrared spectra reported in the same study.

From these results it seems more likely that pyridine at elevated pressures possesses a monoclinic structure such as $P2_1/m$ (C_{2h}^2) with Z = 4, according to which $3A_g+3B_g$ rotational, and $3A_g+3B_g$ translational modes could be expected in the Raman spectra. Furthermore each internal mode will be split into $A_g + B_g + A_u + B_u$ components. In other words, only two Raman-active components can be obtained, accounting for the doublets observed in some of the Raman-active vibrations in pyridine-d_5.

Since the multiplicity expected for the pyridine solid was not obtained, the Raman spectra of the internal modes were relatively uncomplicated. The assignment of most of the internal modes could thus be done with a fair amount of certainty. The C-H stretching region was somewhat more

complicated (figure 2.3) as many Raman bands are evident in a fairly narrow frequency range. In gaseous pyridine, the C-H stretching region is characterized by the occurrence of many fundamentals in the infrared such as ν_{20a}, ν_{7b}, ν_{13}, ν_{20b} and ν_2 as well as combination bands such as $\nu_{8b} + \nu_{19b}$ and $\nu_{8b} + \nu_{19a}$ [97]. The same applies to the solid state where far more bands are obtained than predicted from the symmetry of pyridine and these have usually been ascribed to combination bands or overtones. The final assignment of the stretching bands in solid pyridine was done by comparing the $\frac{d\nu}{dp}$ values of the vibrations, as combination and overtone bands are expected to be far more pressure sensitive than the fundamental vibrations.

Polarization studies on the Raman spectra of pyridine and the deuterated analogues have been used to determine the symmetry of the vibrations [24,25,89,90]. Low temperature and high resolution FTIR spectra using matrix isolation techniques have also been used to resolve this region[97]. The variation in frequency with pressure for internal stretching modes is larger than for bending modes and was useful in verifying the assignments made with reference to previous studies on vapour, liquid and solid samples.

The lattice modes observed in the Raman spectra of solid pyridine (figure 2.4) and pyridine-d_5 are limited in number, and unless many of these modes occur below 45 cm^{-1}, in a region that could unfortunately not be studied in the present investigations, they are so few in number that it must be concluded that pyridine under these experimental conditions does not have C_{2v}^9-symmetry. It could be argued that many of the lattice modes could be accidentally degenerate, but then it is reasonable to expect that, because of their different sensitivities toward pressure, they should emerge

Figure 2.3:

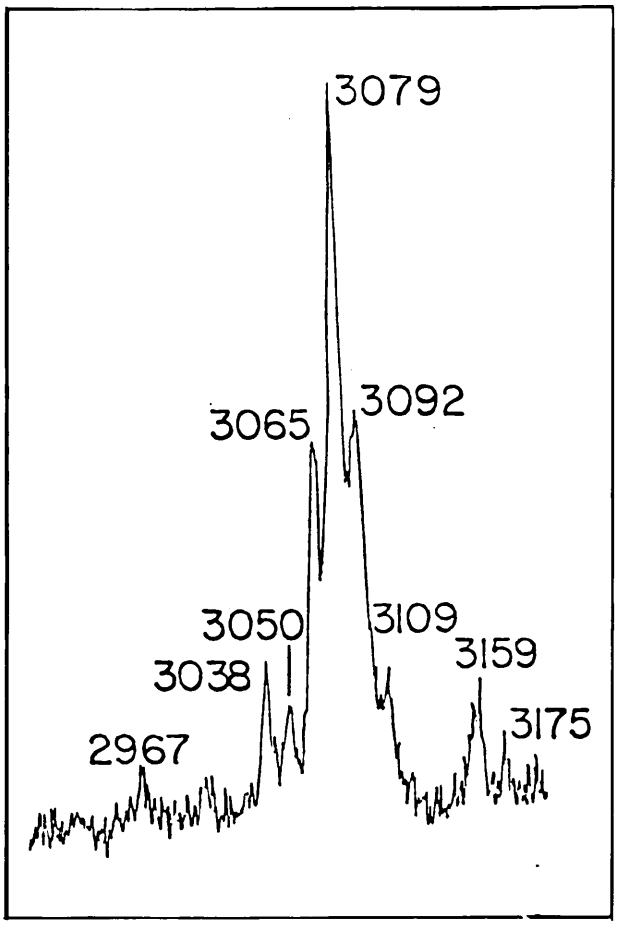

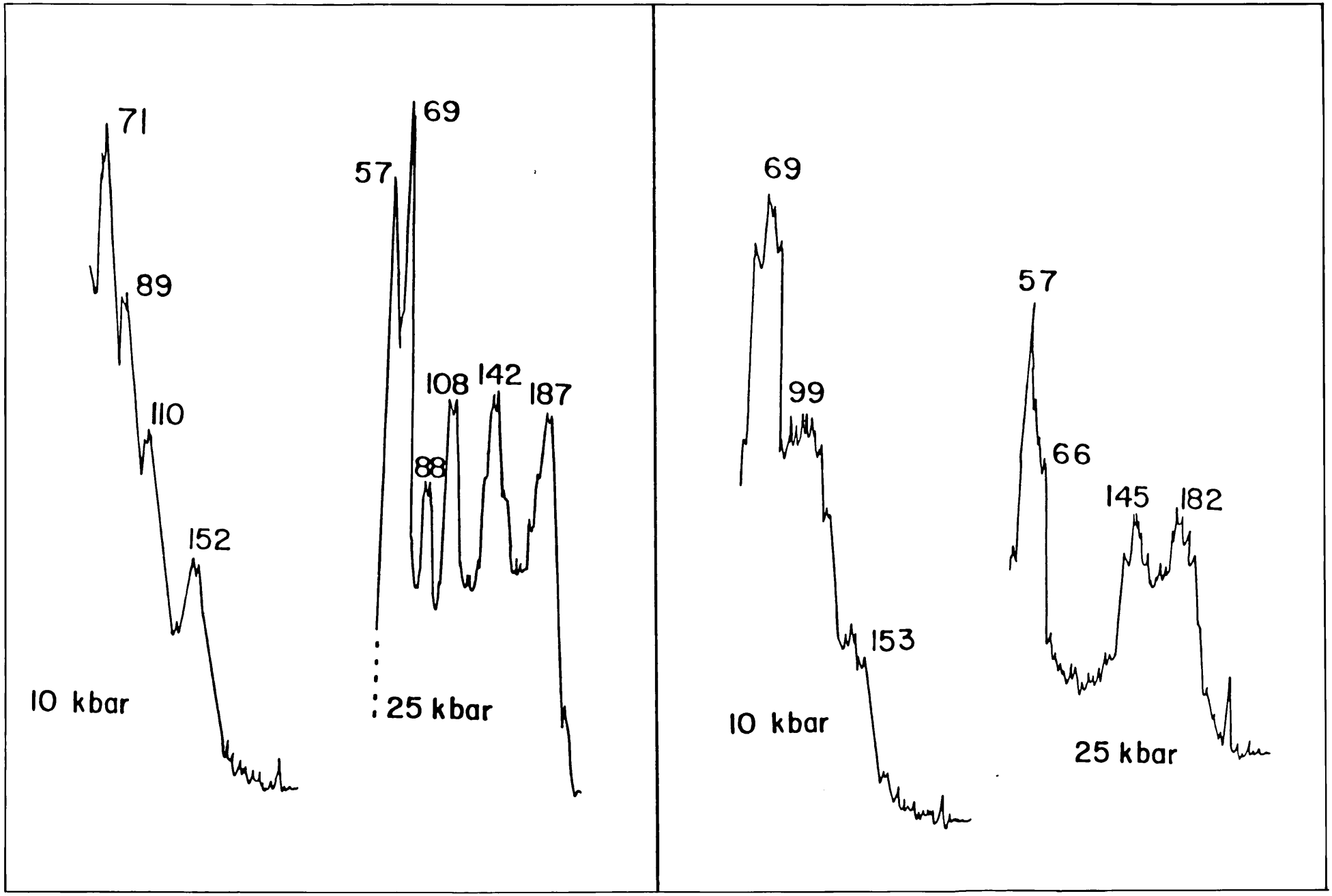

Figure 2.4: "Glassy" modification

as separate components at higher pressures. In a study of benzene under high pressure, good splitting occurred in the i.r. spectrum, but the Raman spectrum was incomplete[2]. Subsequent intensity calculations showed that some lattice modes which were not observed were expected to be orders of magnitude less intense than the observed bands.

The lattice modes of pyridine and pyridine-d_5 in the two phases; as well as $\frac{d\nu}{dp}$ values and isotopic ratios are summarized in table 2.3. In view of the fact that the structure of solid pyridine obtained in this study is not known, only a tentative assignment of the lattice modes can be made. Assuming undistorted pyridine groups, the isotopic ratios should be equal to 0.94, 0.92 and 0.91 for the rotational modes along the x-, y-, and z-axes respectively, while the ratio for the translational modes equals 0.97 (Teller-Redlich product rule,table 2.4).

On this basis, the modes at 153, 91 and possibly 85 cm^{-1} are largely rotational in character, while the ones at 111 and 72 cm^{-1} have, to a large extent, translational character. It is difficult to unambiguously assign the lowest frequency mode at 60 cm^{-1} on the basis of isotopic ratios only, but with the information presently available, it appears as if this could also be a translational mode. Mixing of rotational and translational modes will obviously occur in the crystal lattice, but the ratios can still be used as a guideline in making the above assignments.

Also shown in table 2.3 are the $\frac{1}{\nu} \cdot \frac{d\nu}{dp}$-values for the lattice modes. The compressibility of pyridine is not known, but it can be assumed that it will be of the order of magnitude of 1×10^2 $kbar^{-1}$ usually found for molecular solids[94]. If this is the case, the $\frac{1}{\nu} \cdot \frac{d\nu}{dp}$-values become numerically equal to the Gruneisen parameters for these modes and the average value

Table 2.3: THE LATTICE MODES OF PYRIDINE AND PYRIDINE-d_5 IN TWO DIFFERENT PHASES

PHASE I (CRYSTALLINE) 11 kbar							PHASE II (CRYSTALLINE) 25 kbar						
PYRIDINE			PYRIDINE-d_5				PYRIDINE			PYRIDINE-d_5			
ν cm^{-1}	$d\nu/dp$ cm^{-1} $kbar^{-1}$	$1/\nu \cdot d\nu/dp$ $x10^2$ $kbar^{-1}$	ν cm^{-1}	$d\nu/dp$ cm^{-1} $kbar^{-1}$	$1/\nu \cdot d\nu/dp$ $x10^2$ $kbar^{-1}$	Average Ratio d/H	ν cm^{-1}	$d\nu/dp$ cm^{-1} $kbar^{-1}$	$1/\nu \cdot d\nu/dp$ $x10^2$ $kbar^{-1}$	ν cm^{-1}	$d\nu/dp$ cm^{-1} $kbar^{-1}$	$1/\nu \cdot d\nu/dp$ $x10^2$ $kbar^{-1}$	Average Ratio d/H
-	-	-	-	-	-	-	-	-	-	41	-	-	-
-	-	-	-	-	-	-	57	0.59	1.04	53	0.60	1.13	0.94
60	1.11	1.85	57	0.93	1.63	0.95	69	0.52	0.75	66	0.66	1.00	0.96
72	1.29	1.79	70	1.25	1.79	0.97	87	0.97	1.11	83	0.66	0.80	0.96
85[1]	0.94[2]	1.11	80	0.85	1.06	0.94	96	0.94	0.98	89	0.85	0.96	0.93
91	1.39	1.53	85	1.31	1.54	0.93	108	0.99	0.92	101	0.97	0.96	0.95
111	2.25	2.03	108	2.30	2.13	0.97	142	1.58	1.11	135	1.26	0.93	0.96
153	2.86	1.87	143	2.34	1.64	0.93	187	1.74	0.93	168	1.67	0.99	0.91

1 This peak is seen only as a weak shoulder at 11 kbar. The value used was extrapolated.

2. There were not enough values to calculate the $d\nu/dp$ for each phase separately.

Table 2.4: Isotopic ratios calculated for the rotational and translational modes

The rotational modes will give the following isotopic ratios:-

$$\frac{R_{B_1'}}{R_{B_1}} = \left[\frac{I_y}{I_y'}\right]^{\frac{1}{2}} = \left[\frac{170.2}{200.4}\right]^{\frac{1}{2}} = 0.92$$

$$\frac{R_{A_2'}}{R_{A_2}} = \left[\frac{I_z}{I_z'}\right]^{\frac{1}{2}} = \left[\frac{83.36}{101.2}\right]^{\frac{1}{2}} = 0.91$$

$$\frac{R_{B_2'}}{R_{B_2}} = \left[\frac{I_x}{I_x'}\right]^{\frac{1}{2}} = \left[\frac{86.84}{99.2}\right]^{\frac{1}{2}} = 0.94$$

$$\text{Translational modes} = \left[\frac{19.04}{84.07}\right]^{\frac{1}{2}} = 0.97$$

is calculated to be equal to 1.70 for pyridine and 1.63 for pyridine-d_5. For this type of molecular solid at ambient conditions, an average value close to 3.5 is expected[94] as has, for example, also been observed in 4-cyanopyridine[101], naphthalene and anthracene[66]. The fact that the average γ_i values are lower in this phase of pyridine than the ones in comparable molecular solids can possibly be accounted for by assuming that the phase observed here is a less compressible higher phase of pyridine, and that the more compressible lower phase which compares with the phases observed at ambient conditions in benzene and 4-cyanopyridine, is the one with C_{2v}^9-symmetry observed in the X-ray study[62]. When compounds such as benzene and 4-cyanopyridine undergo phase transitions to Phase II, this phase is characterized by much lower $\frac{d\nu}{dp}$-values of the Raman bands than those determined for Phase I.

If the phase diagram of pyridine resembles that of benzene shown in figure 2.2[3], with the important difference that it is shifted down the temperature axis so that at 25° C the liquid/solid transition occurs at $\approx$ 10 kbar, then it could be argued that Phase I of pyridine either exists over a narrow pressure range at ambient temperatures, or cannot be observed under these conditions. Some differences in the lattice modes of pyridine are evident between 10 and 13 kbar. This can be ascribed either to the existence of a new phase in a narrow pressure range, or to the fact that pyridine becomes a true crystalline solid over this pressure range. The possibility can, however, not be totally ignored that the pressure range over which Phase I exists at 25° C is too narrow for the detection of this phase in a DAC where the pressure cannot be adjusted in small enough increments.

If phase I of pyridine has the same structure as phase I of benzene, i.e. Pbca (D_{2h}^{15}), then the limited number of translational and rotational modes that occur in the Raman spectra can be accounted for, while the splittings observed in some of the internal pyridine modes can be explained in terms of A_g/B_g splittings.

2.3.2 Solidification of Pyridine, Phase II

The pressure dependences of some of the more important vibrations of solid pyridine and pyridine-d_5 are given in figure 2.5. The pressure dependence of the lattice modes observed in pyridine is shown in figure 2.6 and the results are summarized in table 2.3.

Figure 2.6:

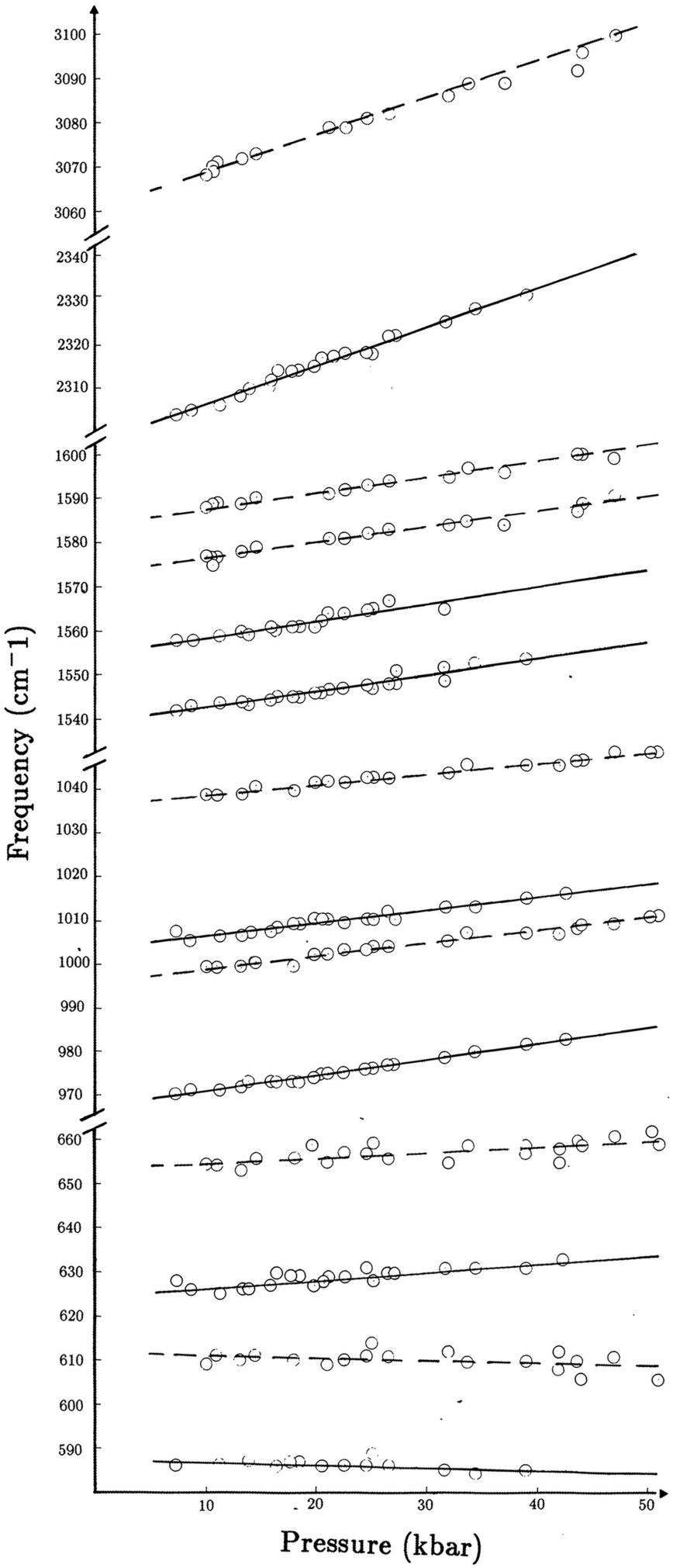

Figure 2.6:

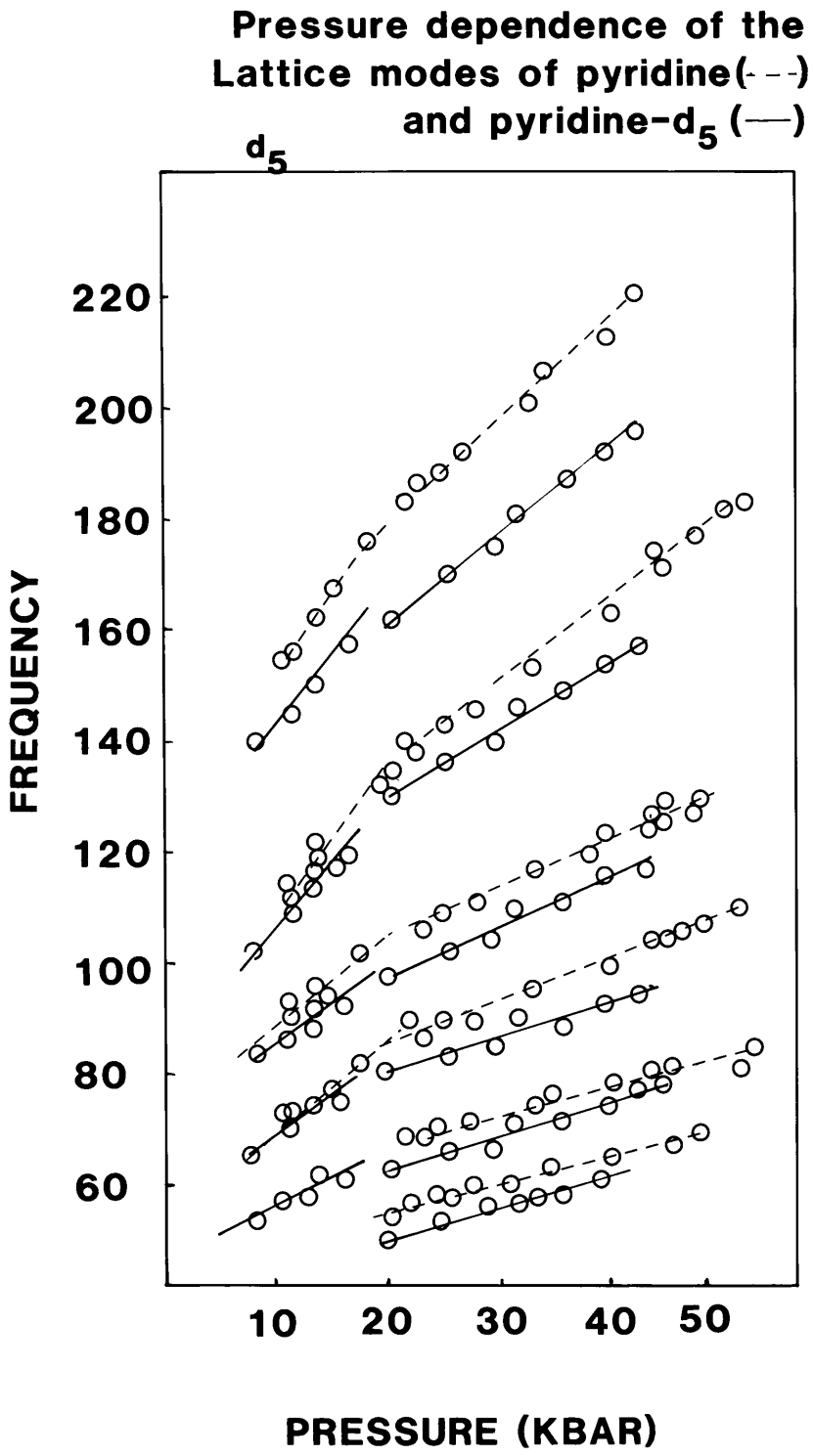

Mode	Spec.	Description	Vapour IR	Liquid Raman	Liquid IR	Crystalline Pyridine-d_5 Phase I,11 kbar	$1/\nu \cdot d\nu/dp$ $kbar^{-1}$ $x10^4$	Crystalline Pyridine-d_5 Phase II,25 kbar	$1/\nu \cdot d\nu/d$ $kbar^{-1}$ $x10^4$
ν_{17a}	A_2	Out-of plane H bend	815	-	-	824 w,br	6.5	823/829 vvw,br	7.2
ν_{17b}	B_1	Out-of plane H bend	-	-	-	-	-	-	-
ν_{18a}	A_1	In-plane H bend	-	824	-	824 w,br	6.5	823/829 vvw,br	7.2
ν_{18b}	B_2	In-plane H bend	-	835	-	843 w	5.1	847[2] w	5.9
ν_{19a}	A_1	C-C ring stretch	-	1339	-	-	-	-	-
ν_{19b}	B_2	C-C ring stretch	-	1228	-	-	-	-	-
ν_{20a}	A_1	C-H stretch	-	2252	-	2260[2] w	2.4	2267 w,br	4.7
ν_{20b}	B_2	C-H stretch	-	2281	-	2284 w	4.2	2294/2300 w	1.5

1 Asymmetrical 2 Could be split

It is evident from figure 2.6 that a phase transition occurs just below 20 kbar in both pyridine and pyridine-d_5 [46]. This phase transition has since also been reported by other workers[106]. The phase transition is not characterized by the appearance of additional lattice modes, except for the lowest lying one occurring at $\approx 55cm^{-1}$ at 20 kbar in pyridine but this could also be due to the fact that it was difficult to record spectra below $50cm^{-1}$ using the DAC and that the upward frequency shifts of the lattice modes with pressure caused the appearance of this mode. The same behaviour has been observed in pyridine-d_5. It is further evident from figure 2.4 that there are significant differences in the intensities of the lattice modes in spectra recorded at 10 kbar and 25 kbar respectively. These differences are clearly evident just below and above the phase transition pressure in both pyridine and pyridine-d_5. The new phase is therefore not characterized by either the appearance of additional bands or large shifts in the lattice mode frequencies and could only be detected by means of abrupt changes in $\frac{d\nu}{dp}$-values and variations in the intensities of these modes. The same behaviour has been reported in the II-III phase transitions in benzene[2].

The $\frac{d\nu}{dp}$ values in this higher phase were generally lower than in the lower pressure phase, indicating a loss of sensitivity of the vibrations to pressure, and thus a stabilization of the molecules in a crystal lattice with a more well-defined symmetry and less thermal motion of the molecules.

At pressures higher than 40 kbar in pyridine and 35 kbar in pyridine-d_5, the lattice modes weakened and broadened considerably. The broadening of the bands could be accounted for by shear stress in the DAC. However, the R_1 and R_2 lines of ruby chips in the cell did not show this to be the case. Furthermore, both sharp and broad internal modes were obtained

in spectra up to 45 kbar. It is uncertain at this stage whether a phase transition occurs above these pressures.

The phase transition occurring just below 20 kbar is analogous to the one reported in the II-III transition in benzene in that the changes which take place in the Raman spectra are relatively mild[79]. The transition is characterized by significant differences in the intensities of the peaks (figure 2.4).

It has already been mentioned that the solidification of pyridine by compression yields two modifications, one the so-called "glassy" state (figure 2.4).

2.3.3 Glassy modification

In figure 2.4 it is shown that two forms of the solid are obtained, the one already described having narrow lattice modes, while the other gives rise to three lattice modes which are broader than those of the first modification. The modification giving rise to broad bands will be referred to as the "glassy" modification, and the one giving rise to the narrow, well-defined lattice vibrations will be referred to as the crystalline modification.

The internal modes of the two modifications do not differ appreciably although some of the modes, particularly the C-H stretching ones, are broader than in the crystalline modification. Transformation of the one form into the other could not be obtained at ambient temperatures and the formation of either of the modifications could not be controlled under existing experimental conditions. It has also been noted that cooling of liquid pyridine yielded samples which were either "glassy" or crystalline,

there being no control of the formation of either modification[16,56]. It is possible that the modification giving rise to the broader lattice-modes could be the "glassy" state obtained in a previous infrared study[16].

The "glassy" modification of pyridine has also been obtained by freezing pyridine under pressure in a study by Kim, Salvador and Sherman[51]. However, it was concluded in this study that pyridine may pass through a metastable glass phase before entering the crystalline phase at 6.5 kbar. The present results are in disagreement with this observation, both as far as the freezing point and pressure stability range of the "glassy" phase are concerned.

Moisture did not play a role in the formation of the "glassy" form, since compression experiments in which pyridine was deliberately exposed to moisture before compression, did not give rise to solid samples which resemble the "glassy" modification. Shifts have also been reported, particularly in the ν_6-region when pyridine complexes with water[90]. The largest Fermi resonance due to H-bonding between pyridine and water was observed in the ν_{8a} vibration where $\nu_{8a} = 1582$ cm^{-1} for dry pyridine and $\nu = 1593$ cm^{-1} for wet pyridine. Extrapolation of the plot of pressure vs frequency to zero yielded $\nu = 1583.5$ cm^{-1}. It can thus be assumed that the pyridine samples used in this study were not wet.

It was initially thought that twinning of the crystals on solidification was taking place in this modification. It is however difficult to explain the presence of such broad ill-defined lattice modes. It appears more likely that in this modification the solid pyridine molecules lie in non-oriented planar laminae as in a "glassy" phase. If this modification characterized by broad bands is truly a "glassy" state, then it is unlikely that a phase transition

will be observed at the same pressure as in the crystalline modification, if at all. In fact, no major changes in intensity or $\frac{d\nu}{dp}$ are observed up to 40 kbar in the spectra of "glassy" pyridine and pyridine-d_5. The peaks at 99 cm^{-1} for pyridine in this modification occurs at very much the same frequency as the vibrational mode found at lowered temperatures for liquid pyridine[57]. This latter band represents a vibrational mode in the liquid phase. At higher pressures, the two maxima are located on the same peak base, and the extrapolated peak obtained is similar to that found in the literature. The $\frac{d}{H}$ isotopic ratios for these modes in "glassy" pyridine and pyridine-d_5 compare well with those cited in the literature for the vibration in the liquid phase.

In this "glassy" modification, the $\frac{d}{H}$ ratios and $\frac{1}{\nu} \cdot \frac{d\nu}{dp}$ values are different from those in the crystalline modification. The values given by $\frac{1}{\nu} \cdot \frac{d\nu}{dp}$ indicate larger differences from crystalline pyridine and pyridine-d_5 in the lower frequency lattice mode than in the higher frequency mode. This trend is also borne out in a comparative study of $\frac{d}{H}$ ratios where the lower frequency vibrational mode displays more rotational character than the same mode which is translational in the crystalline phases. The value for the higher frequency mode remains relatively unchanged and is rotational in character in both the "glassy" and crystalline phases.

The relative intensities of the ν_1 and ν_{12} modes in the "glassy" state differs only slightly from those in the crystalline state, both for pyridine and pyridine-d_5. The slope for the $\frac{I\nu_{12}}{I\nu_1}$ vs pressure for crystalline pyridine is 0.016 $kbar^{-1}$ while for the "glassy" phase it is 0.027 $kbar^{-1}$. This implies that there is very little competition between the different orientations in the disordered state[51].

Assuming the phase diagram for benzene to be an adequate description of that for pyridine, and assuming the planar monoclinic arrangement of molecules in the higher phase possible, it seems plausible that the formation of the "glassy" or crystalline phase should be statistically controlled according to the orientations of the molecules under any given pressure experiment.

2.3.4 Hydrogen bonding in pyridine

Pyridine is known to have three kinds of self-association [106] viz (i) π-π-bonding between aromatic rings; (ii) hydrogen bonding between a -C-H bond and the N-atom of a neighbouring molecule, and (iii) broadside insertion of a -C-H bond into the aromatic ring of another molecule (figure 2.7). In the case of the π-π bond, the ring vibrations would be expected to display changes on compression while in the case of the hydrogen bonds, a specific -C-H out of plane vibration would be affected.

The geometries of adsorbed pyridine molecules in Surface Enhanced Raman Spectroscopy (see Appendix C) studies is much the same as those given above for associated species i.e. pyridine can bond to a metal surface via a π-bond; in which the pyridine lies flat on the surface of the metal (i), or pyridine may bond via a σ-complex, thus assuming a standing-up position on the metal surface (ii).

Since the geometries of (i) and (ii) are so similar, it is safe to assume that the vibrations of the pyridine molecule in both the surface bonded and hydrogen bonded state ought to have similar trends.

Figure 2.7:

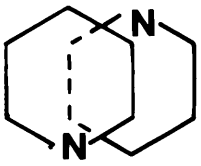

π-π-Bond

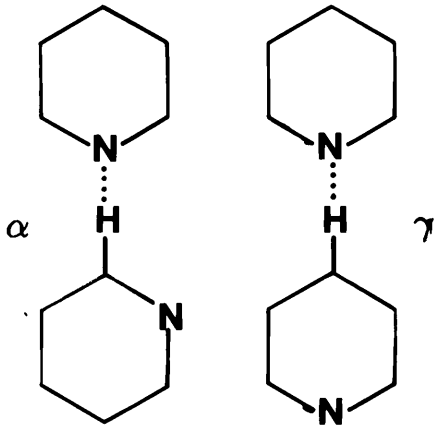

H-Bond

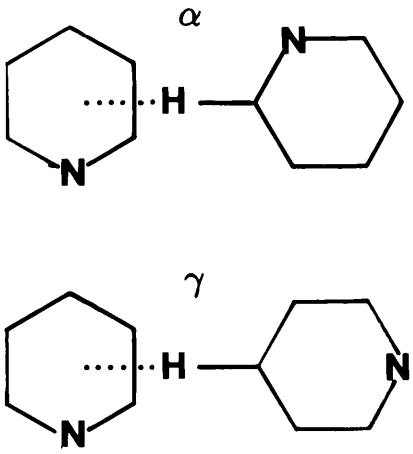

π-H-Bond

Out-of-plane vibrations are expected to be enhanced by π-bond interaction[17]. This would imply that the ν_{16}, ν_4 and ν_5 out-of-plane vibrations would have increased intensities compared to the in-plane ν_1, ν_{12}, and ν_8 vibrations. δ-Bonding on the other hand would affect the C-H stretching vibrations and, depending on the orientation of the associated pyridine molecule, a specific C-H stretching vibration will be affected.

Pyridine-d_5 has stronger association between pairs of molecules than pyridine-h_5[106], therefore any association effects displayed on compression of the samples should be more pronounced in the pyridine-d_5 samples. From table 2.2 it can be seen that no major variation occurred in the intensities of ν_{16}, ν_4, and ν_5 out-of-plane vibrations compared to the ν_1, ν_{12} and ν_8 vibrations. However, the ν_5 out-of-plane hydrogen bending mode which occurs at 942 cm^{-1} in liquid pyridine is shifted by as much as 68 cm^{-1} upon solidification. This shift was confirmed by the corresponding spectra of pyridine-d_5. It is further also of interest to note that ν_2, a prominent C-H stretching mode, shifts upwards by 13 cm^{-1} upon solidification indicating a substantial increase in the C-H bond strength.

It has already been mentioned that hydrogen atoms are involved in the self association of pyridine molecules in the liquid state[106]. The fact that the C-H bonds increase in strength upon solidification shows that the hydrogen bonds either decrease in strength or no longer exist in the solid.

In the case of ν_{13}, a C-H stretching mode of A_1-symmetry, it shifts from 3073 cm^{-1} in the vapour phase to 3057 cm^{-1} in the liquid phase and then upwards again to 3073 cm^{-1} in the solid state. In pyridine-d_5, this mode shifts from 2271 to 2284 cm^{-1} when the compound is solified under pressure.

In the other prominent C-H stretching modes, ν_{20a} (A_1) and ν_{20b} (B_2), no significant shifts could be identified upon solification of pyridine.

The pressure dependences of the internal Raman bands of solid pyridine reveal that in the crystalline Phase I the out-of-plane hydrogen bending modes like ν_{7b} (0.86 $\frac{cm^{-1}}{kbar}$), ν_{10a} (0.54 $\frac{cm^{-1}}{kbar}$), ν_{15} (0.57 $\frac{cm^{-1}}{kbar}$), ν_{17b} (0.55 $\frac{cm^{-1}}{kbar}$) as well as some C-H stretching modes like ν_2 (0.85 $\frac{cm^{-1}}{kbar}$), ν_{20a} (0.60 $\frac{cm^{-1}}{kbar}$) and ν_{20b} (0.97 $\frac{cm^{-1}}{kbar}$) are the most sensitive towards compression. The latter pressure dependences show that, at least as far as these C-H stretching modes are concerned, there are no significant hydrogen bonds in solid pyridine, since an increase in the strength of a hydrogen bond would inevitably weaken the C-H bond that is involved and would therefore cause a downwards frequency shift in the C-H mode upon compression. However, it must be added that the C-H stretching mode ν_{13} ($\frac{d\nu}{dp} = 0.22$ $\frac{cm^{-1}}{kbar}$) is much less sensitive towards pressure than the ones mentioned above. The ν_{13} vibration in the pyridine-d_5 liquid Raman spectrum was obtained as a strong band at 2271 cm^{-1}, while at high pressures it was obtained as a weak band. From these results it appears to be unlikely that solid pyridine is a hydrogen-bonded network and according to the high-pressure Raman spectra it seems much more plausible that π-π interactions between the pyridine rings are of importance.

It must further be noted that ν_2 shifted downwards from 3094 to 3057 cm^{-1} in going from the vapour to liquid phases, proving that C-H—N or even C-H—π interactions are important in the liquid state thereby weakening the C-H bonds. Using the vapour value of ν_2 as a criterion, it must be concluded that some measure of hydrogen bonding still exists in the solid state. The other C-H stretching modes are more difficult to assign unambiguously and

exact correlations between the modes in the liquid and solid states are not always possible.

2.3.5 Vibrational coupling

Since the ν_1 and ν_{12} vibrations both have A_1 symmetry and are found $\approx$ 40 cm^{-1} apart, it is reasonable to expect some Fermi resonance to take place between these two vibrations. Figure 2.8 shows the intensity variation of ν_1 and ν_{12} in both pyridine and pyridine-d_5; while the pressure dependence of the $\frac{I\nu_{12}}{I\nu_1}$ ratio for pyridine is given in figure 2.9. From figure 2.8 it can be seen that there is no evidence of Fermi resonance for pyridine-d_5, and that pyridine shows a pressure dependent Fermi resonance. Figure 2.9, however, shows an approximate 50% increase in $\frac{I\nu_{12}}{I\nu_1}$ for the pyridine samples. This pressure-tuned coupling has since been verified in a study of pyridine in various solvents[106].

A comparison of the $\frac{I\nu_{12}}{I\nu_1}$ ratios of solid pyridine with various complexes is given in the next chapter where the different behaviour of pyridine and pyridine-d_5 upon compression will also be discussed. The intensity of the ν_{12} vibration is shown to be very sensitive to the strength of the M-N bond. The role of the Fermi resonance as opposed to increasing/decreasing M-N bond strength in the intensity of the ν_{12} vibration will thus be further discussed.

Figure 2.8:

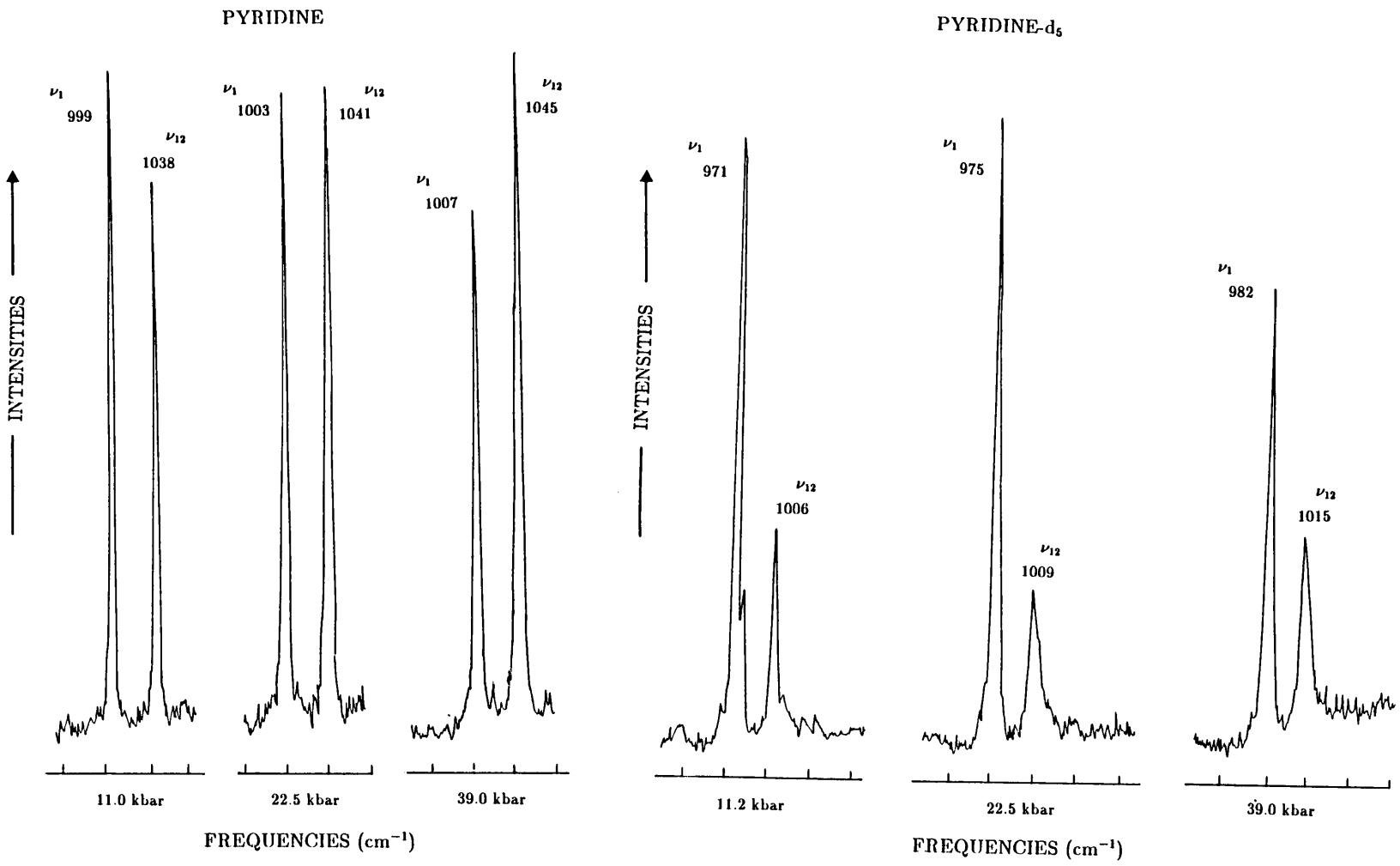

Figure 2.9:

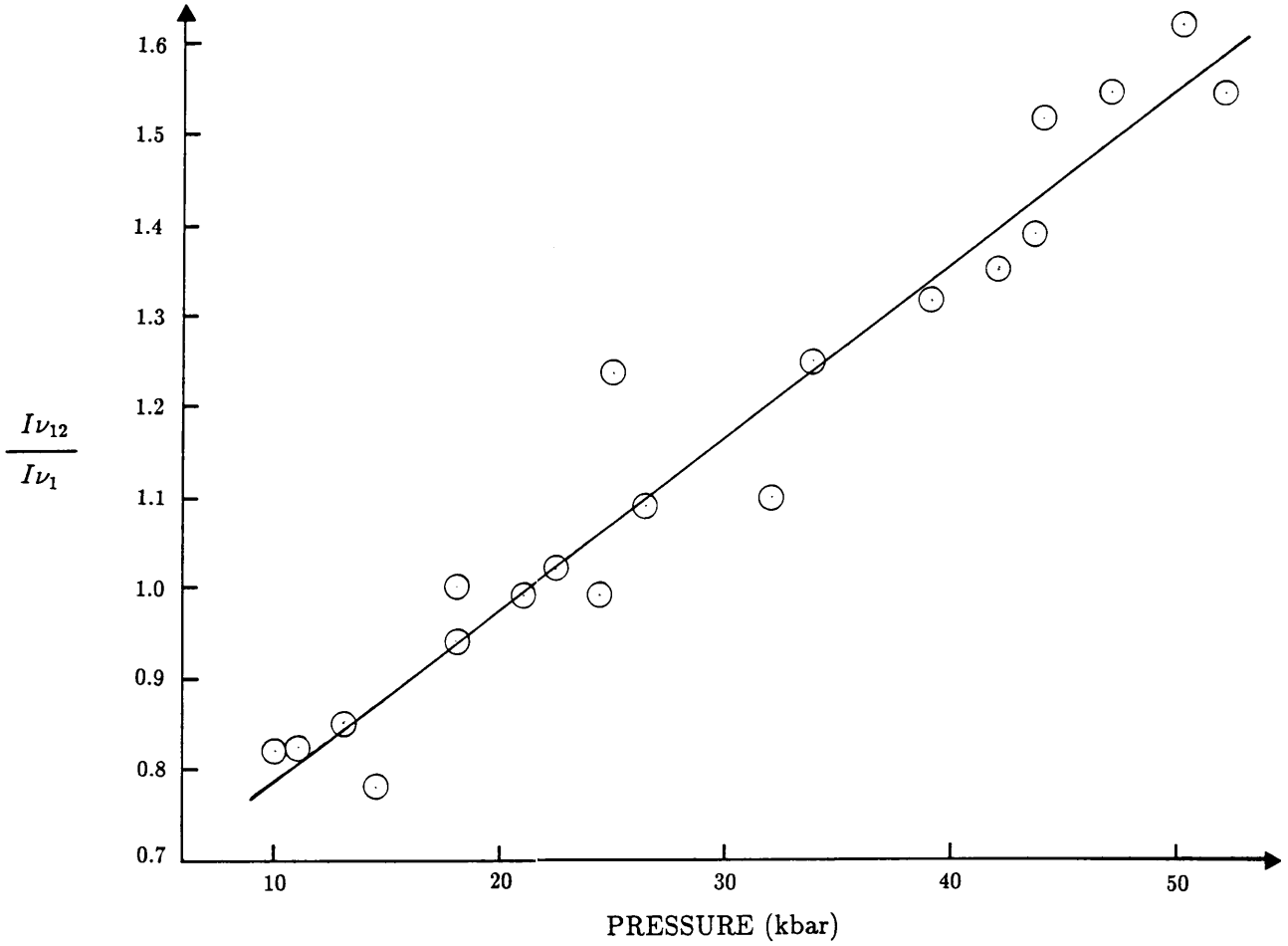

2.4 CONCLUSION

Solidification of liquid pyridine samples in a DAC at ambient temperature at $\approx$ 10 kbar yielded either a crystalline, or a "glassy" modification, the latter characterized by few lattice modes which are much broader than those of the crystalline solid. The pressure shifts obtained in the crystalline phase suggests the phase to be much less compressible than is normally the case with Phase I of planar, aromatic molecules. The Raman spectra of this phase could also not be interpreted in terms of the $Pna2_1$ (C_{2v}^9) structure determined for pyridine by means of X-ray methods at 153 K[62]. This implies that the phase observed in the present investigation is really a high-pressure phase resembling Phase II found in benzene. If the phase diagram for benzene is regarded as representative of this class of molecules then Phase I of pyridine could be orthorhombic with space group $Pna2_1$ (C_{2v}^9) and Phase II could be monoclinic with space group $P2_1/m$ (C_{2h}^2). The Raman spectra of solid pyridine obtained in this study can be much better interpreted in terms of the latter structure.

The pressure dependencies of the lattice modes shows that a phase transition occurs at $\approx$ 20 kbar in pyridine resembling the II-III transition in benzene[2]. This transition is not characterized by the appearance of many new bands, but by abrupt changes in the $\frac{d\nu}{dp}$-values of the lattice modes. The intensities of some lattice modes also change significantly at this pressure.

No major changes in the internal pyridine and pyridine-d_5 modes were obtained under pressure, and assignments of the vibrational modes are similar to those made by previous authors in the gaseous and liquid phases.

From the high pressure Raman studies it seems likely that the π-π interactions of pyridine are of importance in the solid states. It does not seem probable that pyridine exists in a hydrogen-bonded network.

A comparison of the internal pyridine vibrations in the solid state compared with those in metal complexes will be given in the next chapter.

Chapter 3

PRESSURE STUDIES ON SOME METAL DICHLORIDE PYRIDINE$_n$ (n=2,4) COMPLEXES

3.1 INTRODUCTION

Since the vibrational modes have been observed in solid pyridine, it is interesting to compare these results with those of pyridine coordinated to metal ions and in particular to compare the high-pressure behaviour of these species. It was thought that the coordination of the liquid in a known structure would result in specific changes in the vibrational spectra which could easily be interpreted in terms of the metal complex structure. Metal complex formation is also expected to have the same effect as an

increase in pressure on the internal vibrational modes of pyridine, as the pyridine molecules are trapped in a crystal lattice defined by the chosen metal halide frame. Application of further external pressure on such a sample would enhance any steric strain already experienced by the liquid. The vibrational spectra are thus expected to display large shifts in the vibrational modes thus hindered. Internal pyridine vibrations such as ν_1, the totally symmetric C-C stretching mode, and ν_{12}, the symmetric ring bending mode, reflect the strength of M-N bonds and/or hydrogen bond interactions. The hydrogen bonds in these metal complexes may occur between a C-H group and Cl-atom, which will involve a specific C-H group. A C-H stretching vibration might thus be found to behave differently from the others. If, however, a π-π bond is formed, the out-of-plane vibrations of pyridine would be expected to reflect changes on compression. To the author's knowledge, no such study of the pressure effects on the ligand vibrations in a metal halide complex has previously been done.

The vibrations of pyridine adsorbed on metal surfaces has been carefully analyzed to find out how the molecules are bonded to the surface; viz. through the lone-pair electrons; or through the π electrons[23,64]. The Raman bands of pyridine adsorbed on oxides have been used to identify species such as physisorbed, hydrogen bonded-, Lewis-, or Brönstead ones[44,105].

Vibrational studies on the lattice modes of complexes of the type MX_2L_2 (X = halide, L = pyridine or substituted pyridine) are numerous[4,19,32,36]. The first row transition elements of groups VIIa to IIb[26,30,34,59,63,109] and Cd(II) and Hg(II)[9,59,71,109] all have either polymeric octahedral or distorted polymeric octahedral structures excluding Zn(II) which has a slightly distorted tetrahedral shape, and Co(II) which gives both structures

(table 3.1)[34]. $ZnCl_2py_2$ was initially chosen as it has the most simple molecular structure of the above group of compounds. The $NiCl_2(py)_n$ (n = 2,4) have also been studied at high pressures so that it is possible to compare the differences in behaviour between a tetrahedral, polymeric octahedral and octahedral structures. The high pressure Raman spectra of $NiCl_2(py)_4$ show that hydrogen bonds are formed in this complex and it is possible that C-H—π interactions stabilize this complex. The main emphasis of this chapter will, however, be on the $ZnCl_2py_2$ complex. Naturally, compression of these complexes will not only involve changes in the internal pyridine modes, but also in the skeletal modes of the metal complexes.

The possibility that the tetrahedral $ZnCl_2py_2$ molecule, or any other complex, can assume another molecular symmetry under pressure cannot be excluded. Low frequency vibrational spectra have been found to give a good indication of the molecular symmetry present in the metal complex. Distinct differences in the ν M-X stretching vibrations have for example been obtained which are characteristic of specific molecular arrangements[19]. If these complexes were thus to assume another molecular symmetry under pressure then the metal-halide stretching vibrations should indicate this quite clearly.

The vibrational spectra of $ZnCl_2py_2$ have been extensively studied, especially in the region between 250 and 600 cm^{-1} [4,5,6,12,20,95,100,98,102,103,104]. An infrared study from 50 cm^{-1} to 400 cm^{-1} has also been done including most of the lattice modes[10]. Assignments have been based on ligand replacement studies, isotopic labelling and force field calculations. Pressure studies up to 12 kbar have also been published, one of which studied the Zn-Cl modes[99]. The aforementioned study was undertaken to ascertain

Table 3.1:

ION	COMPLEX	STRUCTURE	SPACE GROUP	FACTOR GROUP	Z	M^{II} SYMMETRY	REF
d^4	$CrCl_2py_2$	Monoclinic	$P2_1/n$	C_{2h}^5		Distorted polymeric octahedral	[34]
d^5	$MnCl_2py_2$	Monoclinic	$P2_1/n$		2	Polymeric octahedral with pseudo orthorombic symmetry	[109]
d^6	$FeCl_2py_2$	Monoclinic	$P2_1/n$	C_{2h}^5		Polymeric octahedral	[34]
d^7	γ-$CoCl_2py_2$	Monoclinic	P2/b	C_{2h}^4	8	Polymeric octahedral with pseudo orthorhombic symmetry	[26]
	β-$CoCl_2py_2$	Monoclinic	$P2_1/c$	C_{2h}^5		Tetrahedral	[75]
d^8	$NiCl_2py_2$	Monoclinic	P2/b	C_{2h}^4	2	Polymeric octahedral	[75]
d^9	$CuCl_2py_2$	Monoclinic	$P2_1/n$	C_{2h}^5	2	Distorted polymeric octahedral	[26]
d^{10}	$ZnCl_2py_2$	Monoclinic	$P2_1/c$	C_{2h}^5	4	Tetrahedral	[86,87]
d^{10}	$CdCl_2py_2$	Monoclinic	$P2_1/n$	C_{2h}^5	2	Polymeric octahedral with pseudo orthorhombic symmetry	[109]
d^{10}	$HgCl_2py_2$	Monoclinic	$P2_1/n$	C_{2h}^5	2	Distorted polymeric octahedral	[109]

the effect of a 4-substituent on the pyridine ring, and the effect thereof on the Zn-Cl stretching mode. The π-bonding between Zn and Cl was found to be more sensitive to pressure than the corresponding σ-bonding. The second pressure study[100] to 12 kbar included the whole of the lattice region (no internal pyridine vibrations were reported), and the presence of twenty bands and shoulders were reported.

In the present study, a phase transition at $\approx$ 10 kbar was obtained. Since the previous studies did not report any phase transition in $ZnCl_2py_2$, the present work will deal mainly with the spectral changes at the phase transition and also with a possible mechanism for the transition. In samples which were deliberately improperly dried, the phase transition occurred at higher pressures, i.e. $\approx$ 17 kbar at ambient temperatures, and for this reason may not have been detected in the previous Raman high pressure study to 12 kbar.

The Raman spectra of $NiCl_2py_n$ for both the skeletal (n = 2) [37] and internal pyridine vibrations (n = 2,4) [4] have been reported in the literature. The present study, however, includes high pressure determinations so that a comparison of the above mentioned spectra with those of the $ZnCl_2py_2$ complex may be made. Some interesting aspects concerning the high pressure behaviour of some of the internal pyridine vibrations (notably the C-H stretching vibrations), in the complexes will be discussed in terms of hydrogen bonding association of these complexes. Comparisons of the skeletal M-L modes will also be made.

3.2 CRYSTAL STRUCTURE AND SELECTION RULES

The crystal structure of $ZnCl_2py_2$ is given by the space group $P2_1/c$ (C_{2h}^5) with Z = 4[86,87]. From table 3.2, $3A_g + 3B_g$ translational, $3A_g + 3B_g$ rotational and $9A_g + 9B_g$ skeletal vibrations of $ZnCl_2py_2$ which are Raman active should be obtained in the lattice region. Two types of pyridine rings are present in the crystal structure, i.e. those which form dimer-like pairs and those tipped at $\approx 25°$ from planarity related by the c-glide, and forming an infinite column in the crystal. All vibrations involving zinc and the pyridine molecules are expected to be split. This multiplicity is not observed in any of the Raman studies cited. Another interesting feature of the structure is the bond angles. The Cl-Zn-Cl angle (120.9°) is larger, and the N-Zn-N angle (106.3°) smaller, than that obtained for perfect tetrahedra. The Zn-Cl bond distances are also longer than any of the analogous bond lengths in the 4-substituted pyridine series[88]. These significant differences are attributable to some Cl-H non-bonded interactions.

From the selection rules, a total of thirty bands should be observed in the Raman spectrum of the lattice region of $ZnCl_2py_2$. Due to the limitations of the instrument used, only vibrations occurring above ≈ 50 cm^{-1} could be observed. Although only eight bands were obtained in this region, it must be noted that some of these were broad, implying some overlapping, and previous authors have assigned these to more than one mode[100].

Table 3.2: Lattice vibrations in the $ZnCl_2py_2$ crystal

$ZnCl_2py_2$ has space group $P2_1/c$ with factor group C_{2h}^5 and possible sites $4C_i(2)$, $C_1(4)$ with $Z^b = 4$. All the "atoms" thus occupy the C_1 sites.

now

f^γ	t^γ	C_1	C_{2h}^5	C_s	a_s
12	$3(T_x, T_y, T_z)$	A	A_g	1	3
			B_g	1	3
			A_u	1	3
			B_u	1	3

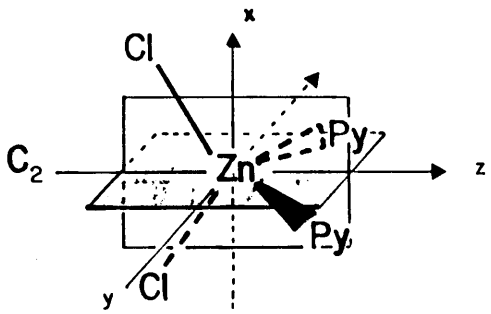

therefore

$$\Gamma_{\text{trans}} = 3(A_g + B_g + A_u + B_u)$$

now

$$\Gamma_{\text{acoust}} = A_u + 2B_u$$

therefore

$$\Gamma_{\text{trans}}^{\text{cryst}} = \Gamma_{\text{trans}} - \Gamma_{\text{acoust}} = 3A_g + 3B_g + 2A_u + B_u$$

A similar mapping for the rotational modes yields

$$\Gamma_{\text{rot}} = 3(A_g + B_g + A_u + B_u)$$

Since only the A_g and B_g modes are Raman-active, $3A_g + 3B_g$ translational and $3A_g + 3B_g$ rotational modes will be found in the Raman spectrum of $ZnCl_2py_2$.

If the pyridine rings are regarded as point groups, then one can say that there are 5 "atoms" in the $ZnCl_2py_2$ molecule. The number of molecular vibrations is given by $3n - 6$, i.e. 9. Since there are four symmetry species, the skeletal modes of $ZnCl_2py_2$ are given by $9A_g + 9B_g + 9A_u + 9B_u$.

3.3 RESULTS

3.3.1 Pressure dependence of the lattice vibrations of different structural types

The most important results obtained involve the changes occurring in the lattice modes of $ZnCl_2py_2$. A plot of the variation with pressure of the lattice frequencies is given in figure 3.1, while table 3.3 gives the $\frac{d\nu}{dp}$ values of the lattice modes in the two solid phases. Below 10 kbar, the assignment of the bands is based on those of previous authors (table 3.4)[65,76,83,100]. The highest occurring peak in the lattice region has been assigned to the ν Zn-Cl stretching mode. No intensity variation takes place on an increase in pressure, but the band moves to higher ν-values. The peak at 154 cm^{-1} has been assigned to ν Zn-N while the vibration at 209 cm^{-1} is assigned also to ν Zn-N, but includes some Cl-Zn-Cl bending motion. The M-N vibrations are generally found to be weaker than the M-Cl vibrations. On compression, the 209 cm^{-1} band increased in wavenumber; the band at 201 cm^{-1}, which is also a ν Zn-N vibration, disappeared, and three new peaks in place of that found at 154 cm^{-1} appeared (figure 3.2). The 201 cm^{-1} peaks consists of ν Zn-N, ν-lattice and δ Cl-Zn-N modes, and a lowering of the symmetry could have separated these modes.

At pressures above 10 kbar, vast changes take place in the lattice modes (figure 3.2). There is a large increase in the number of bands readily definable, and as can be seen, there are also large changes in intensities. The increase in the number of observable bands may be attributed to large pressure shifts, where vibrations under ambient conditions which were too

Figure 3.1:

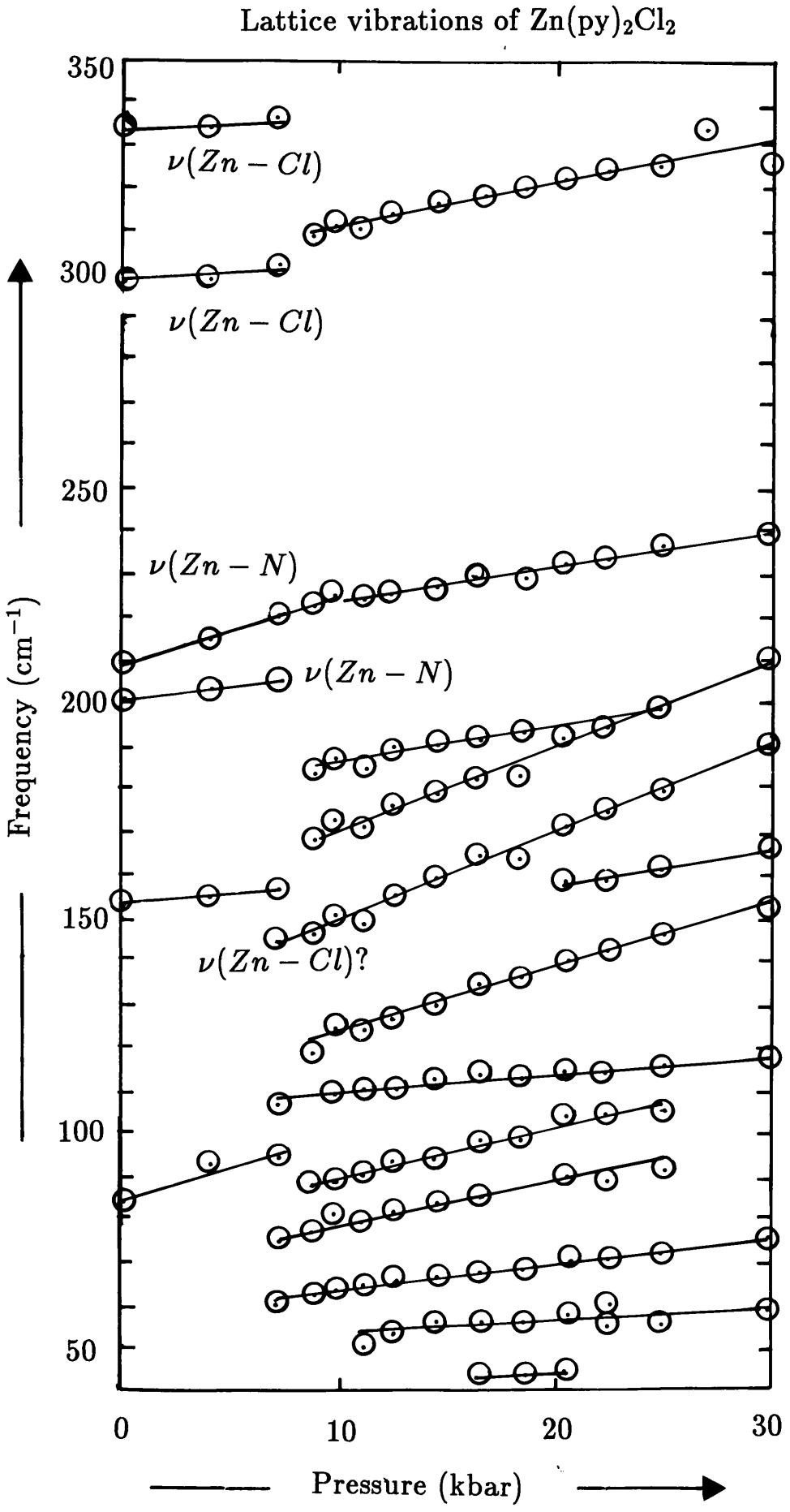

Table 3.4

RAMAN						INFRARED			
DAC	Assignment	Wong	Assignment	Saito & Nakamoto	Assignment	Postmus	Assignment	Barvinok & Panin	Assignment
83s	δCl-Zn-N δN-Zn-N νlattice	83,3							
								94	δ(N-Zn-N)
						109	Lattice	109	δ(X-Zn-N)
						141	Lattice	143	δ(X-Zn-N)
154m	νZn-N δCl-Zn-Cl	151,5	νZn-N,νlattice δCl-Zn-N, δlattice (B_2)	151,2	νN-Zn-N (A_1)	154	δZn-Cl	154	δ(X-Zn-N)
201vw	νZn-N, νZn-Cl δCl-Zn-Cl νlattice	197,0	νZn-Cl, δCl-Zn-Cl, νZn-N	200,0	δCl-Zn-N	200	δZn-Cl	203	ν_{as} Zn-N
209w		204,7	δCl-Zn-Cl, νZn-Cl,νZn-N νlattice	207,6	νZn-N,νZn-Cl				
225vw	νZn-N, δCl-Zn-Cl	222,1	νZn-N, δCl-Zn-N	224,1	νZn-N	218	νZn-N	221	ν_s Zn-N
296m	νZn-Cl, νZn-N, δCl-Zn-Cl	292,9	νZn-Cl, δCl-Zn-Cl, νZn-N	294,8	νZn-Cl, νZn-N	293	νZn-Cl	296	ν_s Zn-Cl
333w	νZn-Cl δCl-Zn-N	326,3	νZn-Cl	330,3	νZn-Cl	326	νZn-Cl	329	ν_{as} Zn-Cl
355vw									

Figure 3.2:

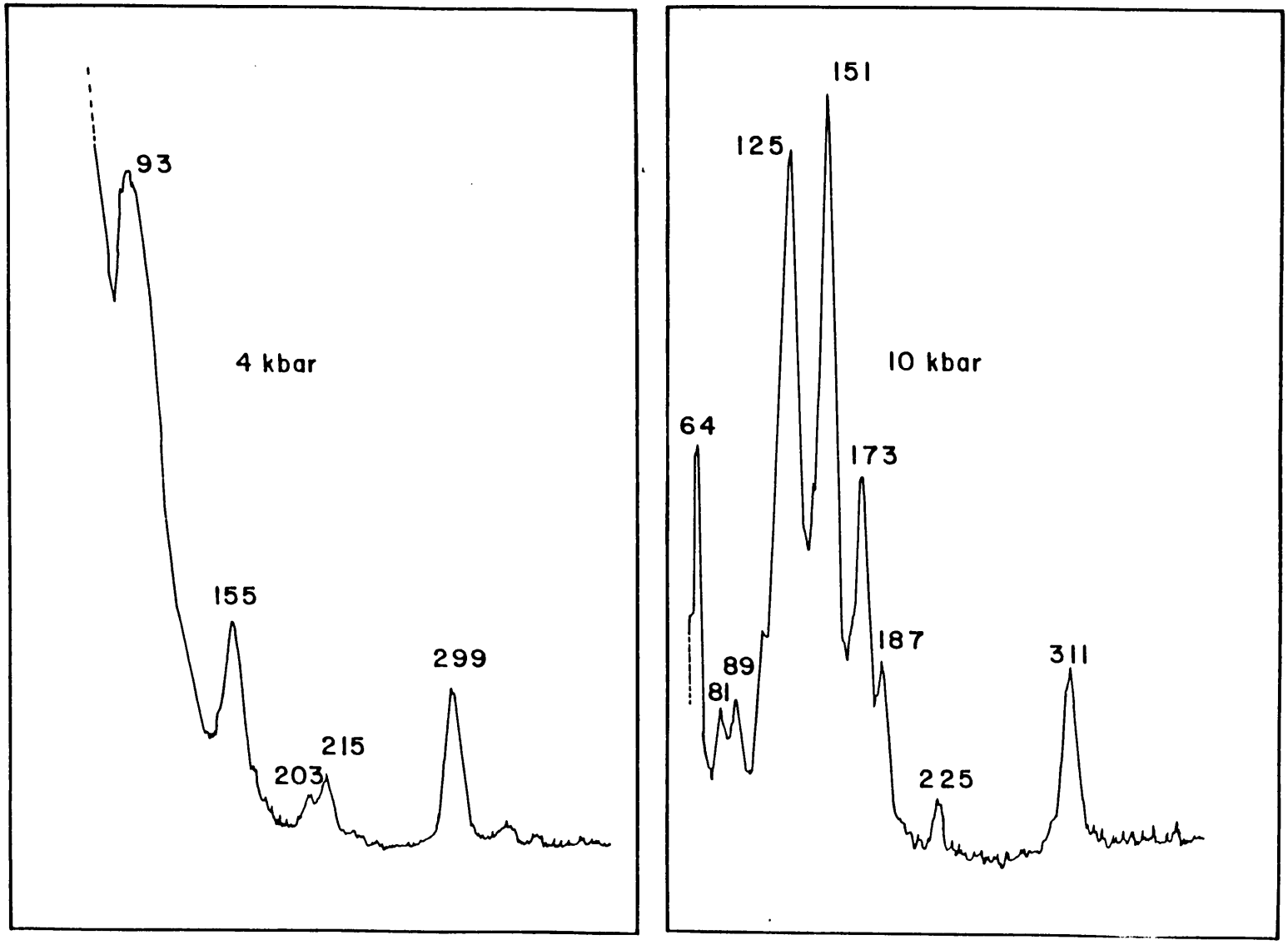

Table 3.4

RAMAN						INFRARED			
DAC	Assignment	Wong	Assignment	Saito & Nakamoto	Assignment	Postmus	Assignment	Barvinok & Panin	Assignment
83s	δCl-Zn-N δN-Zn-N νlattice	83,3							
								94	δ(N-Zn-N)
						109	Lattice	109	δ(X-Zn-N)
						141	Lattice	143	δ(X-Zn-N)
154m	νZn-N δCl-Zn-Cl	151,5	νZn-N,νlattice δCl-Zn-N, δlattice (B_2)	151,2	νN-Zn-N (A_1)	154	δZn-Cl	154	δ(X-Zn-N)
201vw	νZn-N, νZn-Cl δCl-Zn-Cl νlattice	197,0	νZn-Cl, δCl-Zn-Cl, νZn-N	200,0	δCl-Zn-N	200	δZn-Cl	203	ν_{as} Zn-N
209w		204,7	δCl-Zn-Cl, νZn-Cl,νZn-N νlattice	207,6	νZn-N,νZn-Cl				
225vw	νZn-N, δCl-Zn-Cl	222,1	νZn-N, δCl-Zn-N	224,1	νZn-N	218	νZn-N	221	ν_s Zn-N
296m	νZn-Cl, νZn-N, δCl-Zn-Cl	292,9	νZn-Cl, δCl-Zn-Cl, νZn-N	294,8	νZn-Cl, νZn-N	293	νZn-Cl	296	ν_s Zn-Cl
333w	νZn-Cl δCl-Zn-N	326,3	νZn-Cl	330,3	νZn-Cl	326	νZn-Cl	329	ν_{as} Zn-Cl
355vw									

Figure 3.2:

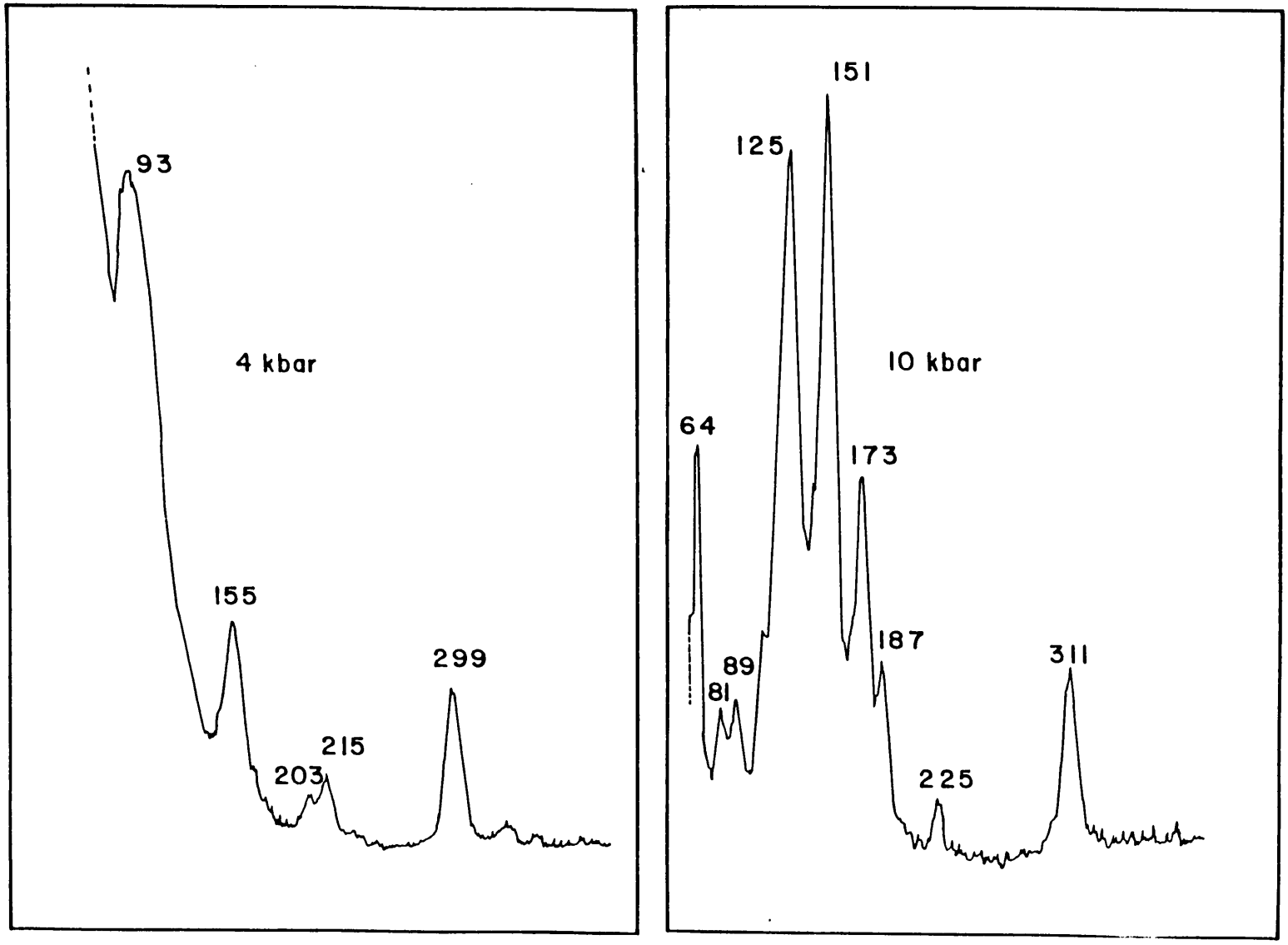

Table 3.3:

$ZnCl_2py_2$ LATTICE MODES				
νcm^{-1} (at atm pressure)	$d\nu/dp$	νcm^{-1} (at 12,5 kbar)	νcm^{-1} (at 20,5 kbar)	$d\nu/dp$
		-	44s	0,46
		54w	58w	0,75
		66s	70s	0,61
		82w	89w	0,88
		93w	104w	1,18
83s	2,03	111w	114w	0,39
		127vs	141vs	1,71
		-	159m	1,15
		156vs	172vs	2,14
154m	0,51	177m	191m	2,07
		190m	195m	0,89
201vw	0,50	-	-	-
209w	1,56	226w	233w	0,86
225vw	2,53	-	-	-
296vw	0,92	314m	322m	1,08
333w	-			
355vw	-			

low to be observed, shifted to higher ν-values. The differences in intensities can also be explained in terms of these ν shifts as previously overlapping bands would be separated from each other at higher pressures as they would have differing $\frac{d\nu}{dp}$ values. If the changes in the spectra occurred gradually over a pressure range, instead of abruptly at a certain pressure as is the case, the above explanation would suffice.

The application of pressure to a coordination compound usually results in an increase in the coordination of the crystal lattice[40,85]; also, the $ZnCl_2py_2$ molecule would be expected to assume the structure of the next higher homologue[40,85], i.e. $CdCl_2py_2$, where $CdCl_2py_2$ has the polymeric octahedral structure. If the $ZnCl_2py_2$ structure were to distort from normal C_{2v} molecular symmetry, either compression of the cis- or trans-ligands will occur, accompanied by a general flattening of the pseudo-tetrahedral shape to give a square-planar as in bis(glycenyl)zinc. A coordination number of six around the Zn^{++} is possible since the octahedral $[Zn(NH_3)_6]^{+2}$ is known to exist[21]. Therefore the polymeric octahedral type structure is theoretically possible. The possibility of dimer formation can also not be excluded.

The probability of structural interconversions under pressure is in most cases very small for nearly pure tetrahedral complexes, as the energy barrier to rearrangement is high. Flattening of the distorted tetrahedral shape to give a square-planar complex would not result in a significant change in the molecular symmetry of the molecule (table 3.5) and would thus not account for the significant increase in the number of bands observed.

The $ZnCl_2py_2$ complex is distorted, and due to the nature of the d^{10} system, there is no ligand field stabilization energy. Conversion from a

Table 3.5: Square-Planar Symmetry

	Symmetry	$\nu(M-X)$	$\nu(M-L)$
trans $-$ $[MX_2L_2]$	D_{2h}	$A_g(R) + B_{3u}(IR)$	$A_g(R) + B_{2u}(IR)$
cis $-$ $[MX_2L_2]$	C_{2v}	$A_1(IR.R) + B_1(IR.R)$	$A_1(IR.R) + B_1(IR.R)$

distorted tetrahedral to a polymeric octahedral structure would involve the formation of new bonds which would stabilize the polymeric octahedral type structure. The chains in the polymeric octahedral structure have a line group isomorphous to D_{2h}; where the pyridine molecules are taken as point masses. Thus $\Gamma_{line}(D_{2h}) = 2A_g + 2A_g + B_{1g} + B_{2g} + B_{3g} + 2B_{1u} + 2B_{2u} + 2B_{3u}$ modes are expected and thus five Raman active modes are predicted. In spectra of polymeric octahedral complexes it is common for more than five bands to be obtained[36]. It has been found that for some compounds, due to slight orientations of the pyridine rings, the symmetry of the species in question is lowered, and thus more bands are allowed in the Raman spectra[36]. The packing of the chains within the crystal structure should also be taken into account as this could give rise to correlation splitting, dependent on the crystallographic space group.

For the distorted polymeric octahedral compound, the line group is isomorphous with the C_{2h} point group. Regarding the pyridine rings as point masses, $\Gamma_{line}(C_{2h}) = 3A_g + 2B_g + 2A_u + 4B_u$ vibrational modes are expected. In the distorted complexes, some ν_{M-X} vibrations occur at higher frequencies than in the undistorted complexes.

If upon the application of pressure, a polymeric octahedral compound were to form analogous to that found for say $CoCl_2py_2$, then two bridging

M-Cl vibrations would be expected which should respond as lattice type modes i.e. high $\frac{d\nu}{dp}$ values, on compression. The ν and $\frac{d\nu}{dp}$ values for $ZnCl_2py_2$ in both phases are given in table 3.3. Two peaks at 151 and 173 cm^{-1} (10 kbar) have lattice type $\frac{d\nu}{dp}$ values. The ratios of the bridging to the terminal ν values are approximately 0.5, i.e. similar to the values obtained for the $CoCl_2py_2$ bridging vibrations (table 3.6)[77]. However, a pressure study on the tetrahedral $CoCl_2py_2$ monomer yielded a polymeric octahedral compound which was also characterized in the infrared by the disappearance of the terminal M-Cl stretches at 347 cm^{-1} and 306 cm^{-1}. The $CoCl_2py_2$ polymeric octahedral species has the bridged Co-Cl stretching modes at much lower frequencies, i.e. 186 cm^{-1} and 174 cm^{-1}[77]. In the case of $ZnCl_2py_2$ there are two Zn-Cl stretching modes. The higher frequency Zn-Cl stretching mode at 333 cm^{-1} (figure 3.1) disappears at the transition pressure, which is characteristic of the structural conversion to a polymeric octahedral complex. However, the lower frequency Zn-Cl stretching mode shifted from 299 cm^{-1} (4 kbar) to 311 cm^{-1} (10 kbar), i.e. an upward shift of frequency with pressure. Formation of both the polymeric octahedral and the tetragonally distorted polymeric octahedral complex should give rise to M-Cl stretching vibrations at lower wavenumbers. In a polymeric octahedral complex, only two M-N vibrations are obtained $\Gamma_{M-N} = A_g + B_{2u}$. Only one of these, the A_g vibration is allowed in the Raman spectrum. In tetrahedral $ZnCl_2py_2$ there are two Raman active Zn-N stretching modes at $\approx$ 200 and $\approx$ 210 cm^{-1}. Above the phase transition, however, only one band is observed (figure 3.1). This is a very good indication of formation of the polymeric octahedral structure in which only one M-N vibration is Raman allowed. From figure 3.3 it can be seen that the Raman spectrum

for the lattice modes of the higher pressure phase of $ZnCl_2py_2$ is very similar to the other polymeric octahedral complexes.

The possibility of dimer or n-mer formation cannot yet be discounted. Although Cl-bridged dimers appear only to form in the gaseous phase in the case of zinc[93], there are a number of such examples, including in the solid phase, in the case of mercury[4]. These dimers would all have both bridging and terminal M-Cl stretches, which would explain the non-disappearance in the Raman spectra of the terminal M-Cl symmetrical stretch in the new phase. The postulated structure is given in figure 3.4, and fits in well with that found for $(ZnCl_2)_2$ in the gaseous phase, with the pyridine molecules serving as layers above and below the Cl-M-Cl bridged layers. The structure is also similar to some $(HgCl_2L_2)_2$ dimers found in the literature[93]. Dimers of this type also have D_{2h} symmetry. The terminal M-Cl stretching vibrations occur much higher than those for $ZnCl_2$ in the various solid phases. This difference between gaseous and solid states is to be expected, the point is that in the polymeric octahedral compounds the terminal M-Cl stretch disappears while bridging M-Cl modes are found at lower, not higher wavenumbers. However, from table 3.6 it can be seen that the M-Cl vibrational ratios are much closer to those found for the polymeric octahedral complexes.

It is useful at this stage to discuss the hydrogen bonding in the $ZnCl_2py_2$ complex. Two types of hydrogen bonding are possible i.e. intramolecular bonding via the ortho positions of the pyridine rings; and intermolecular bonding via the para positions. As has been previously mentioned the Zn-Cl bond lengths in $ZnCl_2py_2$ complex are longer than those of the 4-substituted pyridine series[88]. Since this is the case, there must be

Figure 3.3:

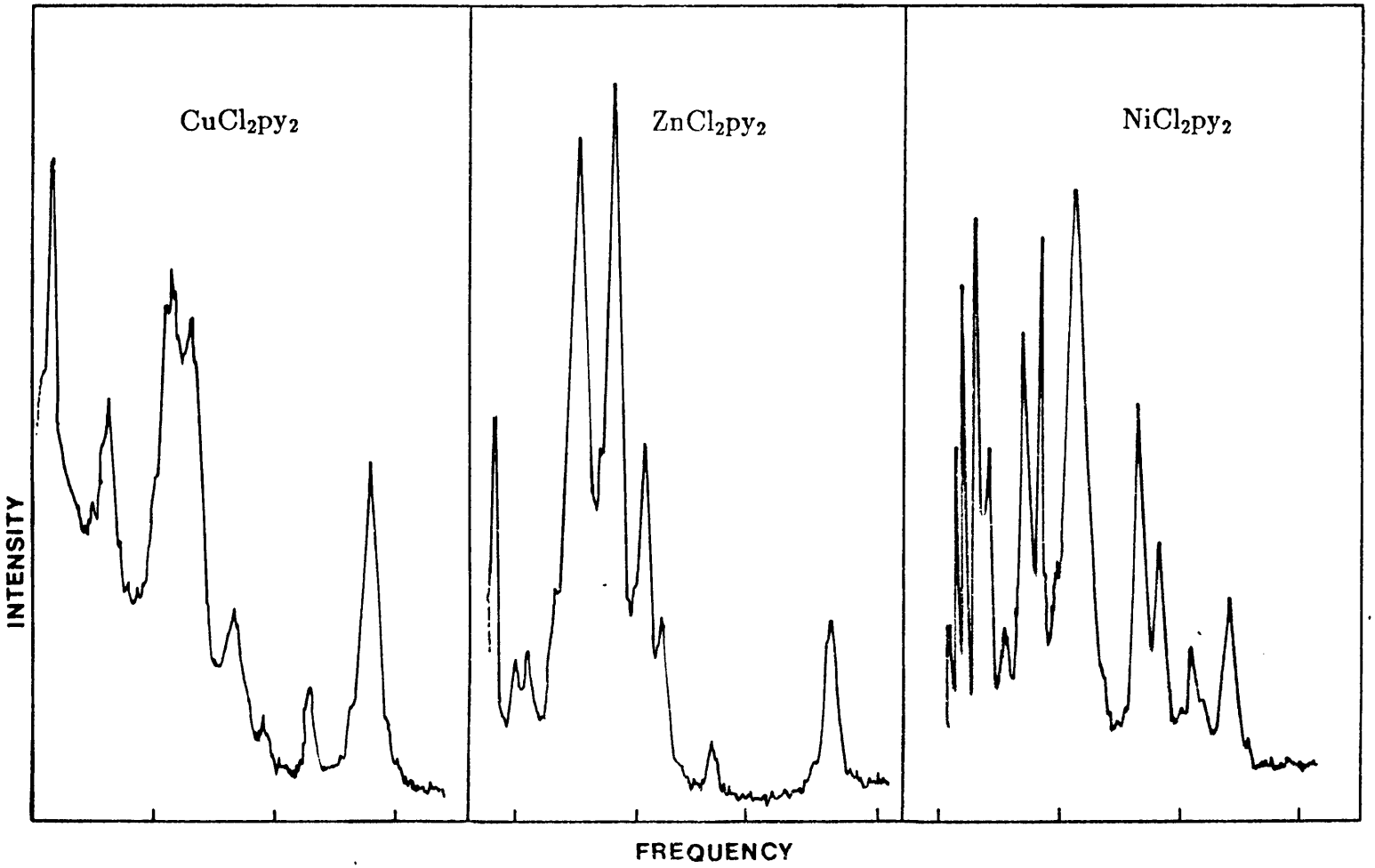

Table 3.6: Metal-Chloride Vibrational Ratios

a) Gas Phase Dimers

$$[ZnCl_2]_2 : \frac{\nu_{M-Cl_{bridging}}(dimer)}{\nu_{M-Cl_{terminal}}(dimer)} = 0.72$$

$$[CoCl_2]_2 : \frac{\nu_{M-Cl_{bridging}}(dimer)}{\nu_{M-Cl_{terminal}}(dimer)} = 0.74$$

$$CoCl_2(monomer) : \frac{\nu_{M-Cl_{bridging}}(dimer)}{\nu_{M-Cl_{terminal}}(monomer)} = 0.62$$

b) Polymeric Octahedral complexes

$$CoCl_2py_2 : \frac{\nu_{M-Cl_{bridging}}(polymer)}{\nu_{M-Cl_{terminal}}(monomer)} = 0.55$$

$$CoBr_2py_2 : \frac{\nu_{M-Cl_{bridging}}(polymer)}{\nu_{M-Cl_{terminal}}(monomer)} = 0.50$$

For $ZnCl_2py_2$ under pressure:

$$\frac{173}{311} = 0.56; \frac{151}{311} = 0.49; \frac{153}{316} = 0.48; \frac{145}{302} = 0.48$$

Figure 3.3:

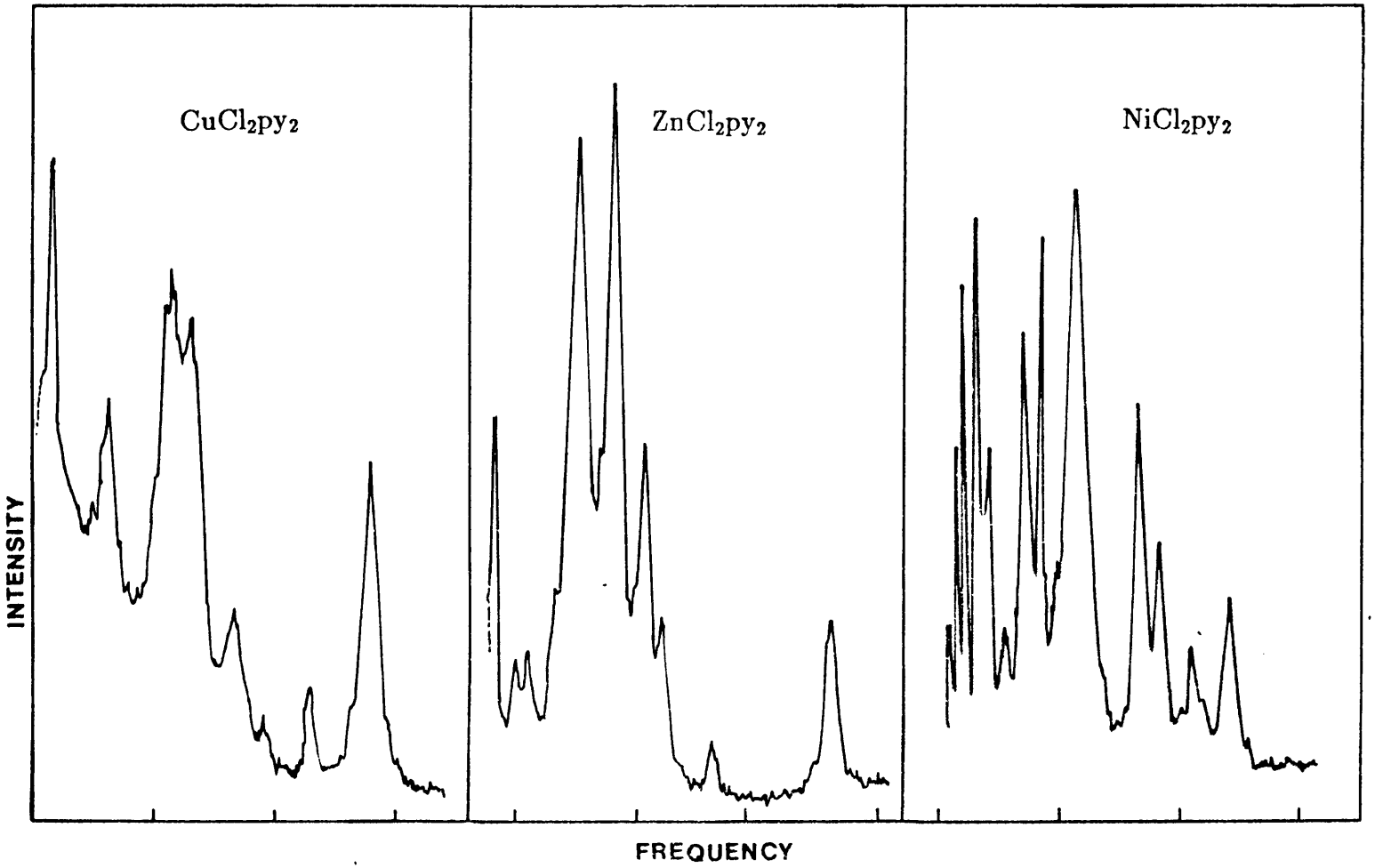

Figure 3.4:

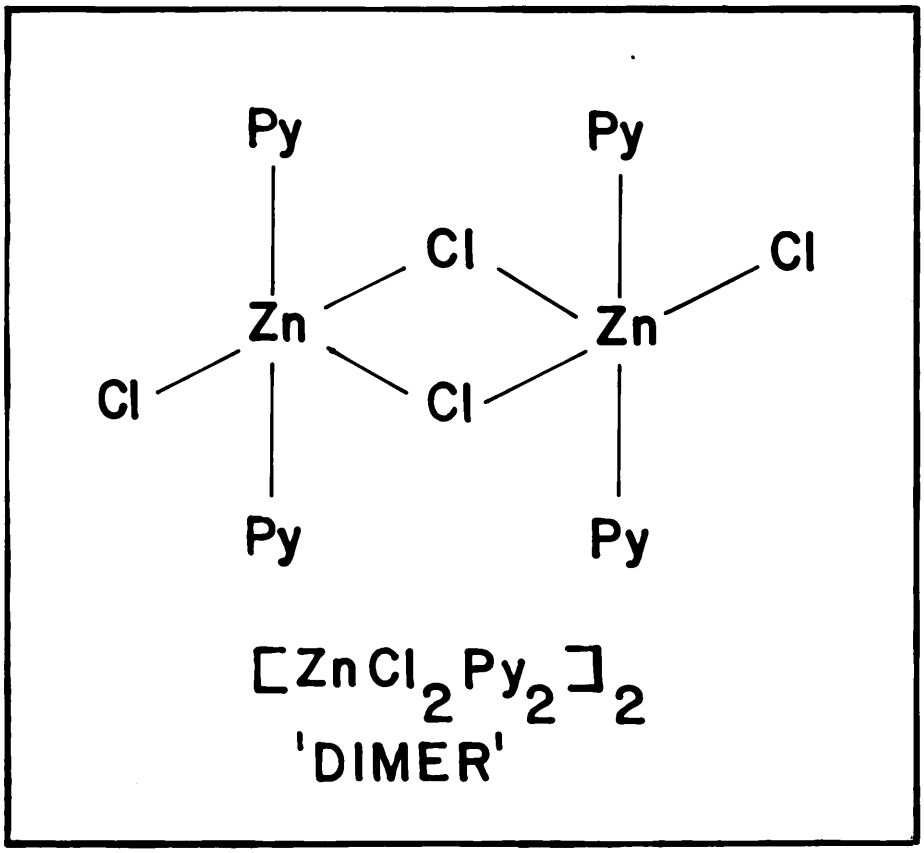

Figure 3.5:

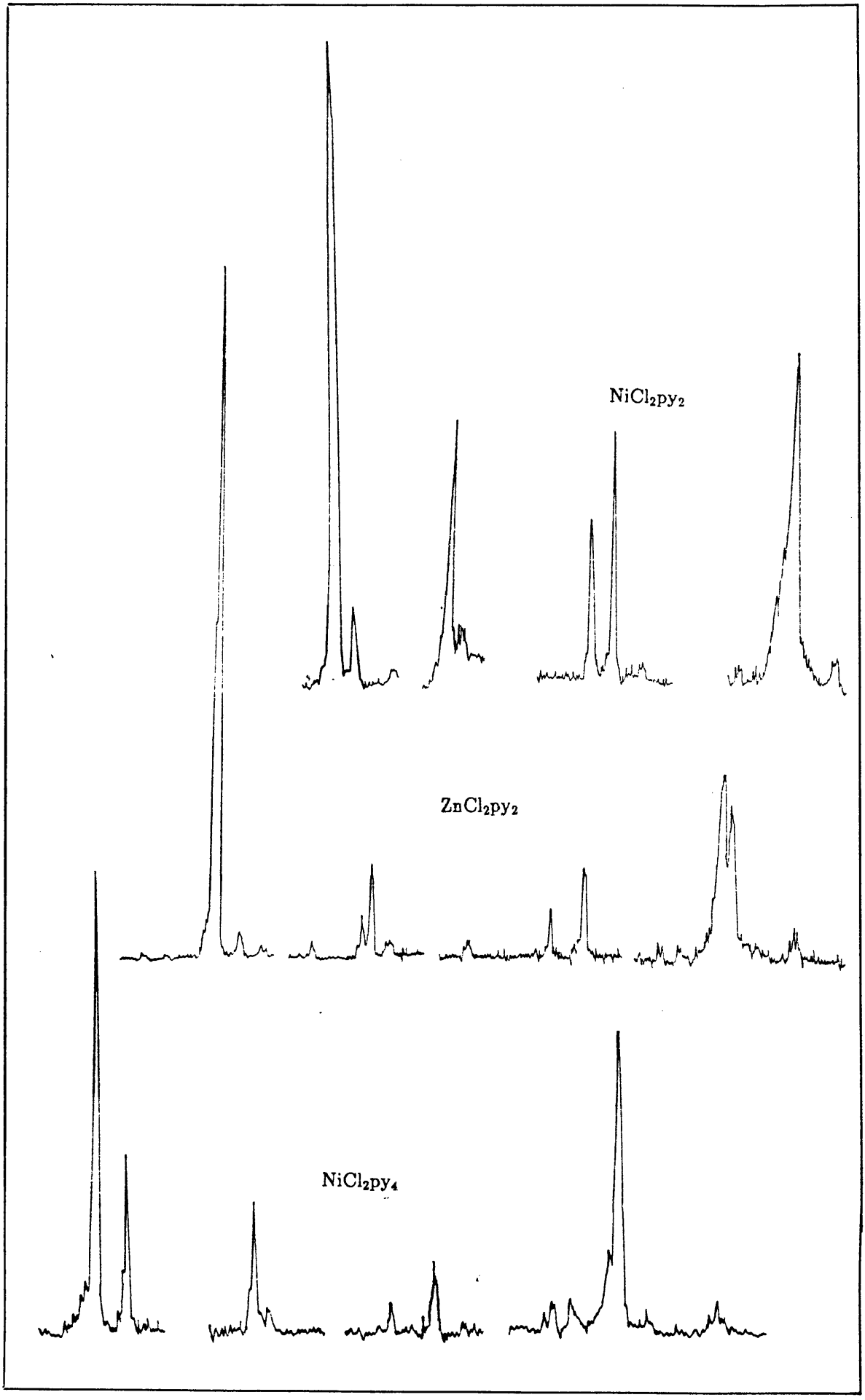

Figure 3.5:

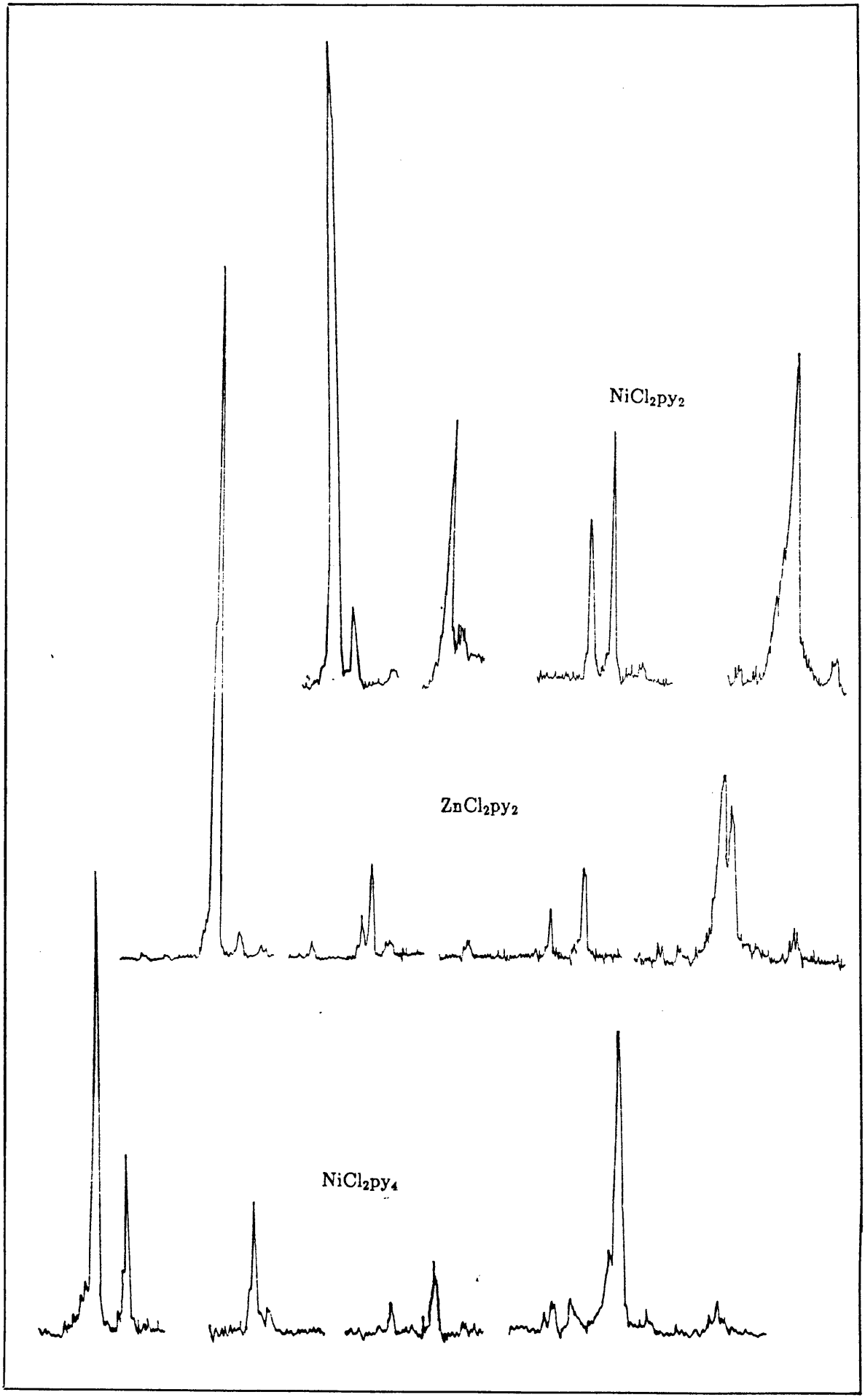

considerable Cl-H interaction via the para position in the pyridine ring. Thus the $ZnCl_2py_2$ molecules are intermolecularly H-bonded. The above study, however, did not exclude the possibility of intra-molecular bonding. Both the $ZnCl_2py_2$ and a (2,6-disubstituted-pyridine)$_2ZnCl_2$ have intermolecular hydrogen bonding. The latter complex, however, could not have the intramolecular H-bonding as both ortho positions on the pyridine ring are occupied. If $ZnCl_2py_2$ has the intramolecular type interaction, then the νZn-Cl mode should be at much higher frequencies than that for the disubstituted species since the latter would also be much heavier. In this work, a Raman spectrum was obtained of (2,6-dibromopyridine)$_2ZnCl_2$. The νZn-Cl mode was obtained at 290 cm^{-1}. The same vibration for $ZnCl_2py_2$ was observed at 296 cm^{-1}. It seems, therefore, that there is only minimal intramolecular association.

A possible explanation for the phase changes observed for $ZnCl_2py_2$ may lie in a combination of the effects of hydrogen-bonding as well as the structural transition from tetrahedral to polymeric octahedral discussed earlier, since a decrease in the Cl-H intermolecular interactions would result in a shorter Zn-Cl bond length, thus explaining the presence of the higher frequency Zn-Cl vibration at $\approx$ 300 cm^{-1}.

3.3.2 Hydrogen bonding as found in the internal pyridine vibrations of $ZnCl_2py_2$

At similar pressures, the frequencies of the internal pyridine vibrations for $ZnCl_2py_2$ were found to be approximately 20 cm^{-1} higher on average than those for uncoordinated pyridine. The differences in the internal pyridine

vibrations depend on the type of coordination of the pyridine to the metal in the complexes[4]. Vibrations involving large changes in volume are particularly sensitive to complexation. Depending on the type of structure, different internal pyridine modes would be expected to be affected.

At pressures above 10 kbar, the spectrum of the internal modes of pyridine in $ZnCl_2py_2$ undergoes marked changes (figures 3.6 and 3.7). The regions most severely affected by the phase change are the C-H bending (1200 cm^{-1}) and C-H stretching (3000 cm^{-1}). These modes are affected by metal complexation and are thus volume sensitive vibrations. In the C-H bending region (figure 3.6) a large downward shift is obtained in the two largest peaks, i.e. the energy of the bending modes has been lowered. In the C-H stretching region a large upward shift of the most intense peak is obtained which implies a shortening of the C-H bond length. It must also be noted that the two shoulders at higher frequencies disappeared, with the simultaneous appearance of one peak at lower frequency. This higher phase spectrum in the C-H region is characteristic of pyridine complexes with no hydrogen bonding[88].

It has been observed that vibrational modes involving large changes in volume are particularly sensitive to pressure. If rotation about the Zn-N axis occurred so that the arrangement of pyridine rings becomes more ordered, with larger interpyridine ring spaces, then the C-H stretching and bending modes would be expected at lower ν-values. The fact that these vibrations did occur at lower ν-values, and that the spectra in these regions become less complex, indicated that an increase in the stabilization of the pyridine rings could possibly have taken place.

Figure 3.6:

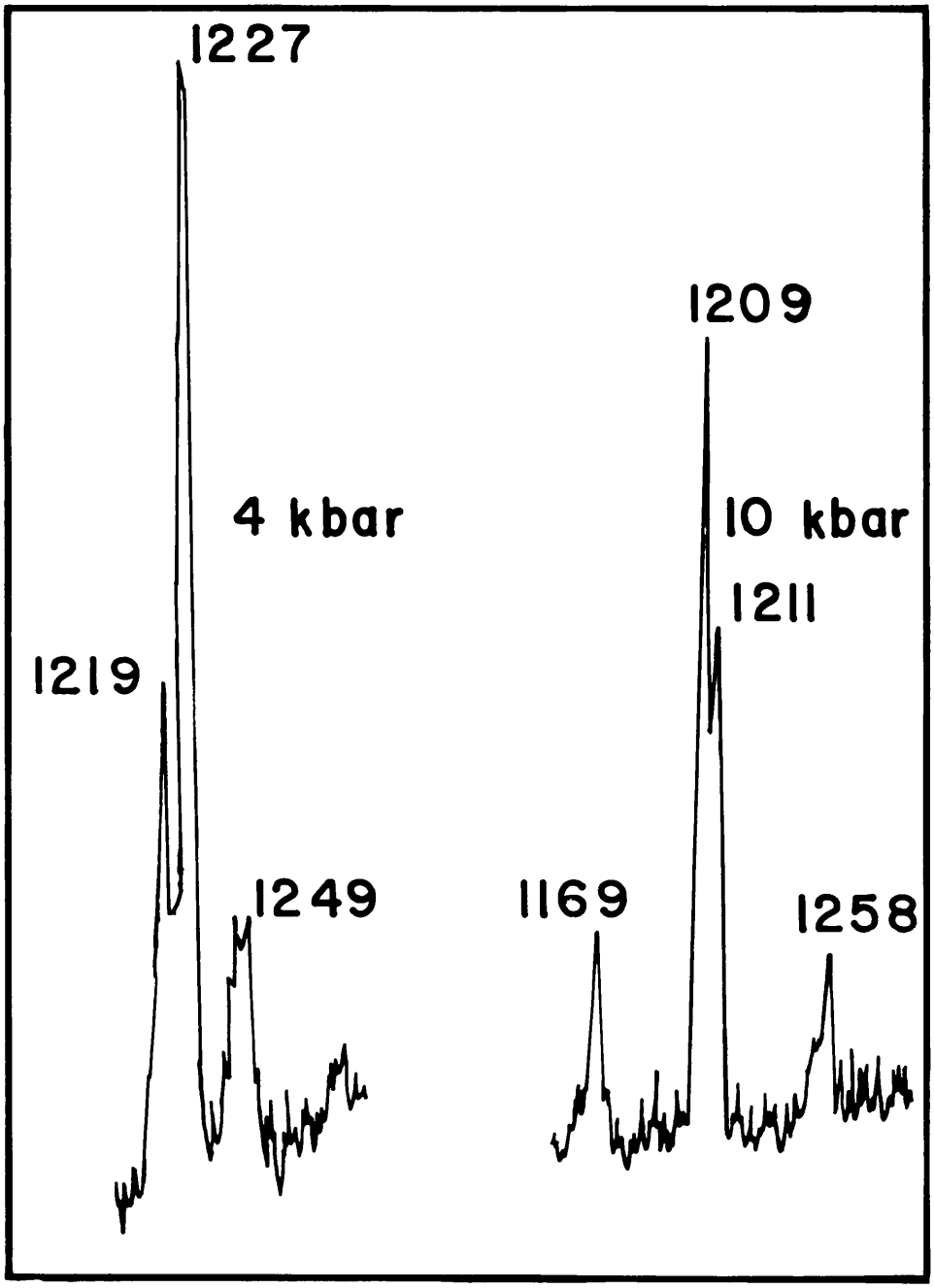

Figure 3.7:

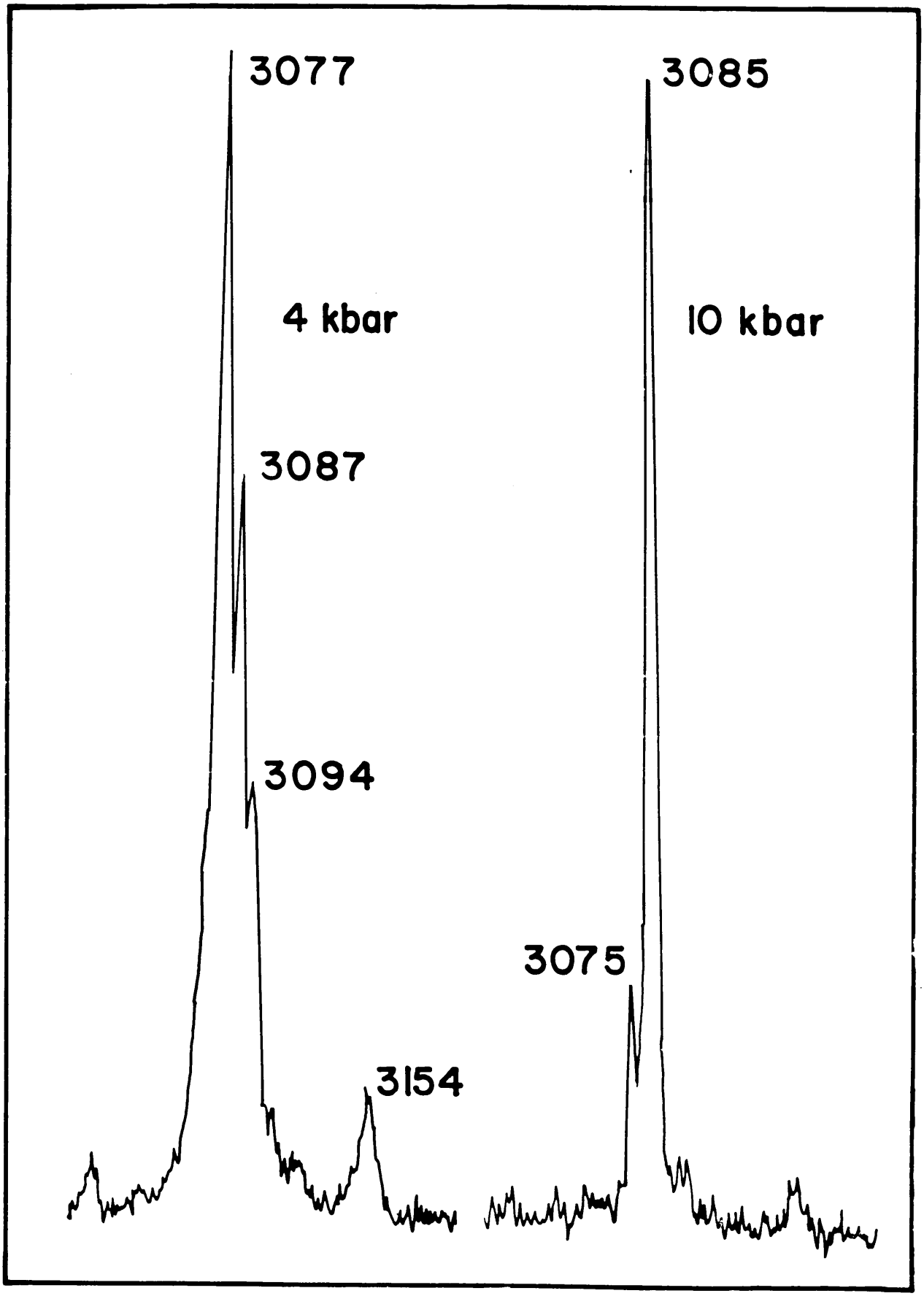

As observed earlier, the higher phase C-H spectrum is characteristic of pyridine complexes with little or no hydrogen bonding. If the hydrogen bonds between the Cl and H atoms were to be broken, then one would expect changes in both the internal C-H modes as well as in the Zn-Cl skeletal modes. It has already been established that the Zn-Cl vibrations of the unsubstituted pyridine complex do not fit in with the values obtained for $(4\text{-R-py})_2ZnCl_2$ complexes which do not have any intermolecular Cl-H contacts[88]. This is a clear indication that the Cl-H contacts which occur intermolecularly via the para-position of the pyridine ring influences the Zn-Cl bond length to a larger extent than the intramolecular Cl-H contacts which occur via the hydrogen atoms on the ortho-positions of the pyridine rings. If the Zn-Cl vibrations were to fit in with the results obtained for the 4-substituted pyridine complexes then the vibrations should be obtained at higher frequencies than those obtained under ambient conditions. It was found that at higher pressures, apart from the normal pressure shifts, the ν Zn-Cl skeletal mode at 299 cm^{-1} undergoes a large shift toward higher ν values, which effect is also observed in the C-H stretching mode (figure 3.7) as mentioned earlier. A similar shift in the ν Zn-N skeletal modes is not observed. This effect corresponds with a substantial shortening of both the Zn-Cl and C-H bond lengths and thus less intermolecular Cl-H interaction. The phase change must thus have included a diminishing Cl-H bonding effect. The structural conversion from tetrahedral to polymeric octahedral as discussed earlier may thus be assumed since the only discrepency is the increase in frequencies of the ν Zn-Cl mode to 311 cm^{-1} (10 kbar). This shift to a higher frequency has, however, now been explained in terms of the diminishing Cl-H contacts at higher pressures.

3.3.3 Important aspects of the pressure dependence of the internal pyridine modes of some $M^{II}Cl_2py_n$(n=2,4) complexes.

The Raman bands occurring in solid pyridine, $Zn(py)_2Cl_2$, $Ni(py)_2Cl_2$ and $Ni(py)_4Cl_2$ are summarized in Table 3.7, while some of the shifts which occur when liquid pyridine is crystallized at 10 kbar or when pyridine is coordinated to a metal ion are given in table 3.8. It is evident in the latter table that several modes are affected when pyridine is crystallized by the application of pressure and it appears as if the ring modes of pyridine are in general less affected than the C-H modes. This has, however, been discussed in detail in the previous chapter.

When liquid pyridine is coordinated to metal(II) ions, several shifts in the frequencies of Raman bands are observed. It is evident that ring vibrations such as ν_1, ν_{6a}, ν_{8a}, ν_{12} are severely affected. However, some C-H stretching bands such as ν_2 and out-of-plane H-bending vibrations such as ν_5 are also affected. In other words, when a σ-bond is formed between the lone pair of electrons on the N-atom and a metal ion, the in-plane hydrogen and C-C vibrations of pyridine reflect these redistributions of electrons very clearly. It is further also of interest to determine whether the positions or intensities of the above-mentioned bands which are affected by coordination accurately reflect the M-N bond strength in a pyridine complex. It has been shown[91] that the frequency of ν_{6a} in the infrared spectra of pyridine of a metal complex is a good measure of the M-N bond strength and this was illustrated by correlating the M-N force constant with the value of ν_{6a} for the polymeric octahedral complexes $Ni(py)_2Cl_2$ and $Cd(py)_2Cl_2$. However,

Table 3.7: Frequencies and assignments of the Raman-active Internal Pyridine Vibrations in Solid Pyridine and $Zn(py)_2Cl_2$, $Ni(py)_2Cl_2$ and $Ni(py)_4Cl_2$ ($\frac{d\nu}{dp}$-values of some modes are indicated between brackets)

Mode	Species	Description	Pyridine	$Zn(py)_2Cl_2$	$Ni(py)_2Cl_2$	$Ni(py)_4Cl_2$
ν_1	A_1	C-C ring stretch	998vs(0.37)	1023vs(0.5)	1017vs(0.40)	1011vs(0.86)
ν_2	A_1	C-H stretch	3070vs(0.86)	3072vs(0.37)	3077m(0.73)	3075vs(0.86)
ν_3	B_2	in-plane H bend	1233w(0.42)	1227m(≈0)	1231m	1235m
ν_4	B_1	out-of-plane ring bend	–	–	–	–
ν_5	B_1	out-of-plane H bend	1010vw(0.43)	1001sh	–	1000sh
ν_{6a}	A_1	in-plane ring bend	609vw	646vw(≈0)	635w	627w
ν_{6b}	B_2	in-plane ring bend	653w	654m(≈0)	651m	649m(0.1)
ν_{7a}	A_1	out-of-plane-bend	3061sh(0.46)	–	3068sh	3067sh(-0.16)
ν_{7b}	B_2	out-of-plane H bend	3042w(0.85)	–	3042w(0.67)	–
ν_{8a}	A_1	C-C ring stretch	1588m(0.30)	1612m(0.2)	1611m	1602m
ν_{8b}	B_2	C-C ring stretch	1577m(0.37)	1577w(0.10)	1578m(0.45)	1570m
ν_{9a}	A_1	in-plane H bend	1233w(0.48)	1226m(≈0)	1233m	1217m
ν_{9b}	B_2	in-plane H bend	1213w(0.40)	1217w(≈0)	1240m	1235w
ν_{10a}	A_2	out-of-plane H bend	899vw(0.54)	–	–	–
ν_{10b}	B_1	out-of-plane H bend	≈960vw(0.26)	–	–	–
ν_{11}	B_1	out-of-plane bend	–	–	–	–
ν_{12}	A_1	in-plane ring bend	1038vs(0.35)	1048w(0.10)	1043m(0.20)	1037m(0.18)
ν_{13}	A_1	C-H stretch	3093w(0.22)	–	–	3079sh
ν_{14}	B_2	C-C ring stretch	–	–	–	–
ν_{15}	B_2	in-plane H bend	1150w(0.58)	1165vw(≈0)	–	1142vw(≈0)
ν_{16a}	A_2	out-of-plane ring bend	384w(0.10)	–	–	388w
ν_{16b}	B_1	out-of-plane ring bend	417w(0.36)	425w	–	–
ν_{17a}	A_2	out-of-plane H bend	986vw	–	–	980vw
ν_{17b}	B_1	out-of-plane H bend	1010w(0.55)	1003(≈0)	–	–
ν_{18a}	A_1	in-plane H bend	1068vw	1072vw	–	1073vw
ν_{18b}	B_2	in-plane H bend	1068vw	–	–	1060w
ν_{19a}	A_1	C-C ring stretch	–	–	–	–
ν_{19b}	B_2	C-C ring stretch	–	–	–	–
ν_{20a}	A_1	C-H stretch	3061w(0.61)	–	3028w	3054m
ν_{20b}	B_2	C-H stretch	3081w(0.96)	–	3009w	–

Table 3.8: The frequency shifts of some Raman-active internal modes of liquid pyridine upon crystallization at 10 kbar and upon coordination to Ni(II) and Zn(II)

Mode	Liquid pyridine	$\Delta\nu$	$\Delta\nu$ liq. pyridine → complex		
	cm^{-1}	liq. pyridine → solid	$Zn(py)_2Cl_2$	$Ni(py)_2Cl_2$	$Ni(py)_4Cl_2$
ν_1-(C-C) ring stretch	991vs	7	32	26	20
ν_2-C-H stretch	3057vs	13	15	20	18
ν_3-in-plane H bend	1227w,sh	6	0	4	8
ν_5-out-of-plane H bend	942vw	68	59	–	58
ν_{6a}-in-plane ring bend	604w	5	42	31	23
ν_{6b}-in-plane ring bend	653	0	1	-2	-4
ν_{8a}-C-C ring stretch	1582s	6	30	29	20
ν_{8b}-C-C ring stretch	1574w,sh	3	3	4	-4
ν_{9a}-in-plane H bend	1217s	16	9	16	over 18
ν_{12}-in-plane ring bend	1031vs	7	17	12	6
ν_{15}-in-plane H bend	1147m	3	18	–	-5
ν_{18a}-in-plane H bend	1069m	-1	3	–	4

in the present study the values of ν_{6a} did not show a direct relationship with the strength of the M-N bonds in the complexes investigated. A possible reason for this behaviour could also be that the frequency of ν_{6a} could also be dependent on the structure of the complex and that it could be inappropriate to compare the values of ν_{6a} in polymeric octahedral ($Ni(py)_2Cl_2$, $Cd(py)_2Cl_2$, $Cu(py)_2Cl_2$), distorted octahedral ($Ni(py)_4Cl_2$) and distorted tetrahedral complexes ($Zn(py)_2Cl_2$).

The ring breathing modes ν_1 and ν_{12} of pyridine have been studied in aqueous solution as functions of concentration and pressure[106], while the pressure dependences of these modes have been studied in various solvents[107]. For certain combinations of solvent and concentration, a strong pressure-dependent Fermi resonance has been observed between ν_1 and ν_{12}. A comparison of the Raman bands in solid pyridine and its complexes reveals that the relative intensity of ν_{12} varies widely (figure 3.8). It ranges from a ratio of $\frac{I\nu_{12}}{I\nu_1} = 0.05$ in $Ni(py)_4Cl_2$ to ratios of 0.65 in $Cd(py)_2Cl_2$ and 0.86 in solid pyridine (13 kbar). The ratios of the intensities $\frac{I\nu_{12}}{I\nu_1}$ are graphically represented against $4\pi^2\mu c^2\nu^2$ in figure 3.9 (μ = reduced mass, ν = wavenumber of the symmetric M-N stretching mode) for the complexes $Cd(py)_2Cl_2$, $Ni(py)_2Cl_2$, $Cu(py)_2Cl_2$, $Ni(py)_4Cl_2$ and $Zn(py)_2Cl_2$. The linear relationship that is evident in figure 3.9 shows that the intensity of the vibration ν_{12}, which is schematically drawn in figure 3.10, together with the totally symmetric ring stretching mode ν_1, is very sensitive with respect to the strength of the M-N bond and can thus be used as a criterion to measure its bond strength. In the lower phase tetrahedral $ZnCl_2py_2$ there are four σ-bonds(sp^3). These result in strong Zn-N bond formation. The higher phase polymeric octahedral $ZnCl_2py_2$ will also have strong Zn-

Figure 3.8:

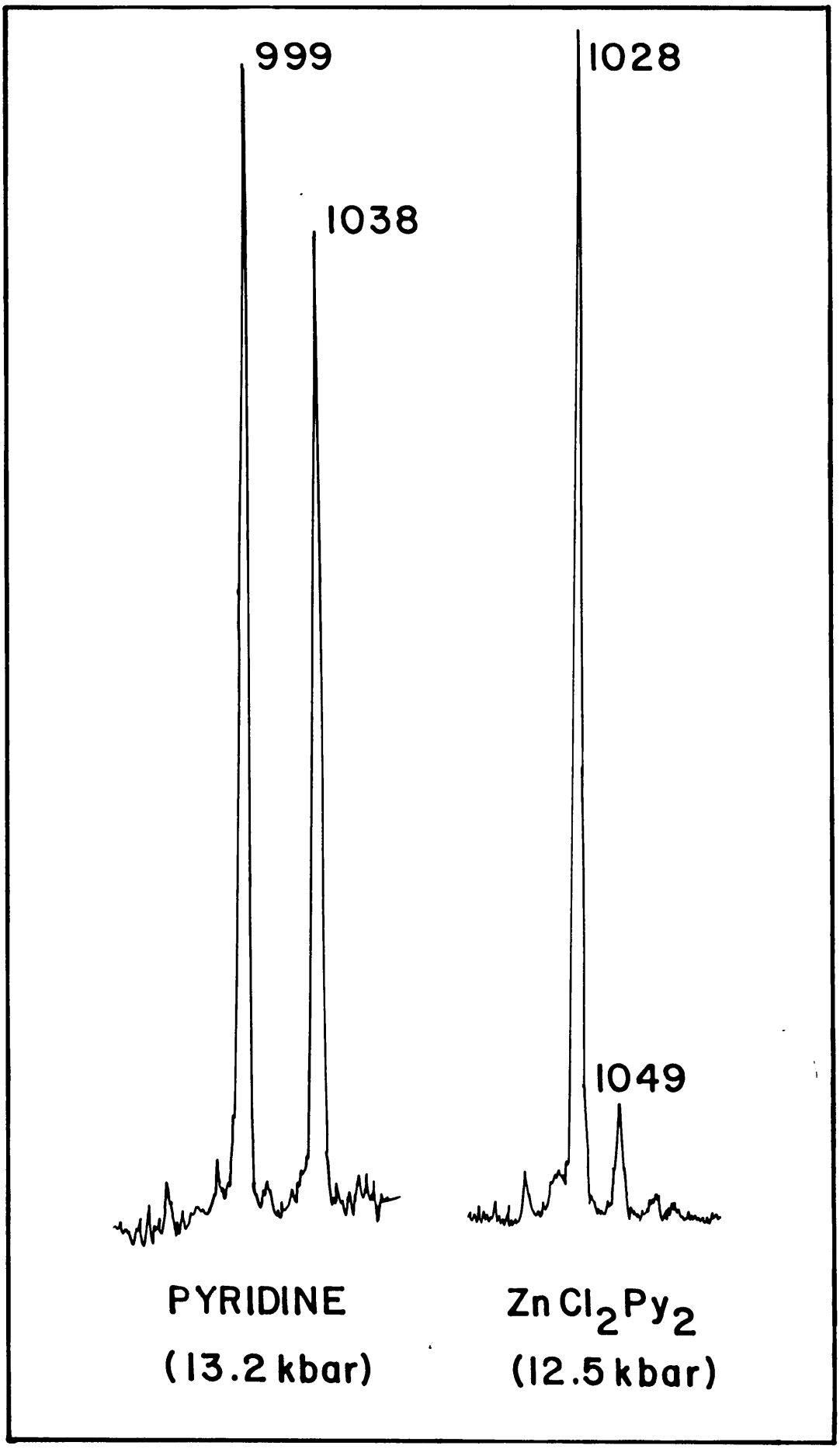

Figure 3.9:

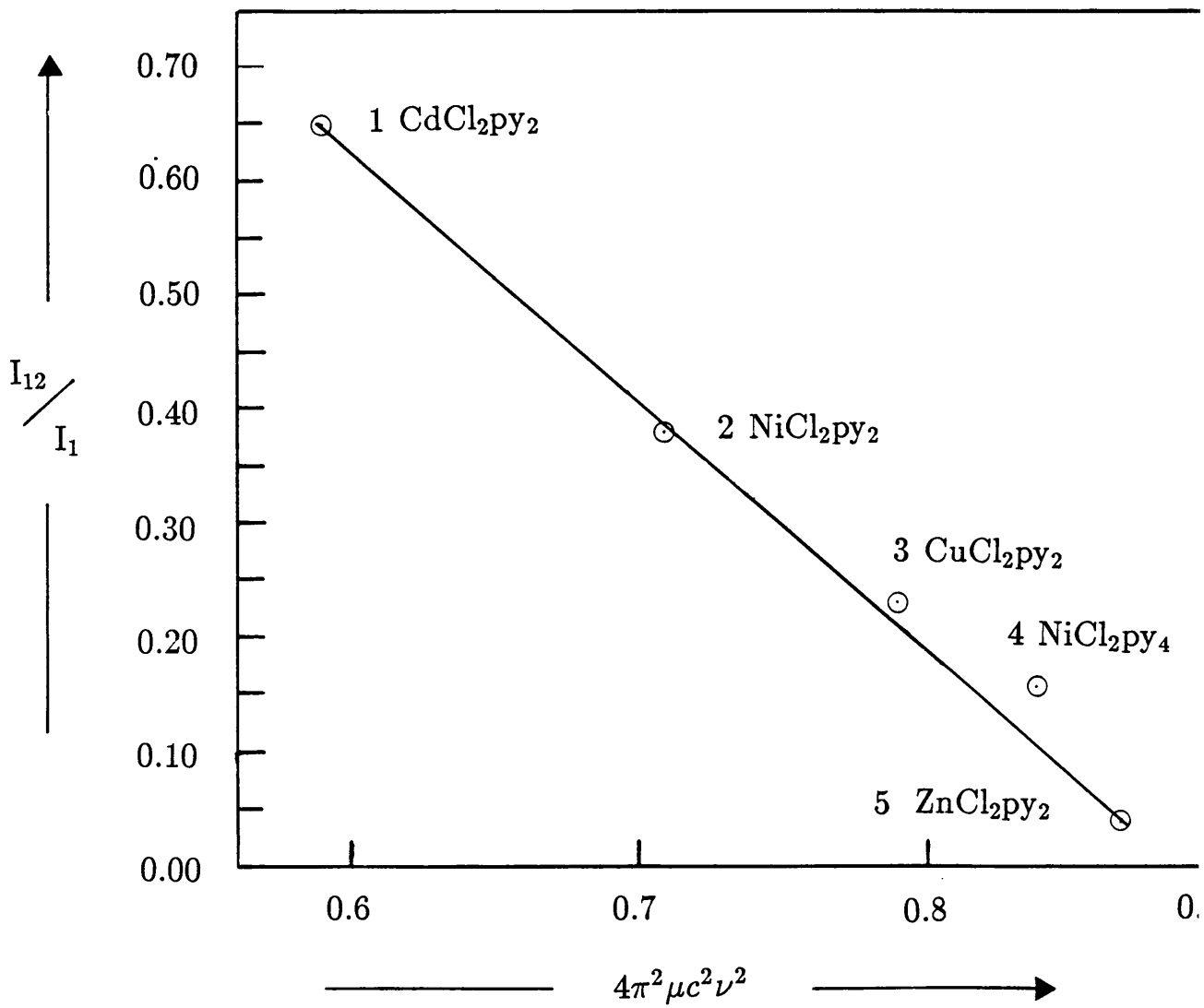

Figure 3.10:

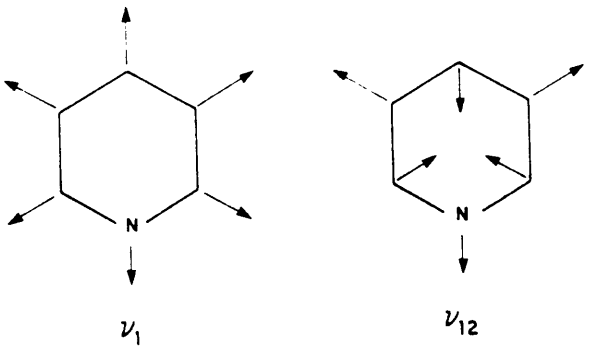

N bonds in the absence of any Jahn-Teller effect. The $NiCl_2py_4$ complex has π-bonding which stabilizes the Ni-N bonds. In $CuCl_2py_2$, despite Jahn-Teller effects, π-bonding is more important than in $NiCl_2py_2$ with the result that stronger Cu-N bonds are formed.

The intensity of ν_{12} was already shown to be very sensitive to isotopic substitution, and this has been explained in terms of the C-D masses which are virtually equal to that of the N-atom, causing the change in the molecular volume to be very small. The ratios of the intensities $\frac{I\nu_{12}}{I\nu_1}$ are graphically represented against ν_s(Ni-N) for $Ni(py)_2Cl_2$ in figure 3.11 and it is clearly evident that a pressure-dependent Fermi resonance also contributes to the intensity of ν_{12} at higher pressures and that it no longer largely depends on the strength of the M-N bond only. Fermi resonance is further proved to be important in figure 3.12 depicting the frequency

separation ν_{12}-ν_1 which is graphically represented against the pressure in kbar for $Ni(py)_2Cl_2$. In the case of $Zn(py)_2Cl_2$, a plot of $\frac{I\nu_{12}}{I\nu_1}$ against the pressure in kbar demonstrates the phase transition which occurs in the compound at $\approx$ 10 kbar rather well (figure 3.13).

The frequency of ν_1 has been used in the past to determine the type of adsorption of pyridine on a surface and it was for example established that ν_1 at 989 cm^{-1} of adsorbed pyridine on alumina surfaces represents a physisorbed species, at 998 cm^{-1} it represents a H-bonded interaction and at 1017 cm^{-1} a Lewis-bonded pyridine is obtained[44,105]. The significant upwards shift in ν_1 upon coordination is therefore in accordance with these values.

The pressure dependences of the internal modes of $Ni(py)_4Cl_2$, $Ni(py)_2Cl_2$ and $Zn(py)_2Cl_2$ are shown in figure 3.14 and those of the main C-H stretching modes in figure 3.15. The only evidence of the existence of hydrogen bonds involving C-H bonds of pyridine was found in the case of the prominent C-H component at 3068 cm^{-1} in $Ni(py)_4Cl_2$. This band shifts downwards upon an increase in the sample pressure (figure 3.15) and therefore represents a slight weakening of one of the C-H bonds upon the concomitant strengthening of the C-H—π or C-H—Cl hydrogen bonds. However, very little can be concluded about the exact nature of these hydrogen bonds from the high-pressure Raman results, in other words, whether there are C-H—π or C-H—Cl interactions.

In $NiCl_2py_4$ indications were found of a weakening of one of the C-H bonds with pressure. The origin of the hydrogen bonds responsible for this weakening could be either C-H—π bonds or C-H—Cl interactions. In deciding which of these are primarily responsible for the weakening of a

C-H bond with the concomitant increase in the strength of the hydrogen bond concerned, a few facts regarding the bonding in the pseudo-octahedral $NiCl_2py_4$ must be considered first.

The undistorted $NiCl_2py_4$ of D_{4h}-symmetry in the "free" state possesses the stereochemical arrangement which allows d_π-electron delocalization between the metal ion orbitals and the π-electrons of the pyridine rings[78]. Such an interaction will be controlled by the d_π-electron delocalization from the nickel ion to the π^* orbitals of the coordinated pyridine molecules. Octahedral complexes of Ni(II) are commonly found; this is, however, not so with mixed complexes of general formula NiX_4Y_2 where X is a stronger ligand than Y[78]. The energy change associated with conversion of a diamagnetic, square planar NiX_4^{+2} complex to a paramagnetic "octahedral" complex $NiCl_2py_4$ is > 0[78]. It is therefore clear that the complex $NiCl_2py_4$ must be stabilized in order to exist at all and this can possibly be achieved by d_π-electron delocalization.

It can be noted that the Ni-N symmetric stretching mode occurs at 207 cm^{-1} in $NiCl_2py_4$, and this is significantly higher than the 188 cm^{-1} in $NiCl_2py_2$ and for that matter, the corresponding ones in $ZnCl_2py_2$ and $CuCl_2py_2$[47]. Some other unique features in the Raman spectra of $NiCl_2py_4$ compared to those of $ZnCl_2py_2$ include the following: ν_1 occurs at 1011 cm^{-1} in $NiCl_2py_4$ compared to 1017 cm^{-1} in $NiCl_2py_2$ and 1023 cm^{-1} in $ZnCl_2py_2$. ν_{6a} Occurs at 627 cm^{-1} in this pseudo-octahedral complex compared to 635 cm^{-1} in $NiCl_2py_2$ and 646 cm^{-1} in $ZnCl_2py_2$. The C-C ring stretching mode, ν_{8a}, occurs at 1602 cm^{-1} in $NiCl_2py_4$. ν_{8b} Occurs at 1570 cm^{-1}, which is lower than the corresponding ones in pyridine, $NiCl_2py_2$ and $ZnCl_2py_2$; the same applies to ν_{9a}, the in-plane H-bending mode at 1217 cm^{-1}. An-

other in-plane H-bending mode, ν_{15}, occurs at 1142 cm^{-1} in $NiCl_2py_2$ and 1150 cm^{-1} in pyridine. It must therefore be concluded that the C-C bonds in the pyridine rings must be weaker in $NiCl_2py_4$ than in the other complexes. (The same can most probably be said of a complex like $CuCl_2py_4$[55]. However, because of its almost spontaneous decomposition to $CuCl_2py_3$, its high-pressure Raman spectra could not be studied in the present investigation. It was evident in preliminary measurements that both $CuCl_2py_3$ and $CuCl_2py_4$ were present in the diamond anvil cell.) The π-electron density of an aromatic ring such as benzene and pyridine is reflected by the frequencies of modes such as the ring breathing mode ν_1 and the C-C stretching modes ν_{8a} and ν_{8b}. From the above mentioned evidence it is clear that the π-electron density of the pyridine rings in $NiCl_2py_4$ is less than that in complexes such as the tetrahedral $ZnCl_2py_2$ and polymeric octahedral $NiCl_2py_2$.

It was previously found, in the case of $CuCl_2py_4$ dissolved in protic solvents, that the d_π-electron delocalization within the complex and the H—π type of interaction of the complex with the protic solvent mutually enhance each other. It is therefore reasonable to assume that if the d_π-electron delocalization within $NiCl_2py_4$ is enhanced at higher pressures that H—π interactions must also occur in the solid state. The fact that one of the C-H stretching modes shows a red shift upon compression, seems to support the assumption that this interaction could be of the C-H—π type, either inter- or intramolecular.

It is possible that this distorted octahedral complex is stabilized by C-H—π interactions, thereby enhancing the dπ-electron back-donation from the central nickel ion, as is the case in $Cu(py)_4Cl_2$[55]. The Ni-N force

constant is higher in $Ni(py)_4Cl_2$ than in $Ni(py)_2Cl_2$ and is also higher than the corresponding M-N ones in $Zn(py)_2Cl_2$, $Cd(py)_2Cl_2$ and $Cu(py)_2Cl_2$.

The pressure dependences of ν_1 in the complexes are also significantly higher than $\frac{d\nu_1}{dp}$ in solid pyridine, once again demonstrating the effect of an increasing M-N bond strength (at higher pressures) on the frequency of this band. On the other hand, $\frac{d\nu_{12}}{dp}$ in solid pyridine is significantly lower than the corresponding ratio's in the complexes. The significant difference in the pressure dependence of ν_{12} between pyridine and pyridine-d_5 has already been discussed[106]. This has been ascribed to the trigonal symmetry of this mode in which the N atom and two C-H groups undergo breathing vibrations out-of-phase with the other three C-H groups (figure 3.10). When the hydrogen atoms are replaced by deuterium atoms, the masses of N and C-D are almost equal and the change in molecular volume becomes very small. The same argument seems to hold in the case of an increasingly stronger bond between N and the metal ions, causing the molecular volume to be likewise small and thereby explaining the small pressure dependence of ν_{12}, particularly in the case of the more strongly bonded pyridine molecules in $Zn(py)_2Cl_2$ ($\frac{d\nu_{12}}{dp} = 0.10\frac{cm^{-1}}{kbar}$) and $Ni(py)_2Cl_2$ ($\frac{d\nu_{12}}{dp} = 0.18\frac{cm^{-1}}{kbar}$).

These results can be compared and contrasted with those obtained on chemisorbed pyridine as far as the nature of bonding and the molecular geometry are concerned, where it is a well-known fact that pyridine can π-bond to eg. the surface of Ag(III) and consequently lie flat, while it can also nitrogen-lone-pair bond at higher chemisorption coverages. It has been observed that ν_1 is selectively enhanced for chemisorbed pyridine[23]. At higher exposures ($\approx$20L, L=layers) ν_{12} becomes observable and at even higher exposures (>44L) ν_1 and ν_{12} are almost equal in intensity[23]. In

other words a strong mode selective enhancement is dependent on the orientation of the molecule with respect to the surface. In the case of bulk solid pyridine, where surface charge modulation at the surface is not a factor, ν_{12} has an intensity which is almost equal to that of ν_1. In complexes such as $Ni(py)_4Cl_2$ and $Zn(py)_2Cl_2$, however, it is of much lower intensity. As a matter of fact, a linear relationship exists between the intensity of ν_{12} and the strength of the M-N bond, irrespective of the structure of the complex.

3.4 CONCLUSION

The application of pressure on a coordination compound usually results in an increase in the coordination number about the metal ion concerned. The metal ion is also expected to assume the structure of the next higher homologue[40,85]. If these rules were to hold in the case of $ZnCl_2py_2$, then the phase change observed above 10 kbar should result in the formation of the polymeric octahedral type complex. This transition has occured. The dramatic changes in the lattice modes is good evidence for this.

Compression of a hydrogen bonded compound is expected to increase the hydrogen bonded contacts[85]. This should cause the C-H and Zn-Cl stretching modes to shift downward since they are weakened by the increasing strength of the H-Cl bond. This, however, has been found not be the case for $ZnCl_2py_2$, as one of the stretching modes shifts upward. The Zn-Cl bond length is thus shortened, resulting in a higher frequency Zn-Cl stretching mode. Similarly a reduction of intermolecular H-bonding resulted in shorter C-H bond lengths; and lower frequency C-H bending

vibrations. Careful analysis of the $ZnCl_2py_2$ structure will show that two types of hydrogen bonding exists within the structure, i.e. intermolecular and intramolecular H-bonding. Applying the above pressure-rule to the one type of H-bonding will necessarily exclude the compliance of the second type of H-bonding in the structure to the rule.

Since the only internal pyridine vibrations to undergo any dramatic changes at the phase transition are those mentioned above, it is thought that a reduction in the intermolecular Cl-H non-bonded interactions also takes place, accounting for the anomolous behaviour of one of the νZn-Cl stretching modes in the high pressure polymeric octahedral structure. If the phase transition includes some change in the strength of intermolecular H-bonds, then the profound effect that moisture has on the transition pressure can be easily understood.

Neither of the frequencies of the internal Raman modes observed in the complexes studied, nor their pressure dependences, reflect the structural differences between pseudo-tetrahedral $ZnCl_2py_2$ and polymeric octahedral $NiCl_2py_2$ complexes. No evidence could be found in these complexes of the existence of strong C-H—π or C-H—Cl hydrogen bonds.

It has been found that the $\frac{I\nu_{12}}{I\nu_1}$ ratio is a good indication of the strength of the M-N bond in these divalent metal complexes. However, no evidence of a relationship between type of structure and the Fermi resonance ratio exists.

It can therefore be concluded that the structure adopted by the MCl_2py_2 coordination compounds, namely pseudo-tetrahedral and polymeric octahedral, have little effect on the internal pyridine vibrations. This is in direct contrast to the strength of the M-N bonds which clearly influences

the intensities, frequencies and pressure dependences of the internal Raman bands.

Chapter 4

SINGLE CRYSTAL RAMAN POLARIZATION STUDIES ON $CdCl_2py_2$ AND $CuCl_2py_2$

4.1 INTRODUCTION

In the previous chapter it was found that $ZnCl_2py_2$ undergoes a phase transition at elevated pressures. On consideration of the pressure effects on such compounds[85,40], it was concluded that the new phase is polymeric octahedral (which includes tetragonally distorted structures). Further study into these MX_2py_2 polymeric octahedral compounds revealed a great deal of confusion in the assignment of the vibrations for such systems[35]. Molecular symmetries were postulated on the basis of M-Cl bridging and terminal vibrations only; where the assignments given to these bands were also uncertain as the vibrational studies did not always go

below 200 cm^{-1}[19]. Comparison of the high pressure $ZnCl_2py_2$ spectra with those of the polymeric octahedral compounds was thus made exceedingly difficult.

The d^{10} nature of Zn(II) and its next higher homologue Cd(II) increases the importance of vibrational spectra in the elucidation of the coordination geometry of $ZnCl_2py_2$ and $CdCl_2py_2$, as these complexes cannot be studied by magnetic or electronic spectral means.

Various methods of determining the different types of vibrations in the infrared and Raman spectra of polymeric octahedral MCl_2py_2 complexes have already been employed. These include isotopic labelling[36,37,38,80], ligand exchange[36], temperature studies[36] and some comparisons with analogous compounds. As far as isotopic dilution methods are concerned, some of the predicted frequency shifts are small. Since the spectra are complicated by the appearance of a great many modes, with coupling occurring between different vibrations of the same symmetry; inducing shifts in modes which are not strictly M-N vibrations; an unambiguous interpretation of these results is often not possible. The presence of large shifts can only be used to attribute some M-N character to a vibrational mode.

Assignment of the M-Cl vibrations based on the replacement of Cl with Br must also be regarded as tentative as the structures of MX_2py_2 complexes of the chlorides and bromides although sometimes similar, are not strictly isomorphous[59]. Temperature studies have been useful in resolving overlapping bands; so as to correlate the spectra with a particular type of structure. These studies generally require that the assignment of bands is already made. The possibility of the occurrence of a phase transition

on cooling must also not be overlooked. Comparison of the spectra of analogous compounds can be useful in that general vibrational regions can be identified. This is of particular importance in the M-Cl bridging vibrations. There is a wealth of infrared spectra available for such metal-chloride bridging systems[19,36,80,18,32], but very few Raman studies have been reported[37]. The non-coincidence of Raman and infrared spectra in non-centrosymmetrical complexes imply that the assignments made in the infrared cannot be directly correlated with the Raman spectra.

No polarized single-crystal Raman study on any of the polymeric octahedral MCl_2py_2 (M=Cr,Mn,Fe,Co,Ni,Cu,Cd,Hg) complexes has as yet appeared in the literature. Such studies can be used to ascertain directly the symmetry of the vibration, and together with the reliable vibrational studies already published, some degree of certainty as to the type and symmetry of the observed vibrations can be obtained. However, such a single-crystal Raman study has two prerequisites i.e. the thorough knowledge of the crystal structure of the complex in question; and the deduction of the total number of vibrations expected for the polymeric octahedral structure. The methods used in the derivation of the vibrational modes will be described in the next section.

The choice of the $CdCl_2py_2$ and $CuCl_2py_2$ complexes for polarized single-crystal Raman study was based on the following :

a) The crystal structures of both complexes have already been published[71,63].

b) Generally it has been found difficult to obtain single crystals in the MCl_2py_2 polymeric octahedral series[59]. It was possible to grow needle-shaped crystals for both $CdCl_2py_2$ and $CuCl_2py_2$.

c) The 4880Å excitation line of the Ar ion laser could be used for both of these complexes to give reasonable Raman spectra. Since most of the polymeric octahedral MCl_2py_2 complexes are highly coloured, it is generally difficult to obtain good Raman spectra for this series of complexes.

d) The $CdCl_2py_2(d^{10})$ is expected to give the spectrum closest to that of a postulated polymeric octahedral $ZnCl_2py_2$ complex. The $CuCl_2py_2$ on the other hand is a prime example of a tetragonally distorted polymeric octahedral complex. Differences between the $CdCl_2py_2$ and $CuCl_2py_2$ vibrational spectra should arise only from the differences in bond strength of the two metal ions; resulting in slight shifts in the vibrations; and from the distortion of the M-Cl bridge in the $CuCl_2py_2$ complex; as both structures are monoclinic with space group $P2_1/n$ and are thus isomorphous. This isomorphism can be used to directly compare the vibrations of the $CuCl_2py_2$ and $CdCl_2py_2$ complexes.

4.2 CRYSTAL STRUCTURE

Both $CuCl_2py_2$[63] and $CdCl_2py_2$[71] are monoclinic and belong to the space group $P2_1/n$ (C_{2h}^5) with Z=2 and two chains present in the primitive unit cell. The unit cell and atomic parameters are given in table 4.1.

The molecular structures are polymeric octahedral with the octahedra around the metal linked via Cl atoms to give polymeric octahedral chains, see figure 4.1.

The $CuCl_2py_2$ has a tetragonally distorted polymeric octahedral structure arising from two Cu-Cl bond lengths in the chain.

Table 4.1:

	$CdCl_2py_2$	$CuCl_2py_2$
a	17.78	16.97
b	8.67	8.56
c	3.81	3.85
β	91.6°	91.98°

	x	y	z	x	y	z
M	0	0	0	0	0	0
Cl	1.3957	−1.2069	1.9400	1.3330	−1.2207	1.4676
N	1.5504	1.7661	0.0876	1.3576	1.4757	0.0654

Figure 4.1:

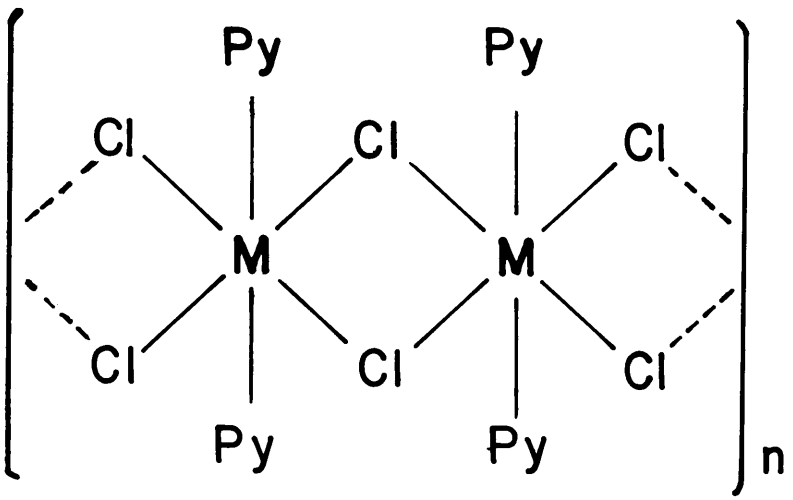

4.3 RAMAN TENSORS

The Raman tensors for "free" molecules can be used to determine the relative intensities of the internal modes of the molecule within the crystal. For such non-polar skeletal modes the Raman tensors are represented by[60,61]:

$$\alpha_0\left[S_\ell^{(P)}\right] = \sum_{k=1}^{N_{M_S}^{PC}}\left[a_{j\ell k}T_k^{+}\alpha(Q_{jk})T_k\right] \tag{4.1}$$

where: $S_\ell^{(P)}$ = symmetry coordinates of the reproducible representation $\gamma^{(P)}$ of the unit cell group.

$N_{M_s}^{PC}$ = number of ions or molecules of M_s type in the primitive cell (PC).

Q_{jk} = normal modes

$a_{j\ell k}$ = coefficients of $S_\ell^{(P)}$ expressed as a linear combination of Q_{jk}.

T_k = quasi-unitary matrix giving the relative orientation of the axes $(x,y,z)_k$ of the k^{th} molecule of ion with respect to the crystal axes.

$\alpha(Q_{jk})$ = Raman tensor of the non-polar mode Q_j of the k^{th} ion or molecule.

and for polar internal modes by:

$$\alpha_0\left[S_\ell^{(P)}\right] = \sum_{k=1}^{N_{M_S}^{PC}}\left[a_{j\ell k}T_k(R_x,R_y,R_z)_{jk}\xi_{jk}^{i}T_k\right] \tag{4.2}$$

where: ξ_{jk}^{i} = polarization vectors (assumed to be orthogonal)

$a_{j\ell k}$ = coefficients of $S_\ell^{(P)}$ expressed as a function of the direction of ξ_{jk}.

R_x, R_y, R_z = polar Raman tensors in the point group P_{M_s} of the ion or molecule.

The transformation matrix T for a molecule in the primitive unit cell of the crystal can be obtained from the equation[61]:

$$T_k = (r^+ r)^{-1} r^+ R_k \tag{4.3}$$

where r = 6×3 matrix representing the $4Cl^-$ and two pyridine groups (regarded as a point mass) in the ideal $MCl_2Cl'_2py_2$ molecule.

R_k = 6×3 matrix giving the coordinates of the k^{th} $MCl_2Cl'_2py_2$ unit in the crystal.

r^+ = transpose of r.

In the crystal structures of both $CdCl_2py_2$ and $CuCl_2py_2$, the pyridine molecules are tilted $\approx 10°$ from the crystal y-axis; and the crystallographic z-axis is found in the M-Cl plane, connecting the metal atoms. Thus the "ideal" structure given in terms of the free $MCl_2Cl'_2py_2$ octahedral unit is given in figure 4.2.

The bond lengths and bond angles for the two complexes are given by:

	$CdCl_2py_2$	$CuCl_2py_2$
$M-Cl$	2.65	2.298, 3.026
$M-N$	2.35	2.004
angles	90°	90°

Figure 4.2:

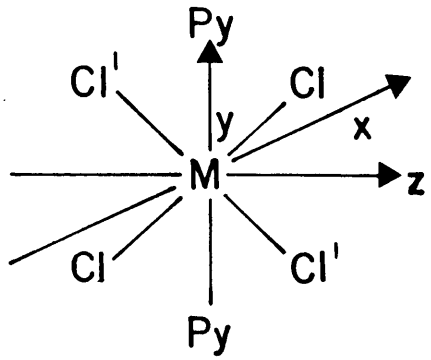

From figure 4.2, the idealized positional matrices are given by:

$$\begin{pmatrix} 0 & 0 & 0 \\ 1.87 & 0 & 1.87 \\ -1.87 & 0 & 1.87 \\ -1.87 & 0 & -1.87 \\ 1.87 & 0 & -1.87 \\ 0 & 2.35 & 0 \\ 0 & -2.35 & 0 \end{pmatrix} \quad \text{and} \quad \begin{pmatrix} 0 & 0 & 0 \\ 2.66 & 0 & 2.66 \\ -2.66 & 0 & 2.66 \\ -2.66 & 0 & -2.66 \\ 2.66 & 0 & -2.66 \\ 0 & 2.00 & 0 \\ 0 & -2.00 & 0 \end{pmatrix}$$

for $CdCl_2Cl'_2py_2$ and $CuCl_2CL'_2py_2$ respectively.

Normalization of these matrices yields:

$$r = \begin{pmatrix} 0 & 0 & 0 \\ 0.707 & 0 & 0.707 \\ -0.707 & 0 & 0.707 \\ -0.707 & 0 & -0.707 \\ 0.707 & 0 & -0.707 \\ 0 & 1 & 0 \\ 0 & -1 & 0 \end{pmatrix}$$

$$\text{and thus} (r^{+}r)^{-1} = \begin{pmatrix} 0.5 & 0 & 0 \\ 0 & 0.5 & 0 \\ 0 & 0 & 0.5 \end{pmatrix}$$

The coordinates of the atoms in the "real" primitive unit cell of $CdCl_2py_2$ and $CuCl_2py_2$ are given below:

$CdCl_2py_2$			$CuCl_2py_2$		
Positions	atom	Coordinates	Positions	atom	Coordinates
a	Cd	(0,0,0)	a	Cu	(0,0,0)
e	Cl	(x,y,z), $(\bar{x},\bar{y},\bar{z})$	e	Cl	(x,y,z), $(\bar{x},\bar{y},\bar{z})$
	x=1.39, y=-1.20, z=1.94			x=1.33, y=-1.22, z=1.47	
e	N	(x,y,z), $(\bar{x},\bar{y},\bar{z})$	e	N	(x,y,z), $(\bar{x},\bar{y},\bar{z})$
	x=1.55, y=1.76, z=0.08			x=1.36, y=1.46, z=0.06	

For the idealized $MCl_2Cl'_2py_2$ unit; the two Cl' atoms are not found in the primitive unit cell. Since the M-Cl chain is assumed to be symmetrical for the purposes of the calculation in both $CdCl_2py_2$ and $CuCl_2py_2$, the extrapolated vectors for the Cl'_2 atoms may be given by the vectors $(\bar{x},\bar{y},z)$ and $(x,y,\bar{z})$. From the coordinates given by the primitive unit cell, and the extrapolated vectors for the Cl'_2 atoms, R_k for $CdCl_2py_2$ and $CuCl_2py_2$ may be respectively derived where

$$R_k(CdCl_2py_2) = \begin{pmatrix} 0 & 0 & 0 \\ 1.39 & -1.20 & 1.94 \\ -1.39 & 1.20 & 1.94 \\ -1.39 & 1.20 & -1.94 \\ 1.39 & -1.20 & -1.94 \\ 1.55 & 1.76 & 0.08 \\ -1.55 & -1.76 & -0.08 \end{pmatrix} \text{and} R_k(CuCl_2py_2) = \begin{pmatrix} 0 & 0 & 0 \\ 1.33 & -1.22 & 1.47 \\ -1.33 & 1.22 & 1.47 \\ -1.33 & 1.22 & -1.47 \\ 1.33 & -1.22 & -1.47 \\ 1.36 & 1.48 & 0.06 \\ -1.36 & -1.48 & -0.06 \end{pmatrix}$$

It has been standard practice up to now to introduce a correction factor c[45] based on the calculated ratios of one of the edges of the "ideal" and "real" octahedra. However, normalization of the R_k matrices would have

the effect of normalizing all the edges of the 'real' octahedra so that both the 'real' and the 'ideal' octahedra have all their edges normalized to the same length. For $CdCl_2py_2$ and $CuCl_2py_2$, the normalized R_k^n matrices are given respectively by

$$\begin{pmatrix} 0 & 0 & 0 \\ 0.52 & -0.45 & 0.73 \\ -0.52 & 0.45 & 0.73 \\ -0.52 & 0.45 & -0.73 \\ 0.52 & -0.45 & -0.73 \\ 0.66 & 0.75 & 0.03 \\ -0.66 & -0.75 & -0.03 \end{pmatrix} \text{ and } \begin{pmatrix} 0 & 0 & 0 \\ 0.57 & -0.52 & 0.63 \\ -0.57 & 0.52 & 0.63 \\ -0.57 & 0.52 & -0.63 \\ 0.57 & -0.52 & -0.63 \\ 0.68 & 0.74 & 0.03 \\ -0.68 & -0.74 & -0.03 \end{pmatrix}$$

Substitution of the above matrices into equation 4.3 gives the following transformation matrices:

$$T_k(CdCl_2py_2) = \begin{pmatrix} 0.73 & -0.63 & 0 \\ 0.66 & 0.75 & 0.03 \\ 0 & 0 & 1.06 \end{pmatrix}$$

$$\text{and}T_k(CuCl_2py_2) = \begin{pmatrix} 0.81 & -0.74 & 0 \\ 0.68 & 0.74 & 0.03 \\ 0 & 0 & 0.89 \end{pmatrix}$$

The matrices of the polarizability tensors for the $MCl_2Cl'_2py_2$ unit with D_{2h} molecular symmetry are given by the following:

$$A_g = \begin{pmatrix} a & 0 & 0 \\ 0 & b & 0 \\ 0 & 0 & c \end{pmatrix} B_{1g} = \begin{pmatrix} 0 & d & 0 \\ d & 0 & 0 \\ 0 & 0 & 0 \end{pmatrix} B_{2g} = \begin{pmatrix} 0 & 0 & e \\ 0 & 0 & 0 \\ e & 0 & 0 \end{pmatrix} B_{3g} = \begin{pmatrix} 0 & 0 & 0 \\ 0 & 0 & f \\ 0 & f & 0 \end{pmatrix}$$

However, these matrices are calculated using the z-axis as the unique axis, i.e.

Interchange of the z and y axes gives:

$$A_g = \begin{pmatrix} a & 0 & 0 \\ 0 & c & 0 \\ 0 & 0 & b \end{pmatrix} B_{1g} = \begin{pmatrix} 0 & d & 0 \\ 0 & 0 & 0 \\ d & 0 & 0 \end{pmatrix} B_{2g} = \begin{pmatrix} 0 & 0 & e \\ e & 0 & 0 \\ 0 & 0 & 0 \end{pmatrix} B_{3g} = \begin{pmatrix} 0 & 0 & 0 \\ 0 & 0 & f \\ 0 & f & 0 \end{pmatrix}$$

By substitution of these tensors into equation 4.1; the Raman tensors $\alpha_0(S_\ell^{(P)})$ can be calculated for the internal modes of the $MCl_2Cl'_2py_2$ unit using the intensities obtained in the Raman spectra (eg. figure 4.3). The results are summarized in table 4.2 below.

Table 4.2:

	$CdCl_2py_2$	$CuCl_2py_2$
D_{2h}	C_{2h}	C_{2h}
	A_g	A_g
$\alpha_0(S_1^{A_g})$	$\begin{pmatrix} 0.53a+0.44b & -0.46a+0.50b & 0.02b \\ -0.46a+0.50b & 0.40a+0.56b & 0.02b \\ 0.02b & 0.02b & 1.12c \end{pmatrix}$	$\begin{pmatrix} 0.66a+0.46b & -0.60a+0.50b & 0.02b \\ -0.60a+0.50b & 0.55a+0.55b & 0.02b \\ 0.02b & 0.02b & 0.79c \end{pmatrix}$
	A_g	A_g
$\alpha_0(S_1^{B_{2g}})$	$\begin{pmatrix} 0.96d & 0.13d & 0.02d \\ 0.13d & -0.95d & -0.02d \\ 0.02d & -0.02d & 0 \end{pmatrix}$	$\begin{pmatrix} 1.10d & 0.10d & 0.02d \\ 0.10d & -1.10d & -0.02d \\ 0.02d & -0.02d & 0 \end{pmatrix}$
	B_g	B_g
$\alpha_0(S_1^{B_{1g}})$	$\begin{pmatrix} 0 & 0 & 0.77e \\ 0 & 0 & -0.67e \\ 0.77e & -0.67e & 0 \end{pmatrix}$	$\begin{pmatrix} 0 & 0 & 0.72e \\ 0 & 0 & -0.66e \\ 0.72e & -0.66e & 0 \end{pmatrix}$
	B_g	B_g
$\alpha_0(S_1^{B_{3g}})$	$\begin{pmatrix} 0 & 0 & 0.70f \\ 0 & 0 & 0.80f \\ 0.70f & 0.80f & 0.06f \end{pmatrix}$	$\begin{pmatrix} 0 & 0 & 0.61f \\ 0 & 0 & 0.66f \\ 0.61f & 0.66f & 0.05f \end{pmatrix}$

Thus for both $CdCl_2py_2$ and $CuCl_2py_2$; only two types of tensors are obtained i.e. the A_g and B_{2g} tensors which have A_g character under C_{2h} symmetry; and the B_{1g} and B_{3g} tensors which have B_g character under C_{2h} symmetry.

4.4 SELECTION RULES

There has been a great deal of controversy surrounding the treatment of the vibrations of the halogen-bridged chain polymers. The prediction of the vibrational spectra has been based on the "MCl_2py_2" octahedral monomer[80,95], and an attempt has also been made to approximate the structure to a particular line group symmetry[36]. The former approach ignores the fact that certain rotations in the monomer occur as chain modes in the polymeric compound. The line group analyses is generally found to be a good approximation of the structure of these chain systems[35], however, the choice of axes is not the same as that physically found in the crystal, i.e. the axes used in the determination of the Raman tensors of the crystal.

In the calculation of the polarizability tensors for both $CdCl_2py_2$ and $CuCl_2py_2$; D_{2h} symmetry was originally assumed. The resultant transformation matrix in effect then converted the "ideal" D_{2h} unit into the "real" positions as described by the crystal structures. Two kinds of tensors, A_g and B_g, belonging to C_{2h} symmetry were obtained. If the previously derived Raman tensors are thus to be used in the prediction of the vibrational modes, then these vibrational modes must be described in terms of a mapping of D_{2h} onto C_{2h} molecular symmetry.

In the line group analysis, assuming D_{2h} molecular symmetry, $\Gamma_{vib} = 2A_g + B_{1g} + B_{2g} + B_{3g} + 2B_{1u} + 2B_{2u} + 2B_{3u}$. If the point group is assumed to be C_{2h}, then $\Gamma_{vib} = 3A_g + 2B_g + 2A_u + 4B_u$. As can be seen, both D_{2h} and C_{2h} symmetries yield the same number of Raman and infrared active vibrations.

If a correlation between the two molecular symmetries D_{2h} and C_{2h} is carried out, and mapped onto the C_{2h} crystal symmetry, then the following is obtained:

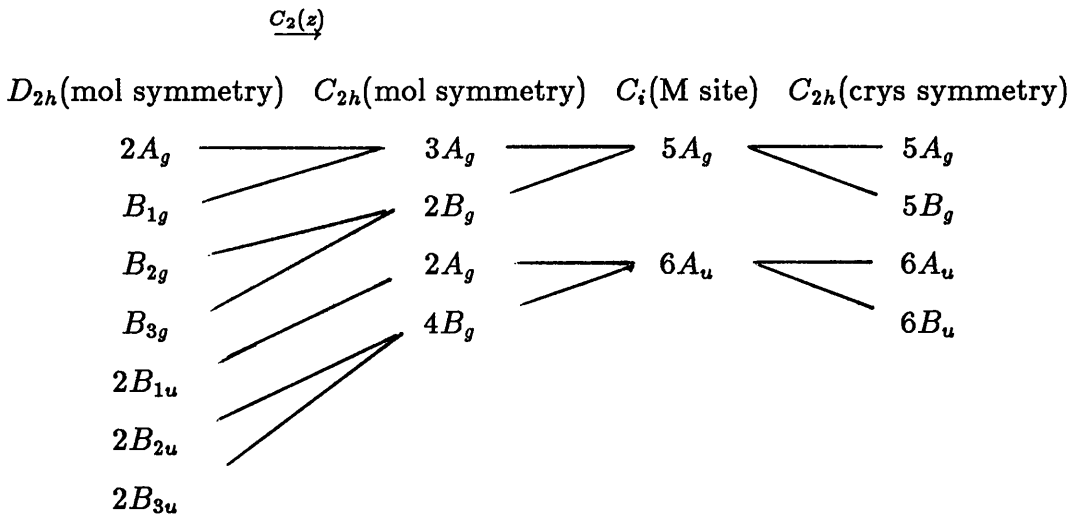

where $\Gamma[\nu(MCl_2)_n] = A_g(R) + B_g(R) + A_u(IR) + B_u(IR)$ are the in-plane chain modes; $\Gamma[\nu(MCl_2)_n = B_u(IR)$, are the out-of-plane chain modes; $\Gamma[\nu(M-N)] = A_g(R) + B_u(IR)$ are the M-N stretching modes, and $\Gamma[\delta(N-M-Cl)] = A_g(R) + B_g(R) + A_u(IR) + B_u(IR)$ are the N-M-Cl bending modes. All the Raman active modes will be further split into $A_g + B_g$; and all the infrared vibrations into $A_u + B_u$ components.

A factor group analysis[1] can also be done for the isomorphous $CdCl_2py_2$ and $CuCl_2py_2$ complexes. The results are tabulated below:

C_{2h}^5 no 14	A_g	B_g	A_g	B_g
N (total)	6	6	9	9
T_A	0	0	1	2
T	0	0	2	1
$R^*_{(z)}$	1	1	0	0
N (internal)	5	5	6	6
Raman activity	xx	xz		
	yy	yz		
	zz			
	xy			

where T_A = acoustic modes; T = translational modes;

$R_{(z)}$ = rotatory modes of chain; N (internal) = internal chain modes.

*Note: $R_{(y)}$ = rotation about the N-M-N axis which is equivalent to an in-plane $[MX_2]_n$ chain mode. Similarly $R_{(x)}$ = rotation about Cl—Cl axis which is equivalent to an out-of-plane $[MX_2]_n$ chain mode, and must thus be excluded in the factor group analysis.

It is thus obvious that the vibrations of the polymeric octahedral complexes can be described in terms of octahedral coordination about the metal atom, where adequate care is taken to exclude rotations which are in fact chain modes.

Further, a point group analysis yields:

Coordinates	Sites	A_g	B_g	A_u	B_u
$M-N(2)$	$C_1(e)$	1	1	1	1
$M-Cl(2)$	$C_1(e)$	1	1	1	1
$Cl-M-Cl(2)$	$C_1(e)$	1	$1^\dagger$	1	1
$N-M-N(2)$	$C_1(e)$	$1^\dagger$	1	1	1
$N-M-Cl(2)$	$C_1(e)$	1	1	1	1
$N-M-Cl(2)$	$C_1(e)$	1	1	1	1
		5	5	6	6

$\dagger$ = less one redundancy.

In the free chain a total of 10 Raman active modes could be observed. Since there are two chains present in each unit cell, some further correlation splitting of these modes might be expected, as has been found for $MnCl_2py_2$[37].

4.5 RESULTS

The crystals of both $CdCl_2py_2$ and $CuCl_2py_2$ are fragile and needle-shaped. In the Raman experiments on these crystals, it was found that using different incident directions yielded different intensities in equivalent experiments. This was found to be especially true for the $CdCl_2py_2$ crystals which were $\ll 1$ mm in diameter. The necessity of normalizing equivalent experiments and then using these adjustments to compare the inequivalent experiments can thus be understood. It is also obvious that the polarizations obtained must be regarded as a qualitative indication of the

symmetry of the vibration. Any quantitative calculations of the indices in the Raman polarizability tensors can only be regarded as approximations as these indices are directly proportional to the intensities of the vibrations, i.e. $I_{ij}^{observed} = (\text{matrix index})_{ij}^2$ for the index in the i^{th} row and j^{th} column of the Raman tensor.

If these vibrations are analyzed in terms of a D_{2h}-model, vibrations having $A_g + B_{2g}$ and/or $B_{1g} + B_{3g}$ symmetry are not observed to split into these components. If a C_{2h}-model is used, the great majority of vibrations predicted are observed in the Raman spectra for both $CuCl_2py_2$ and $CdCl_2py_2$. In other words, correlation splitting into A_g and B_g modes was obtained, especially in the case of the bridging M-Cl modes.

Table 4.3 gives the assignments and spectra of analogous compounds which have already appeared in the literature:

Table 4.3:

	$[\nu(M-Cl)]_n$	$\nu_s(M-N)$	$[\nu(M-Cl)]_n$	δ(N-M-X)	Rocking, Torsional and Lattice modes
$MnCl_2py_2$	207m	160w/157m	137s	123s 93s	59s 34sh 30sh 26s 16s
$FeCl_2py_2$	223m	191w	160s	143s 98s	72s
$NiCl_2py_2$	222m	197w	167s	147s 109s	52s
$CdCl_2py_2$	208m	-	130m	-	120m(unassigned)
$HgCl_2py_2$	204s	122m	162m	-	74w 60vw.

As can be seen, no Raman spectra for $CuCl_2py_2$ have appeared in the literature, and only three Raman bands have been reported for $CdCl_2py_2$ where only two of these were assigned[39].

A comparison of the $CuCl_2py_2$ and $CdCl_2py_2$ vibrations with those of the analogous compounds, together with the knowledge of the symmetry of the bands as obtained from the single crystal measurements yielded the following assignments under C_{2h} symmetry:

	A_g $[\nu(M-Cl)]_n$	A_g $\nu(M-N)$	B_g $[\nu(M-Cl)]_n$	B_g $\delta(N-M-Cl)$	A_g $\delta(N-M-Cl)$	unassigned modes
Cu_2py_2	$230cm^{-1}$	$194cm^{-1}$	$150cm^{-1}$	$122cm^{-1}$	$110cm^{-1}$	$168,73$ $37,31cm^{-1}$
$CdCl_2py_2$	$208cm^{-1}$	$150cm^{-1}$	$127cm^{-1}$	$116cm^{-1}$	$83cm^{-1}$	$66,45$ $29,24cm^{-1}$

4.6 LIGAND FIELD EFFECTS

A plot of the number of d electrons of the M^{II} ion against Raman frequency for the five assigned vibrations is given in figure 4.4. The closed shell $M^{II}_n(d^5)$ and $Cd_{II}(d^{10})$ ions give the lowest vibrations. This is to be expected since these metal ions do not bond as strongly to the ligands as the other metal ions, due to the greater amount of "shielding" of the nucleus.

These weaker bonds thus give rise to longer bond lengths and the vibrational energies are thus lower. In a given series of metal complexes, the wavenumbers of the vibrations should vary according to the Irving-Williams series[32], i.e. $Mn^{+2} < Fe^{+2} < Co^{+2} \leq Ni^{+2} < Cu^{+2} > Zn^{+2}$. A change from 1^{st} to 2^{nd} transition series is accompanied by a shift to a lower frequency. The complexes under consideration should thus show the trend $Mn^{+2} < Fe^{+2} < Ni^{+2} < Cu^{+2} \gg Cd^{+2}$ due to the much larger mass of Cd. From figure 4.4 the only exception to this trend is $CuCl_2py_2$. This is due to the Jahn-Teller induced tetragonal distortion found in Cu^{II} complexes.

Comparison of a and c in figure 4.4, which are both M-Cl stretching modes, and d and e, which are both N-M-Cl bending modes, shows that in both vibrations the A_g type vibration conforms to the Irving-Williams series whereas the B_g mode is found at a lower than expected wavenumber. In the totally symmetrical A_g mode the influence of the one longer M-Cl bond would be minimized as the modes involve both short and long M-Cl bonds to an equal extent, i.e. the vibrational energy is related to an average Cu-Cl bond length. This is not the case in an asymmetric vibration.

Although $CdCl_2py_2$ and $CuCl_2py_2$ have isomorphous structures, it has been found that $CuCl_2py_2$ displays far more splitting of bands than $CdCl_2py_2$. the vibrations displaying this splitting are the $B_g[\nu(M-Cl)]_n$, $B_g\delta(N-M-Cl)$ and the $A_g\delta(N-M-Cl)$ modes. $MnCl_2py_2$ was found to display some correlation splitting in the ν_s(M-N) mode. The $CuCl_2py_2$ complex did not show any splitting of the ν_s(M-N) mode. Generally, the effect of correlation splitting on the ν(M-X) is less than on ν(M-M) modes. The splitting thus obtained in the $CuCl_2py_2$ complex, since it involves only modes related to the M-Cl bond, must be directly coupled to the Jahn-Teller distortion mentioned earlier.

The vibrations, as assigned, thus obey the Irving-Williams series, with some understandable exceptions in the case of $CuCl_2py_2$; and the polarization results obtained are compatible with the symmetries of these vibrations. There are, however, some other bands occurring at lower wavenumbers which are unassigned, and are suspected to be the lattice modes.

4.7 CONCLUSION

It has been found that single crystal polarization studies can be used in studies on MCl_2py_2 polymeric octahedral complexes in order to determine the symmetry of the vibrations. Although the dimensions of the crystals made the calculations extremely difficult, nevertheless, meaningful polarization data were obtained. The treatment of the MCl_2py_2 complex in terms of a factor group and point group analysis[1] has been found to best describe the Raman spectra obtained in the single crystal studies. Due care must be taken to exclude any rotations which occur in the free "MX_4L_2" model, but are in fact chain modes in the MX_2L_2 model.

Chapter 5

A RAMAN STUDY OF THE DECOMPOSITION OF AMMONIUM METAVANADATE UNDER HIGH TEMPERATURES AND PRESSURES

5.1 INTRODUCTION

Ammonium metavanadate is the precursor to a number of industrially important vanadium compounds. It is well-known that NH_4VO_3 decomposes at high temperatures to give the catalyst V_2O_5. This thermal decomposi-

tion reaction has been studied by many investigators[13,14,15,50,81,84] and yet no consensus has been reached on the mechanism through which the reaction proceeds. It has however been established that the decomposition does not occur in a single step, as the intermediate $(NH_4)_2V_6O_{16}$ has already been identified.

The vibrational spectra of NH_4VO_3 at elevated pressures and temperatures have not been previously studied. Spectral information obtained in such studies could be useful in the elucidation of the decomposition mechanism of NH_4VO_3 to V_2O_5. This decomposition has been found to be strongly dependent on reaction conditions[13,14,15], and exclusion of oxygen from the atmosphere (as is the case in the high pressure diamond anvil cell), will lead to different products than those obtained by heating NH_4VO_3 in air.

In order to study the mechanism of the reaction by vibrational spectroscopic means, it is essential that the assignment of the bands occurring in the NH_4VO_3 spectra is known. Infrared and Raman spectra of NH_4VO_3 have already been published[67,68], and the results compared with those of the alkali metavanadates. These spectra have also been recorded at low temperatures[67,68], but most of the bands have only been tentatively assigned. Assignment of the lattice modes has also been made where the existence of oxygen bridged $(VO_3)_n^{-n}$ chains in the crystal has been ignored[67,68]. In this study, a factor group analysis will be used to determine the vibrations occurring in the $(VO_3)_n^{-n}$ chain.

An important facet in the structure of NH_4VO_3 is the strength and nature of the hydrogen bonding occurring in this system. Unique information can be obtained by monitoring these hydrogen bonds at elevated temper-

atures and pressures. Infrared studies of some isotopic diluted samples of NH_4VO_3 were also carried out as an aid in the assignment of some of the bands. These results in conjunction with the Raman spectra are used to elucidate some of the interesting bonding properties found in NH_4VO_3.

5.2 CRYSTAL STRUCTURE AND SELECTION RULES

The crystal chemistry of several metavanadates which have the pyroxene structure (figure 5.1), including that of the ammonium salt, have already been summarized[43]. Crystal structures of these metavanadates are characterized by a $(VO_3^-)_\infty$ chain in which vanadium is in the +5 oxidation state. This chain extends along the c-axis with the alkali metal or ammonium cations linking the adjacent chains[43]. The recommended atomic nomenclature for these metavanadates is summarized in figure 5.1. From the hydrogen-bonding arrangement given in this figure it is evident that the NH_4^+-ion is sixfold coordinated, since two single, and two bifurcated hydrogen bonds are formed with the surrounding anions[43].

From this arrangement of the NH_4^+-ion, it could be expected that the hydrogen bonds will have some dynamic character, i.e. be of a fluxional nature[53]. The normal N-H-O(2) hydrogen bonds have bond angles equal to 169° and 176° respectively, while the N-H-O(1) bifurcated bond has an angle equal to 153°. These H-bonds are thus all almost straight line bonds. The N-H-O(3) bifurcated H-bond is however highly bent, the angle being equal to 120°[43]. The question now arises whether this highly bent H-bond

will become asymmetric at elevated temperatures, i.e. whether the H-atom will become progressively more associated with a specific acceptor atom[53]. This implies that these latter H-bonds will be expected to become stronger at higher temperatures. Normal hydrogen bonds will on the other hand be expected to become weaker at higher temperatures (Appendix B).

NH_4VO_3 belongs to the orthorhombic space group $P_{bcm}(D_{2h}^n)$ with Z=4[43]. The N, V, O(1), O(2), H(1) and H(2) atoms all occupy the 4(d) sites, with a site symmetry of C_s. The O(3) atoms are situated on the 4(d) sites with a site symmetry of C_2 while the H(3) atoms occupy the 8(c) sites with C_1 symmetry.

If a line group of C_{2v} symmetry is assumed for the chains in NH_4VO_3[41], the 21 vibrations can be classified as $\Gamma_{int} = 7A_1 + 4A_2 + 4B_1 + 6B_2$. These modes include four V-O(3) stretching modes, ten bending modes, and three torsional vibrations. If the vibrations of both the NH_4^+ and VO_3^- groups in NH_4VO_3 are analyzed, the results given in table 5.1 are obtained[1]. Further discussion of these vibrations will be given when the spectral results are analyzed.

5.3 RESULTS AND DISCUSSION

The Raman and infrared spectra of NH_4VO_3 under ambient conditions are given in figures 5.2 and 5.3 respectively; and are summarized in tables 5.2 and 5.3 together with the assignment of the vibrations. The pressure and temperature dependencies of the bands are also given. It is immediately evident from figure 5.2 that the Raman-active NH_4^+ vibrations are extremely weak compared to the VO_3^- vibrations. This is however not the case in the

Table 5.1: The vibrations of NH_4VO_4 under Pbcm-D_{2h}^{11}-symmetry*

	A_g	B_{1g}	B_{2g}	B_{3g}	A_u	B_{1u}	B_{2u}	B_{3u}
VO_3^--internal	6	6	4	4	4	4	6	6
NH_4^+-internal	6	6	3	3	3	3	6	6
T-chains	1	1	1	0	0	1	1	1
T-NH_4^+	2	2	1	1	1	1	2	2
R-chain	0	1	0	0	0	0	1	0
R-NH_4^+	1	1	2	2	2	2	1	1
N-total	16	17	11	10	10	11	17	16

*T-transitional; R-rotational

infrared spectra, and is thus the reason for the inclusion of infrared spectra of isotopically dilute species (figure 5.4) in order to facilitate the assignment of the NH_4^+ modes.

5.3.1 The NH_4^+ modes.

Consider the "free" NH_4^+-ion of T_d symmetry. Four internal vibrations are predicted viz $\nu_1(A_1)$, $\nu_2(E)$, $\nu_3(F_2)$. Under P_{bcm} symmetry (D_{2h}''), ν_1 should split into $A_g(R)$, $B_{1g}(R)$, $B_{2g}(R)$, $B_{3g}(R)$, $B_{1u}(IR)$, $B_{2u}(IR)$ and $B_{3u}(IR)$ modes, and both ν_3 and ν_4 give $2A_{1g}(R)$, $2B_{1g}(R)$, $B_{2g}(R)$, $B_{3g}(R)$, $B_{1u}(IR)$, $2B_{2u}(IR)$ and $2B_{3u}(IR)$ as the N atom occupies a C_s site. Extensive correlation splitting of the fundamental NH_4^+ modes is thus expected. However, it is reasonable to expect that the site group splitting of T_d to C_s will predominate whereby ν_1 will remain single, ν_2 will split into two components, and ν_3 and ν_4 will split into three components each.

Table 5.2: The infrared and Raman bands of the lattice and internal VO_3^--modes in NH_4VO_3.**

	NH_4VO_3			ND_4VO_3		
ir	Raman	$d\nu/dT$	$d\nu/dP$	Raman	$d\nu/dT$	Assignment
	71(10)	-0.021	0.36	71(11)	-0.028	Three transla-
	79(8)	-0.021	0.56	76(8)	-0.017	lational and one
	105(5)	-0.018	-	102(4)	≈ 0	rotational mode
	123(3)	-0.075	-	120(4)	-0.050	of the $(VO_3^-)_n$
						chains.
	157(5)	-0.022	-	142(5)	-0.040	$\nu_T(NH_4^+$
	179(4)	-	-	165(4)	-	$\nu_T(NH_4^+$
199*	-	-	-	-	-	$\nu_T(NH_4^+$
	207(15)	0.028	0.11	208(11)	≈ 0	
	222sh	-0.045	≈ 0	220(11)	-0.030	δ(VOV)
242*	-	-	-	224(1)	-	
	258(9)	-0.050	1.1	255(10)	-0.044	
	308sh	-	-	322sh	-	
	321(7)	-	-	334(9)	≈ 0	$\delta(VO_2)$
	340(6)	-	≈ 0	360(6)	-	and $\nu_R(NH_4^+)$
	346sh	-	-	363sh	-	
362	-	-	-	267(3)	-	
	381(5)	-0.050	-	381(4)	-0.050	
502	494(14)	-0.010	0.38	491(13)	-0.010	ν(VOV)_sym
	540(2)	-0.060	-	535(2)	-	Combination
686	646(23)	≈ 0	0.83	643(20)	-0.010	ν(VOV)_asym
850	875sh	-	-	864sh	-	-
897	896(30)	≈ 0	0.23	892(15)	≈ 0	$\nu(VO_2)$_asym
917	927(100)	-0.010	0.18	925(100)	0.010	$\nu(VO_2)$_sym
	1045(1)	-	-	1047sh	-	-
	$\approx$ 1300	-	-	-	-	-

* These infrared bands were taken from [1].

** The relative intensities of the Raman bands are given between brackets.

Table 5.3: The vibrational frequencies of the NH_4^+-ions and their deuterated analogues in NH_4^+.

Assignment	Wavenumbers (cm^{-1})		
	ir	Raman	$d\nu/dT$
$\nu_3(NH_4^+)$	3193	3214	-0.573
$\nu_3(NH_3D^+)$	3183	-	
$\nu_3(NH_4^+)$	3077	3085	0.244
$\nu_3(NH_3D^+)$	2985	-	
$\nu_1(NH_4^+)$	2928	2960	0.21
$2\nu_4(NH_4^+)$	-	2817	
$2\nu_4(NH_4^+)$	2785	2796	
$\nu_3(ND_4^+)$	2362	2405	
$\nu_3(NHD_3^+)$	2355	-	
$2\nu_2(ND_4^+)$	2312	2311	
$\nu_3(NHD_3^+)$	2215	-	
$\nu_1(ND_4^+)$	2190	2216	
$2\nu_4(ND_4^+)$	-	2125	
$2\nu_4(ND_4^+)$	2095	2107	
$\nu_2 + \nu_6(NH_4^+)$	$\approx$ 2006	-	
$\nu_4 + \nu_6(NH_4^+)$	$\approx$ 1758	-	
$\nu_2(NH_4^+)$	1658	1655	-0.017
$\nu_2(NH_3D^+)$	1646	-	
$\nu_4(NH_4^+)$	-	1462sh	
$\nu_4(NH_4^+)$	-	1438	-0.045
$\nu_4(NH_4^+)$	1416	1416	0.005
$\nu_4(NH_3D^+)$	1408	1397	
$\nu_4 + \nu_6(ND_4^+)$	1343	1316	
$\nu_4(NH_3D^+)$	1283	1293	
$\nu_4(NH_3D^+)$	1257	$\approx$ 1240	
$\nu_2(ND_4^+)$	1188	1184	-0.030
$\nu_4(NH_3D^+)$	1120	1121	
$\nu_4(NH_3D^+)$	-	1115	
$\nu_4(ND_4^+)$	-	1080	
$\nu_4(ND_4^+)$	1072	1073	-0.027

In the Raman spectra of the N-H stretching mode region, assignment of individual components is difficult as the spectra are relatively weak. However, in the case of the $\nu_4(F_2)$ vibration, three components at 1416, 1438 and 1462 (sh) cm^{-1} are observed, which most probably represent the site group components of this mode. Deuteration yielded shifts to 1073 and 1080 cm^{-1}. In contrast to this the $\nu_2(E)$ vibrations was observed as a single band in both the infrared and Raman spectra. The vibrations occurring at 2796/2817 cm^{-1} can be assigned to $2\nu_4$; at 2960 cm^{-1} to ν_1 or ν_3; at 3085 cm^{-1} to $\nu_2 + \nu_4$ and the one at 3214 cm^{-1} to ν_3. These assignments are however very tentative. No splitting of the fundamentals ν_1 and ν_3 could be resolved in either the Raman or infrared spectra.

5.3.2 Isotopic dilution studies.

Vibrational spectroscopy, and in particular infrared spectroscopy of the isotopically dilute NH_3D^+ and NHD_3^+ ions has been a powerful tool in the elucidation of the structure of NH_4^+ ions in crystals[70]. This is because the vibrations of these species are not complicated by vibrational coupling between ν_1 and ν_3, for example, or Fermi resonance between vibrational levels ($2\nu_4$, $\nu_2 + \nu_4$, ν_1 and ν_3) as in the case of undeuterated or fully deuterated samples. (Appendix B). Since these NH_3D^+ and NHD_3^+ species are isotopically diluted, their intensities in the vibrational spectra are necessarily low, and samples usually have to be cooled in order to observe all the components. Instrumental limitations precluded such a low temperature study. The original intention of this work was to study the behaviour of the Raman vibrations of NH_4VO_3 under high pressures and temperatures.

With an effective symmetry of C_s for the NH_4^+ ions in NH_4VO_3; ν_1 of the NH_3D^+ species should split into C_s, C_s and $C_1(2)$ components[70]. The bending NH_4^+ mode of T_d-symmetry splits into ν_{4a} and ν_{4bc} for "free" NH_3D^+ groups, and the latter mode splits into six components under C_s symmetry[70]. The three components predicted with the three N-H bond distances of N-H(1):0.82Å, N-H(2):0.94Åand N-H(3):0.97Å(2 bonds)[43]. The NH_3D^+ bonds in the infrared spectra are shown in figure 5.4. There are two components at 3183 and $\approx$ 2985 (very broad) cm^{-1}. In the case of ND_3H^+, two components are evident at 2355 and 2215 cm^{-1} respectively. It can be assumed that these bands represent the very strong N-H-O(2) hydrogen bond, and the bifurcated N-H-O(1) and N-H-O(2) hydrogen bonds respectively. The NH_3D^+ bending mode ν_{4bc} is also split into two components occurring at 1283/1257 cm^{-1} in the infrared spectra and at 1293/1240 cm^{-1} in the Raman spectra.

Although the Raman spectra of the NH_4^+ modes are generally weak and broad, and the infrared spectra of the isotopically dilute samples could only be obtained at room temperature; most of the vibrations of the partially deuterated ammonium ions have been observed and are summarized in table 3. Resolution of all the components under ambient conditions is however not possible, and unambiguous conclusions regarding the structure of a compound studied by such methods can usually only be made if low-temperature results are available.

5.3.3 Hydrogen bonding in NH_4VO_3.

Several criteria have been postulated according to which the existence of hydrogen bonds can be confirmed in ammonium compounds from a study of their vibrational spectra. Two of the most popular criteria are that (i) hydrogen bonding is present if the combination modes $\nu_i + \nu_6$ (i = 2,4) involving the librational mode ν_6 of the NH_4^+ ions are observed in the infrared spectra; and (ii) if the antisymmetric bending mode $\nu_4(NH_4^+)$ is observed above 1400 cm^{-1}. (Appendix B). It has been pointed out[52] that the hydrogen bonds in ammonium halides with a coordination number of 6 or 12 will be highly dynamic and that it is unlikely in these cases that $\nu_i + \nu_6$ will be observed. Occurrence of the $\nu_i + \nu_6$ bands in the infrared spectra of ammonium compounds will thus not depend on the strength of the hydrogen bonds, but rather on the type of hydrogen bond formed. It has further been shown that the ammonium compounds can broadly be classified into two groups[52], namely one in which a volume-effect will predominate the hydrogen bonding according to the degree of compression of the ammonium ion in the crystal; and one in which the acceptor strength of the anion will predominate. Both of these types of hydrogen bonding will affect the ν_{4bc} vibration in a similar manner; ν_1 however will be expected to give an indication of the type of hydrogen bonding present. A plot of the frequencies of ν_1 vs ν_{4bc} will thus be separated according to the acceptor strength of the anion, the coordination number, and various other parameters[52].

In the case of NH_4VO_3 with a coordination number of 6, the fact that $\nu_i+\nu_6$ are easily identified at 2006 cm^{-1} ($\nu_2 + \nu_6$) and $\approx$ 1758 cm^{-1} (ν_4

+ ν_6) under ambient conditions, illustrates that the hydrogen bonds are not fluxional. It could be inappropriate to compare the ν_1 vs ν_4 plots for isotopically isolated species of the ammonium halides[52] with the results obtained for NH_4VO_3. However, if this is done, then the 1257 cm^{-1} (ν_4 of NH_3D^+) plot correlates with the ammonium halides where the anion acceptor strength dominates the hydrogen bonding, rather than the case in which the volume effect dominates. This conclusion is substantiated by the occurrence of the combination modes $\nu_i + \nu_6$ in the infrared spectra of NH_4VO_3. On the other hand, the 1283/2216 cm^{-1} pair indicates particularly strong hydrogen bonds, most probably corresponding to the almost straight line N-H(1)-O(2) and N-H(2)-O(2) hydrogen bond interactions (figure 5.1).

5.3.4 Temperature and pressure dependence of the Raman active NH_4^+ vibrations.

The temperature dependence of the Raman active NH_4^+ vibrations is given in figure 5.5. It is evident that ν_3 at 3214 cm^{-1} shifts downward (at a rate of -0,57 $cm^{-1}/°C$) on an increase in temperature, indicating an increase in the strength of the hydrogen bond represented by this vibration. It has previously been mentioned that an unambiguous assignment of modes in this frequency range is impossible. It can however be safely assumed that this highest-frequency vibration corresponds to the N-H(3) asymmetric stretching modes. This could mean that the H(3) hydrogen atom increases its association with one oxygen atom consequently increasing the strength of the particular hydrogen bond.

The other modes in this frequency range i.e. at 3085 and 2960 cm^{-1} shift marginally upward by 0.24 and 0.21 $cm^{-1}/°C$, respectively, as the temperature is increased. The bands representing the N-H(1) and N-H(2) vibrations thus behave normally at elevated temperature, i.e. the strength of the hydrogen bonding is decreased. It must be remembered that the vibrations in the N-H stretching frequency range are strongly coupled, leading to misinterpretation of the thermal behaviour of the vibrational modes. This is probably the reason why ν_3 of NH_4^+ at 2405 cm^{-1} in the Raman spectra does not have the same thermal behaviour as the 3214 cm^{-1} band in the NH_4VO_3 spectra. The $2\nu_2$ vibration occurs close to $\nu_3(NH_4^+)$ and are probably strongly coupled. Unfortunately, the isotopically dilute species NH_3D^+ and ND_3H^+ give rise to such weak features in the Raman spectra that their thermal behaviour could not adequately be monitored.

The two most intense bands in the ν_4 range also display interesting thermal behaviour. The band at 1416 cm^{-1} remains virtually unchanged while the 1438 cm^{-1} band shifts downward on an increase in temperature. Once again it is thus illustrated that the hydrogen bonding in the case of the weak bifurcated bonds increases (the 1416 cm^{-1} band), while the normal, approximately linear hydrogen bonds decrease in strength (the 1438 cm^{-1} band).

In high pressure experiments, an increase in pressure should bring about an increase in the strength of the hydrogen bonding for normal hydrogen bonds[85]. However, up to pressures of 8 kbar, these asymmetric bonding modes remained virtually unaltered.

5.3.5 Librational and translational modes of the NH_4^+ cation.

In addition to the internal modes of the NH_4^+ modes, librational and translational modes involving these cations can also occur. The R2(A′) librational mode under the site group symmetry C_s will split into $A_g(R) + B_{1g}(R) + B_{2u}(IR) + B_{3u}(IR)$ modes under D_{2h} symmetry, while both the $R_x(A'')$ and the $R_y(A'')$ modes will split into $B_{2g}(R) + B_{3g}(R) + A_u + B_{1u}(IR)$ giving rise to the total number of modes indicated in table 5.1.

From the combination modes $\nu_i + \nu_6$, a librational mode ν_6 is calculated to occur at 342-352 cm^{-1}. This vibrational mode, as shown above, is likely to split into R_x, R_y and R_z components under C_s site symmetry, and eventually into further components under D''_{2h} crystal symmetry. In the far infrared spectra of NH_4VO_3, ν_6 has been observed at 362 cm^{-1}, which shifted to 267 cm^{-1} upon deuteration[67]. Present measurements give $\nu_4 + \nu_6(ND_4^+)$ at 1343 cm^{-1} in the infrared spectra, yielding a value of 271 cm^{-1} for ν_6; which is in excellent agreement with the observed value. Neutron scattering results have indicated that two NH_4^+ librations occur at 371 and 308 cm^{-1} respectively[8], while NMR results show that they occur at 371 cm^{-1} (C_2-libration) and at 308 cm^{-1} (C_3-libration)[72]. If the limit of 1776 cm^{-1} and 1725 cm^{-1} of the broad feature assigned to $\nu_4 + \nu_6$ are assumed to represent the combination modes, then ν_6 is calculated to occur at 364 and 309 cm^{-1} respectively, which correspond very closely with the values obtained in the neutron scattering experiments.

If the literature values of 371 and 308 cm^{-1} are assumed for ν_6[8]; then empirical relationships give Ea values of $\approx$ 5.0 and $\approx$ 3.6 kcal/mol

respectively[82]. Correlations have been made between Ea and the frequencies of $\nu_3(NH_3D^+)$ and $\nu_4(ND_3H^+)$ and it is interesting to note that the correlations 3.6 kcal/mol vs 2355 cm^{-1} as well as 3.6 kcal/mol vs 1257 cm^{-1} show that the acceptor strength of the cation dominated in these approximately linear, normal hydrogen bonds. Correlations of 5.0 kcal/mol vs 2216 cm^{-1} and 5.0 kcal/mol vs 1283 cm^{-1} on the other hand indicate the presence of very strong hydrogen bonding. These observations once again prove that even though the ammonium ion in NH_4VO_3 has bifurcated hydrogen bonds, they are not largely dynamical in character.

The Raman bands in the spectral range 308-380 cm^{-1} show anomalous frequency shifts upon deuteration; which can only be explained in terms of a coupling of the NH_4^+ librational modes with the O-V-O bending modes. Furthermore, from figure 5.6 it is clear that the band at 320 cm^{-1} shifts upward above 120°C. This could be linked to an increase in the strength of the bifurcated hydrogen bonds, which would in turn thus also affect the O-V-O bending modes. This upward frequency shift is in direct contrast to the other modes in this frequency range, which shifts downward on an increase in temperature.

Table 5.1 predicts the presence of many NH_4^+ translational modes in the vibrational spectra of NH_4VO_3. Translational modes have been observed at 242 and 199 cm^{-1} in the infrared spectra, shifting to 224 and 192 cm^{-1} upon deutertion[67]. In this study, additional NH_4^+ translational modes have been observed at 179 and 157 cm^{-1} in the Raman spectra (table 5.2); which shift to 165 and 142 cm^{-1} on deuteration.

5.3.6 The $(VO_3)_n^{-n}$ modes.

The V-O stretching modes are given in table 5.1. These can be further subdivided into V-O bridging modes, i.e. $A_g(R) + B_{1g}(R) + B_{2u}(IR) + B_{3u}(IR)$; and two sets of V-O terminal modes having the same symmetries, i.e. $A_g(R) + B_{2g}(R) + B_{2u}(IR) + B_{3u}(IR)$.

When alkali metal vanadates are dissolved in water, it has been found that the $(VO_3)_n^{-n}$ chains remain intact[68], making possible an unambiguous assignment of the assymetrical and symmetrical stretching modes by means of polarization studies in the Raman spectra of these aqaeous solutions.

In the Raman spectra of NH_4VO_3, the symmetrical V-O bridging mode is observed at 494 $cm^{-1}(A_g)$ and the asymmetric mode is observed at 646 cm^{-1} (B_{1g}). An unusual aspect of these modes is the fact that the asymmetric mode is more intense than the symmetrical mode. These modes occur at 502 $cm^{-1}(B_{2u})$ and 686 $cm^{-1}(B_{3u})$ in the infrared spectra.

The frequencies of these vibrations are almost identical in the MVO_3 $(M = K^+, Rb^+, Cs^+, NH_4^+, ND_4^+)$ series. The V-O-N bridging modes must thus be very similar in this series. Now NH_4VO_3 has hydrogen bonded O(3) bridging atoms. Since the NH_4^+ vibrations are similar to those in the rest of the above MVO_3 series, the NH—O(3) hydrogen bond must thus be weak under ambient conditions.

In the Raman spectra of NH_4VO_3, the symmetrical V-O bridging mode is observed at 494 cm^{+1} (A_g) and the asymmetric mode is observed at 646 cm^{+1} (B_{1g}). An unusual aspect of these modes is the fact that the asymmetric mode is more intense than the symmetrical mode. These modes occur at 502 cm^{+1} (B_{2u}) and 686 cm^{+1} (B_{3u}) in the infrared spectra.

The V-O terminal bands occur at 927 cm^{+1} (A_g) in the Raman spectra and at 917 cm^{+1} and 897 cm^{+1} (B_{1g}) in the infrared spectra, while the asymmetric V-O terminal stretching modes occur at 896 cm^{+1} and 875 cm^{+1} (shoulder) in the Raman and 850 cm^{+1} in the infrared spectra.

The pressure dependence of these modes (figure 5.7) shows that the bridging V-O bonds are much more sensitive than the terminal V-O bonds. This is expected, since there are two kinds of bonds in one tetrahedron of the chain: i) those linking the oxygen atoms in the chain (1.803Å) and ii) the terminal oxygen bonds (1.640Åand 1.647Å) [43].

The d shell of the vanadium atom is split so that the three d_ϵ orbitals form a $d^3_\epsilon s$ hybrid with a tetrahedral configuration. The d^2_α orbitals may form π bonds about two of the σ bonds so that it is only natural to expect that the bands will behave differently upon compression. On the other hand, even though the bands in the tetrahedra differ considerably, it can be expected that in a covalently bonded system such as this one, the strain in bond angles will be much more readily tolerated than in the bond lengths[28].

The V-O bending modes however did not undergo other large changes in frequencies or in the splitting of bands. It is possible that the pressure dependence of the Raman bands are also influenced by the hydrogen bonding between the oxygen atoms and the ammonium ions. The terminal V-O stretches at 927 and 896 cm^{+1} were found to be much less pressure sensitive than the V-O bridging modes. Since these terminal V-O stretches shift upward by 0,23 (896 cm^{+1}) and 0,18 (927 cm^{+1})/kbar upon compression, any likely increase in the strength of hydrogen bonds causing negative

frequency shifts at elevated pressures is not sufficient to cause a substantial weakening of the V-O bonds.

Unfortunately a parallel pressure study on the N-H bands was not possible, as these were very weak in the high-pressure cell.

Chapter 6

EXPERIMENTAL

6.1 INSTRUMENTATION

The Raman spectra in chapters 2 and 3 were recorded on a Spex model 1403 instrument double monochromater. This was fitted with a wavenumber "Compudrive" and a photomultiplier tube with a GaAs photocathode, selected for photon counting, which was used to collect the photons. The instrument also had a spectrometer controller, a data acquisition monitor and a "Scamp" processor.

The Raman spectra for chapters 4 and 5 were recorded on a Z-24 Dilor Raman spectrometer. A Coherent Radiation model 90-5 Ar^+ laser was used to excite the spectra. Both the 488,0 and 514,5 nm lines were used.

High pressure Raman experiments were carried out by using a diamond anvil cell. A basic diagram of this cell is given in figure 6.1, while figure 6.2 shows the diamond anvils and gasketing in more detail.

Figure 3.11:

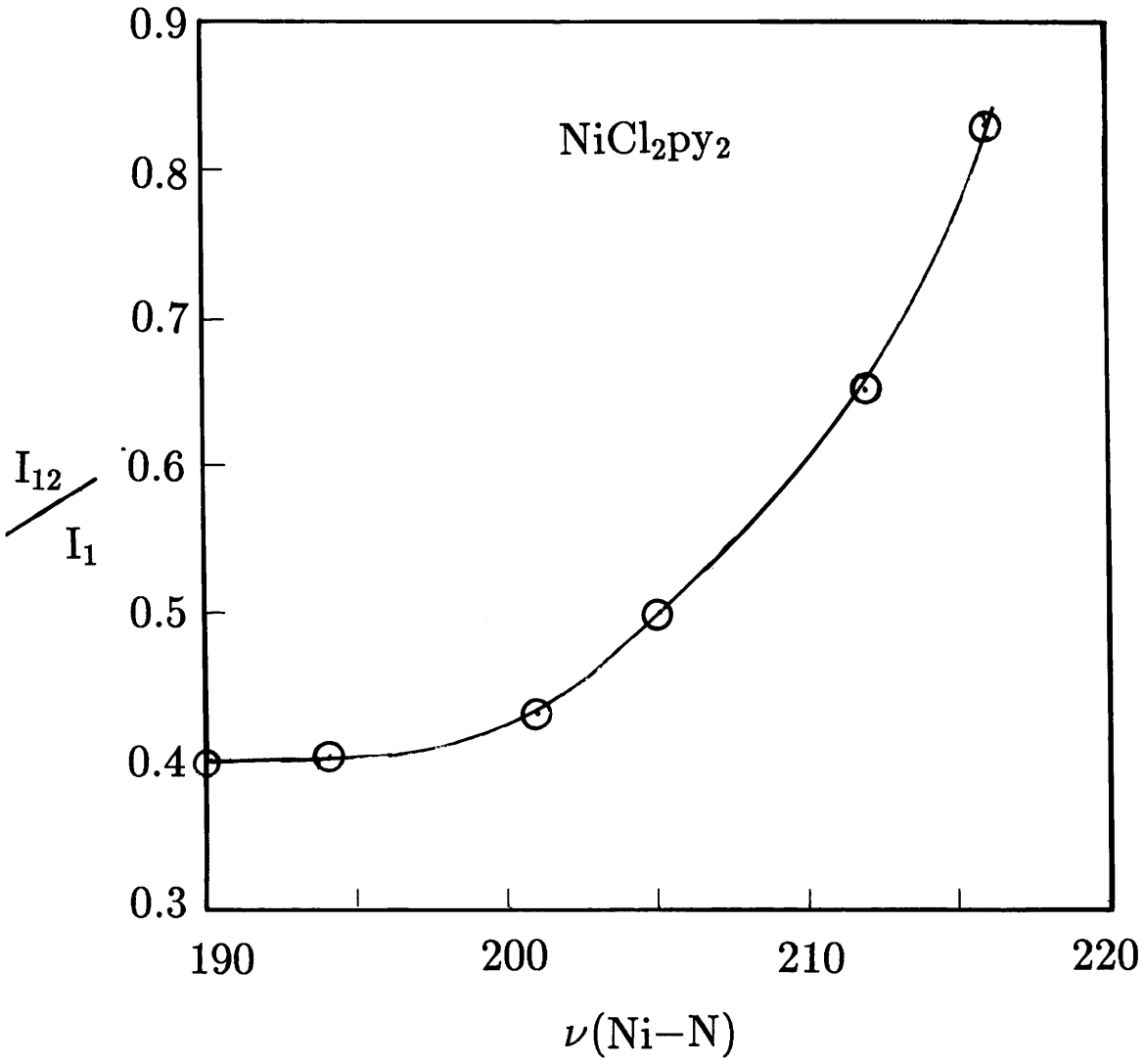

Figure 3.12:

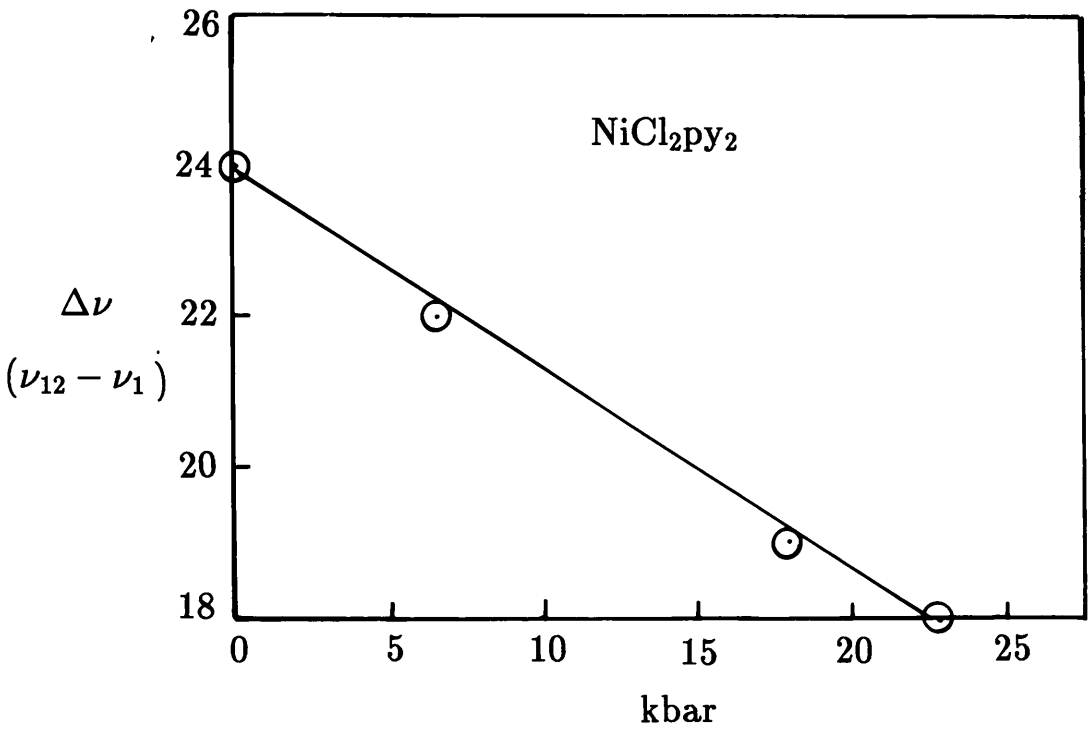

Figure 3.13:

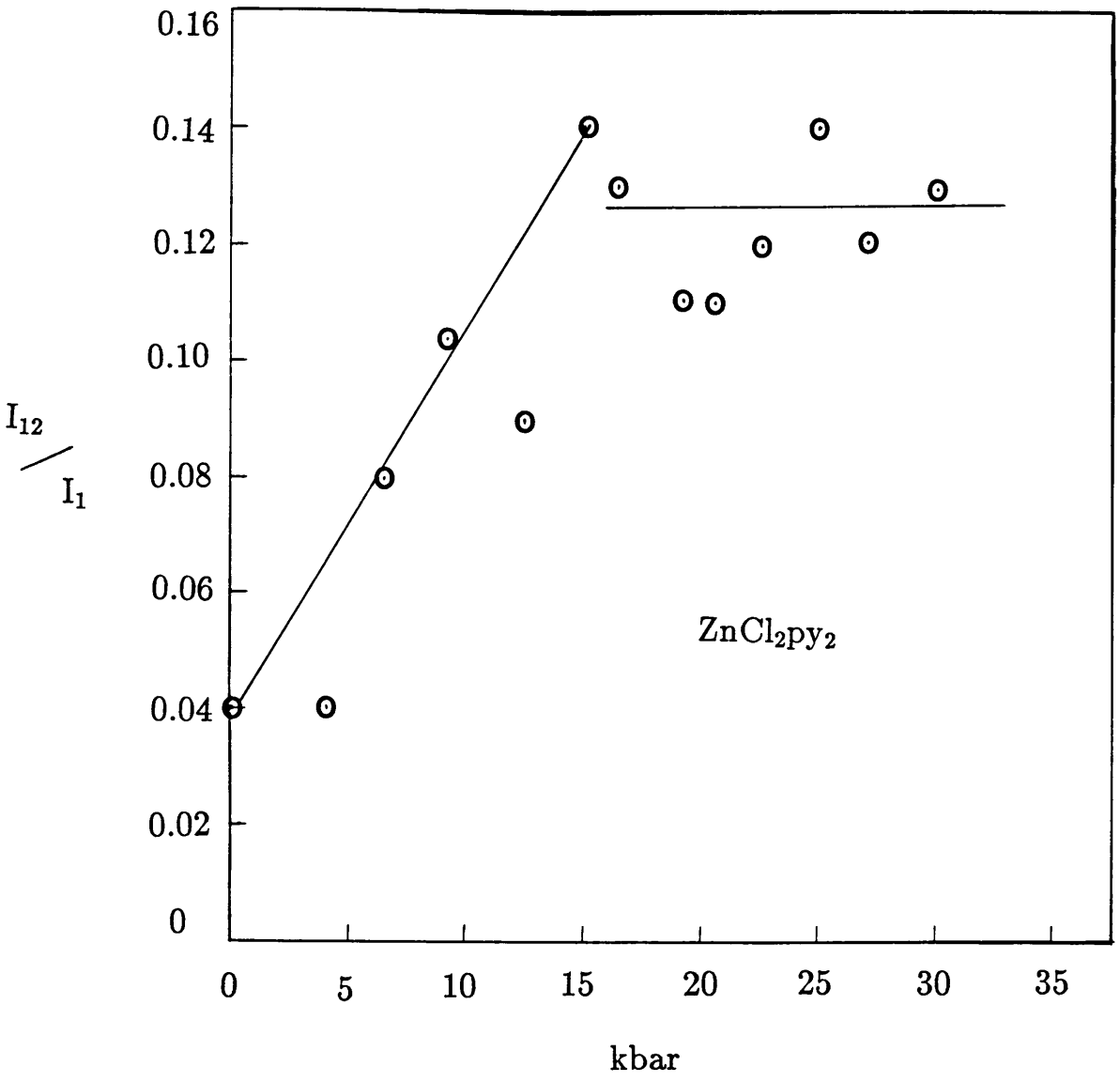

Figure 3.14:

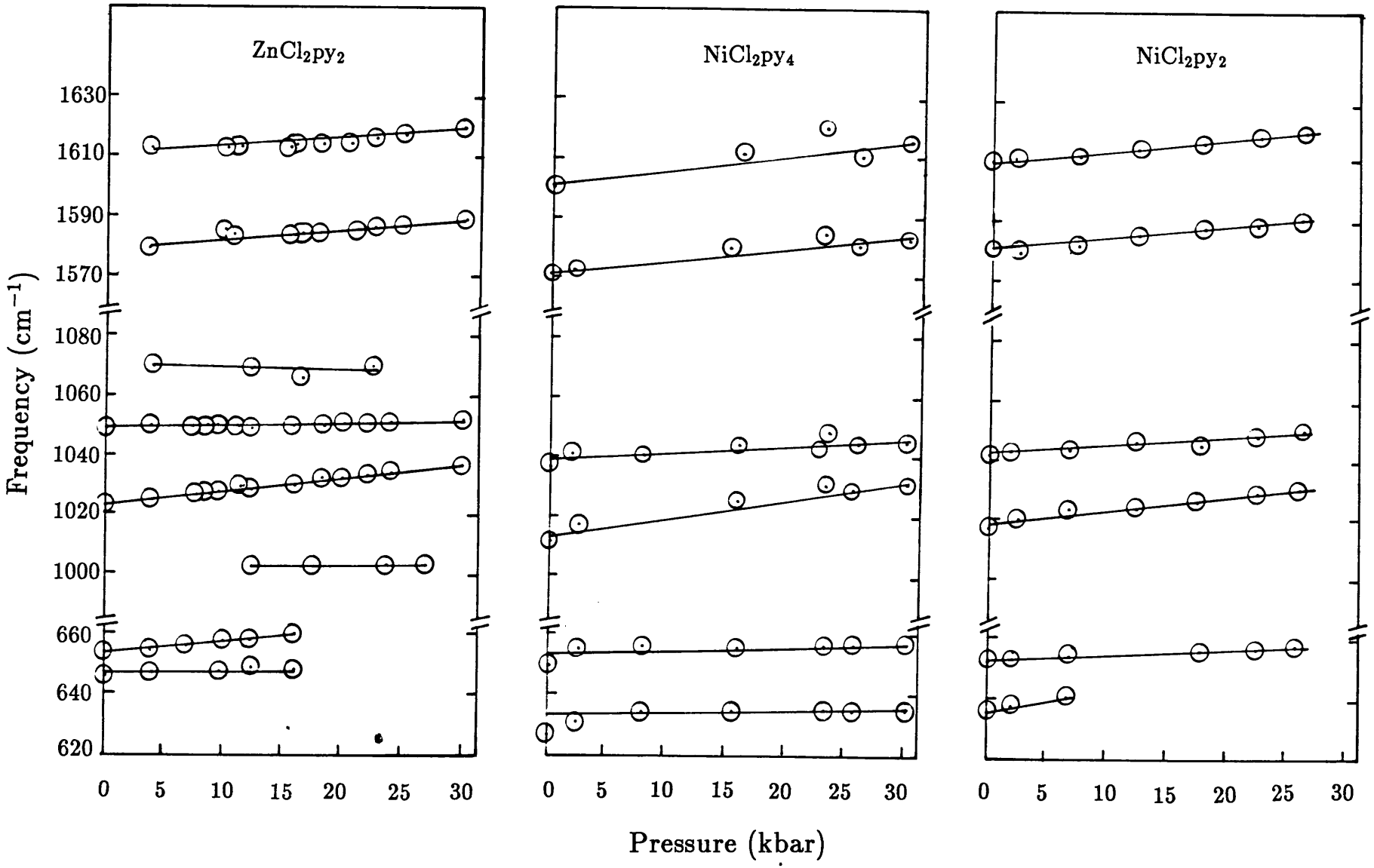

Figure 5.2: The Raman spectra of NH_4VO_3. The frequency ranges in which the N-H bonding and stretching modes occur are shown at increased intensities.

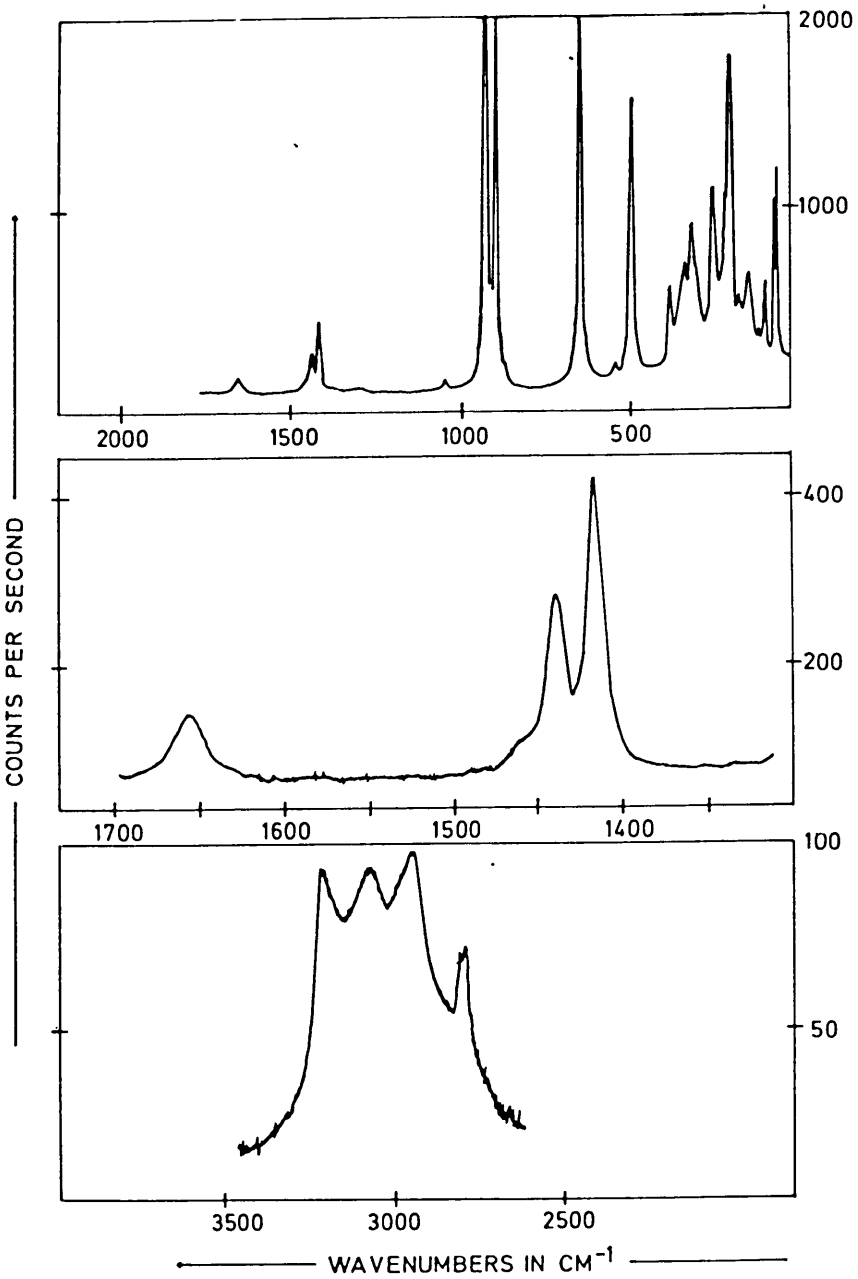

Figure 3.15:

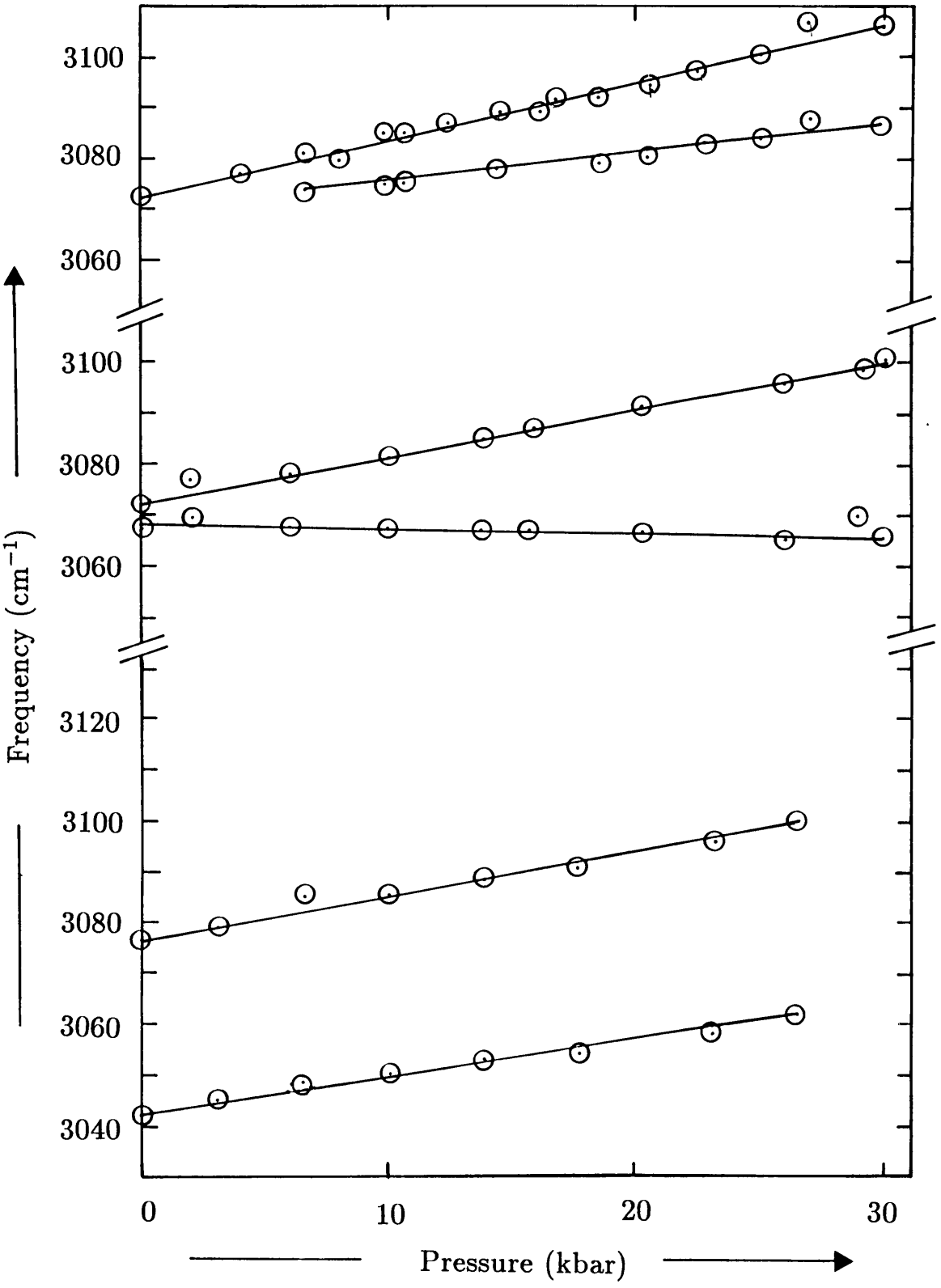

The variation in intensity of the Ag (Cd-Cl) stretching mode at 201 cm^{-1} with different polarizations in the Raman spectra

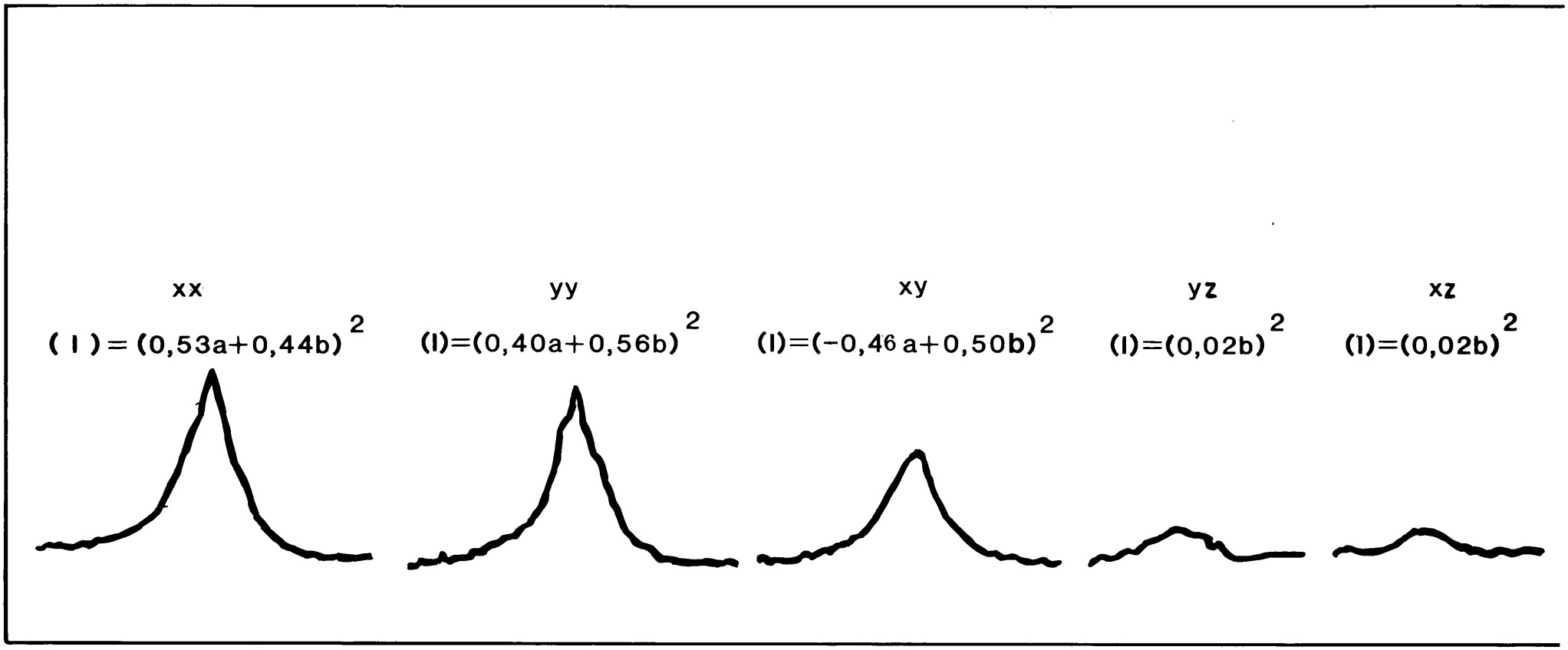

Figure 4.3:

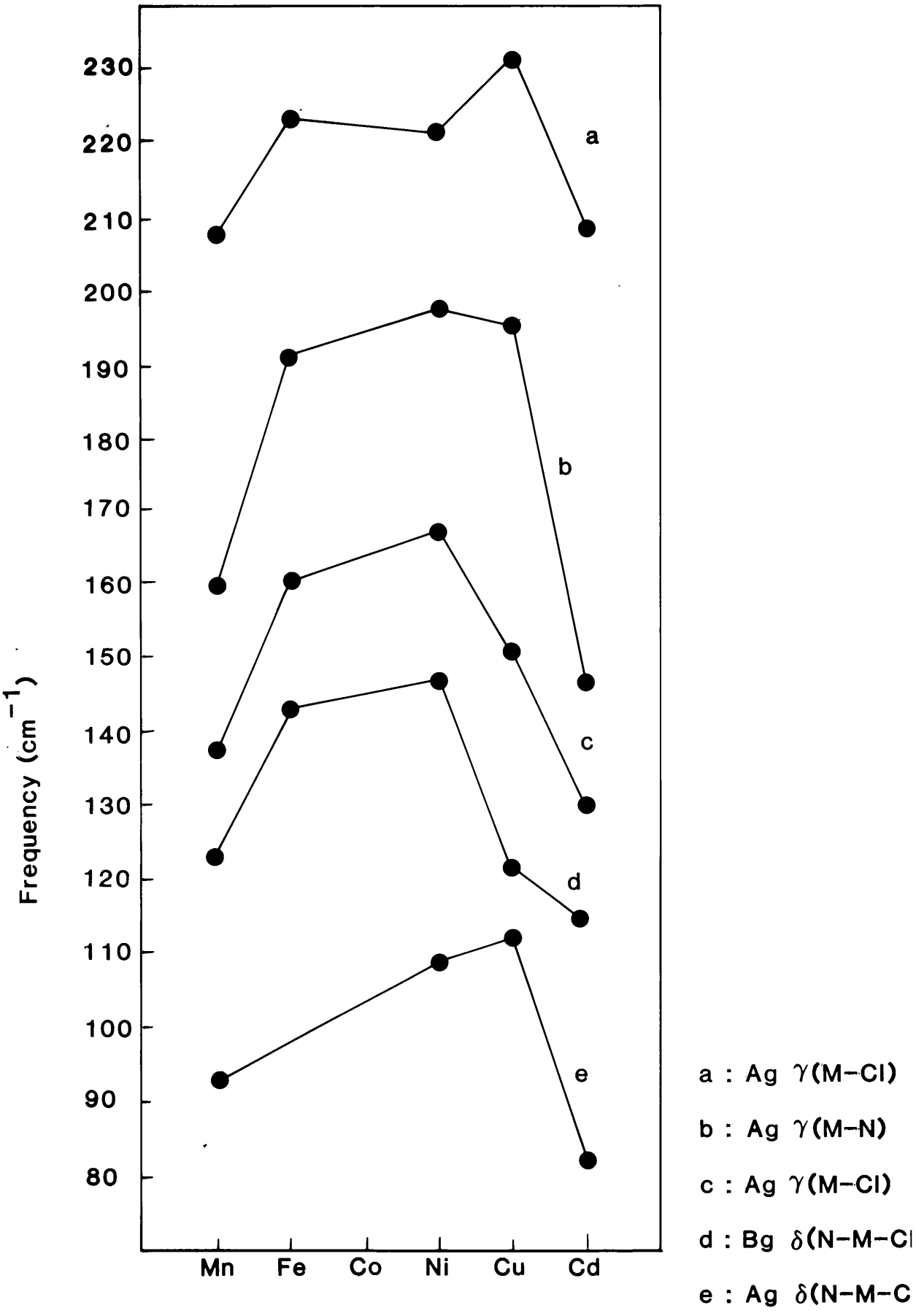

Figure 4.4: **Variation of $\gamma(cm^{-1})$ with change of metal in the MCl_2py_2 complex**

Figure 5.1: The Pyroxene structure showing the recommended atomic nomenclature for Metavanadates [42]

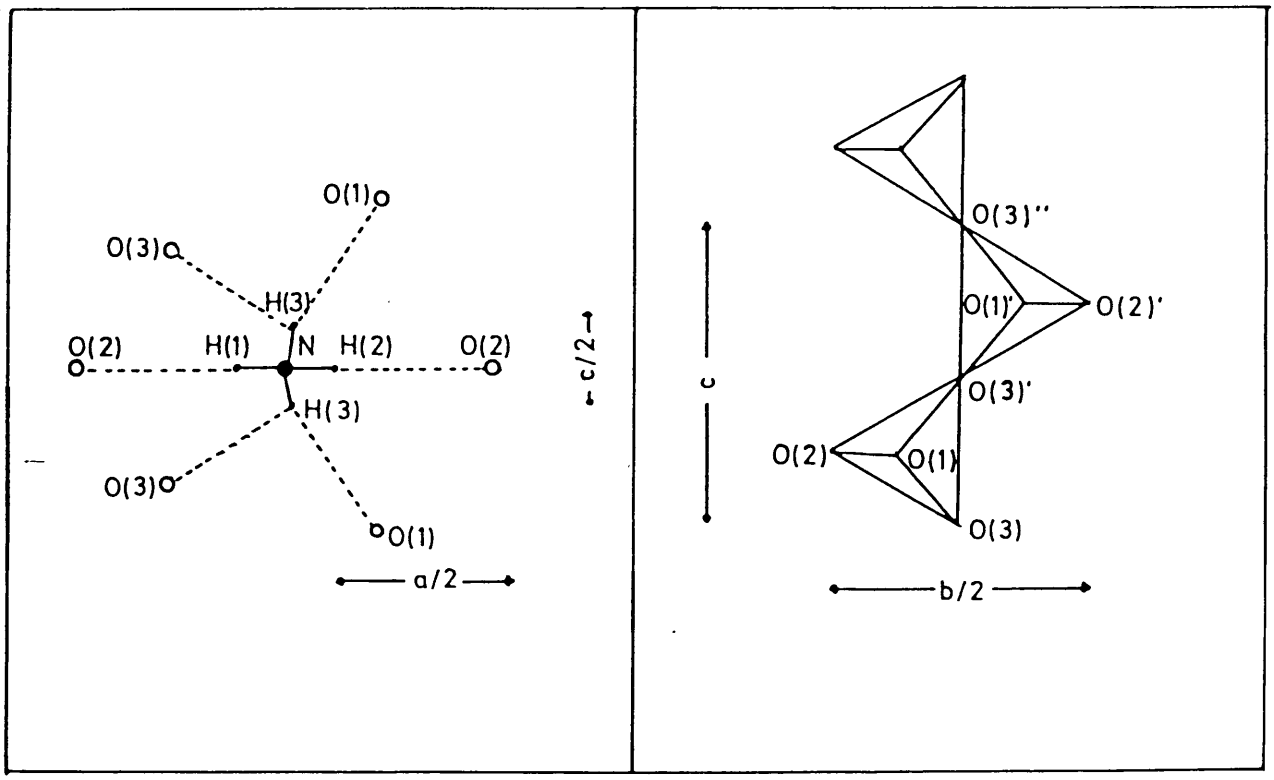

Figure 5.3: The infrared spectra of NH_4VO_3 in the frequency range of 3500 - 450 cm^{-1}.

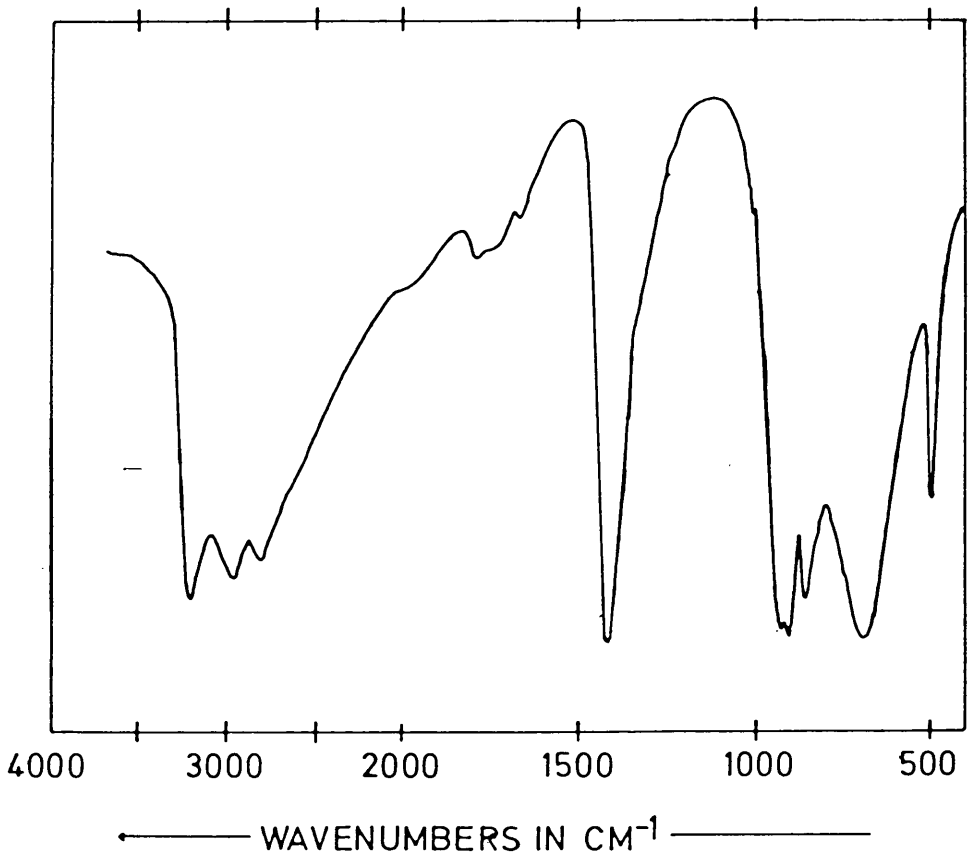

Figure 5.4: The infrared spectra of some isotopically dilute species in NH_4VO_3.

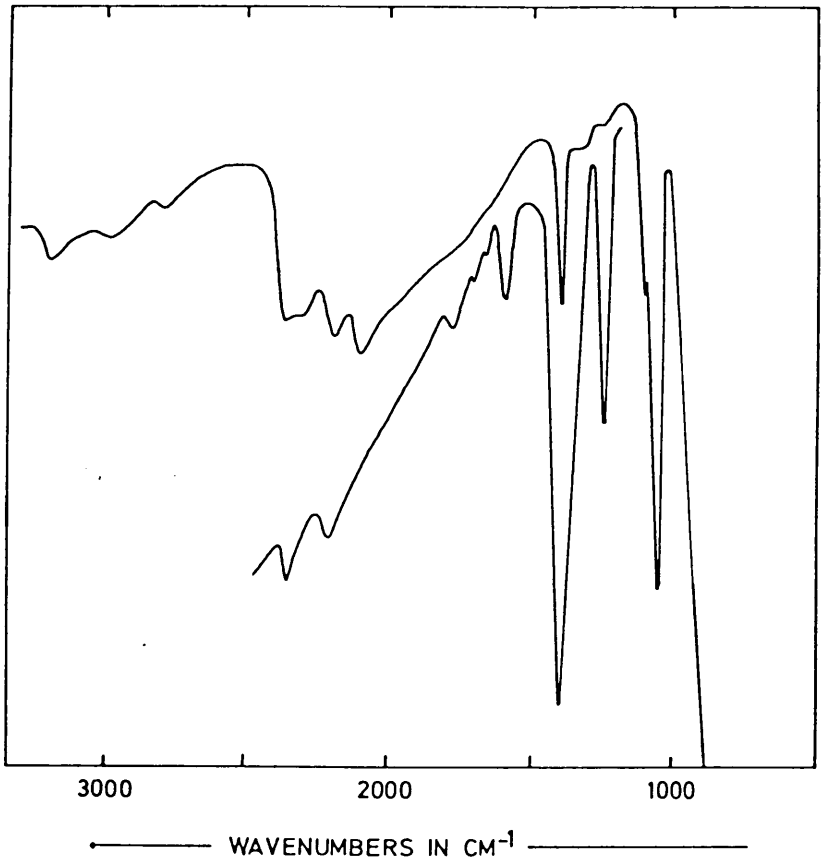

Figure 5.5: The temperature dependence of the Raman bands $\nu_3(NH_4^+)$, $\nu_3(NH_4^+)$, $\nu_1(NH_4^+)$, $\nu_{4a}(NH_4^+)$, $\nu_{4b}(NH_4^+)$, $\nu(VO_2)$sym, $\nu(VO_2)$asym, and a shoulder at 875 cm^{-1}.

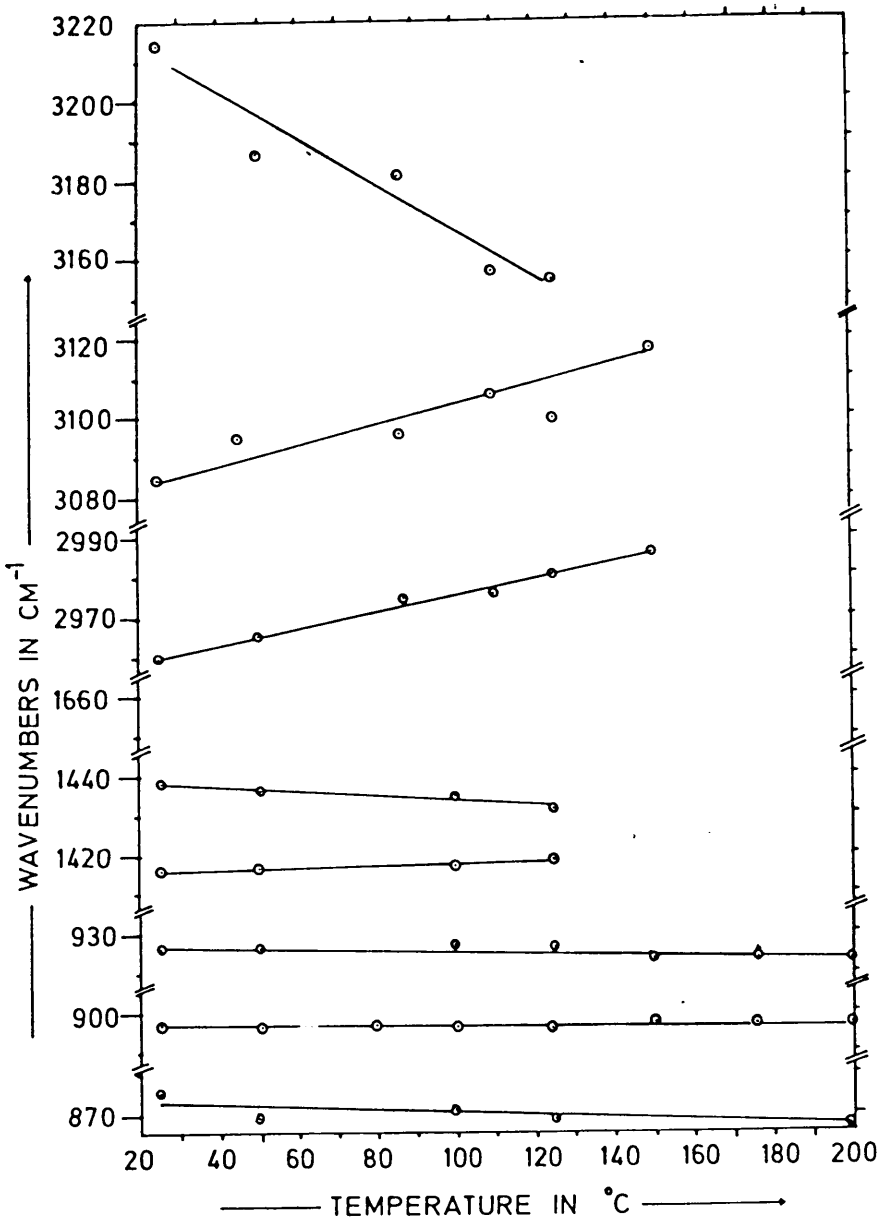

Figure 5.6: The temperature dependence of some low-frequency raman modes in NH_4VO_3.

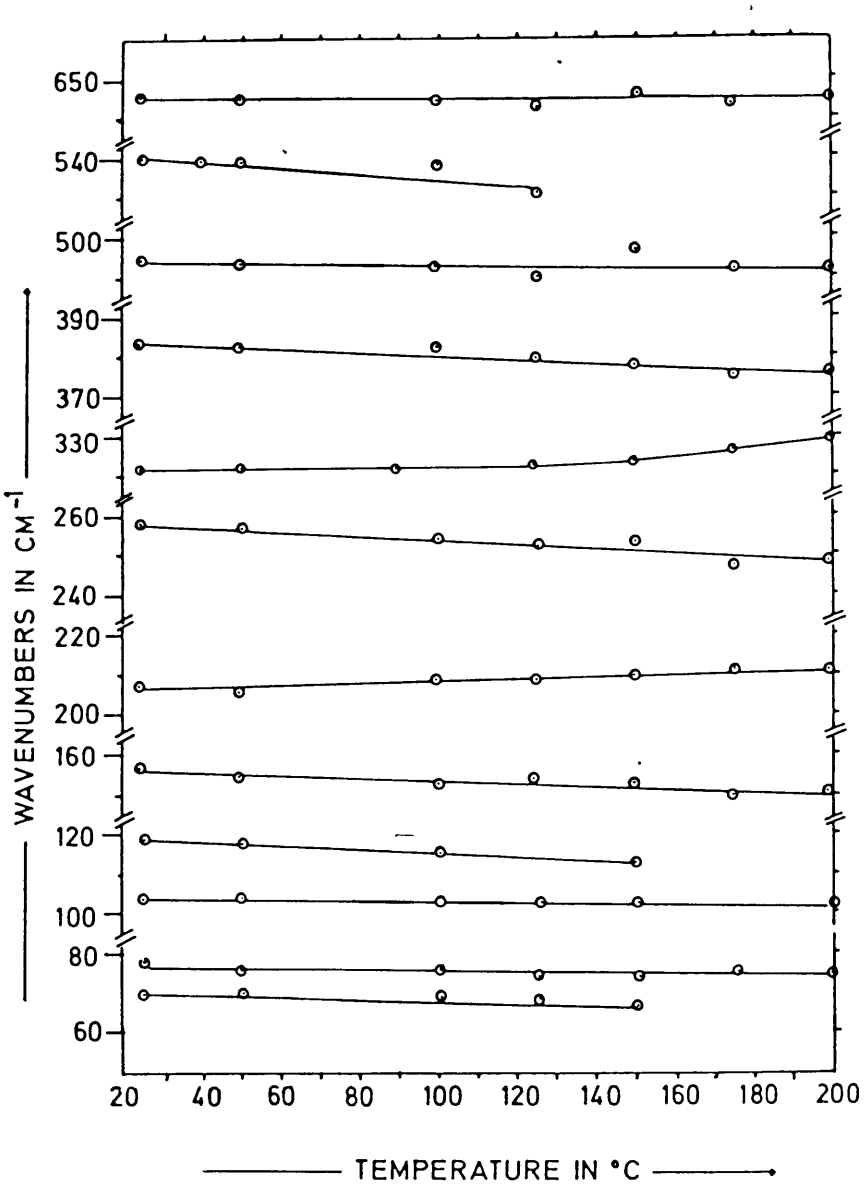

Figure 5.7: The Pressure dependence of some raman-active V-O modes in NH_4VO_3.

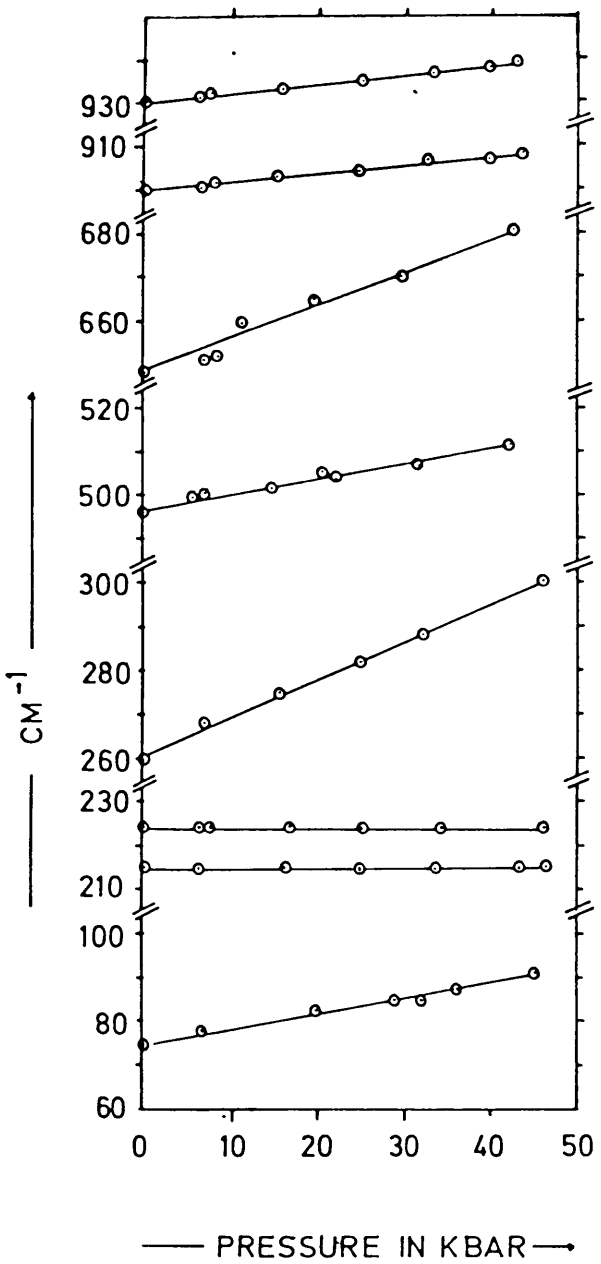

Figure 6.1:

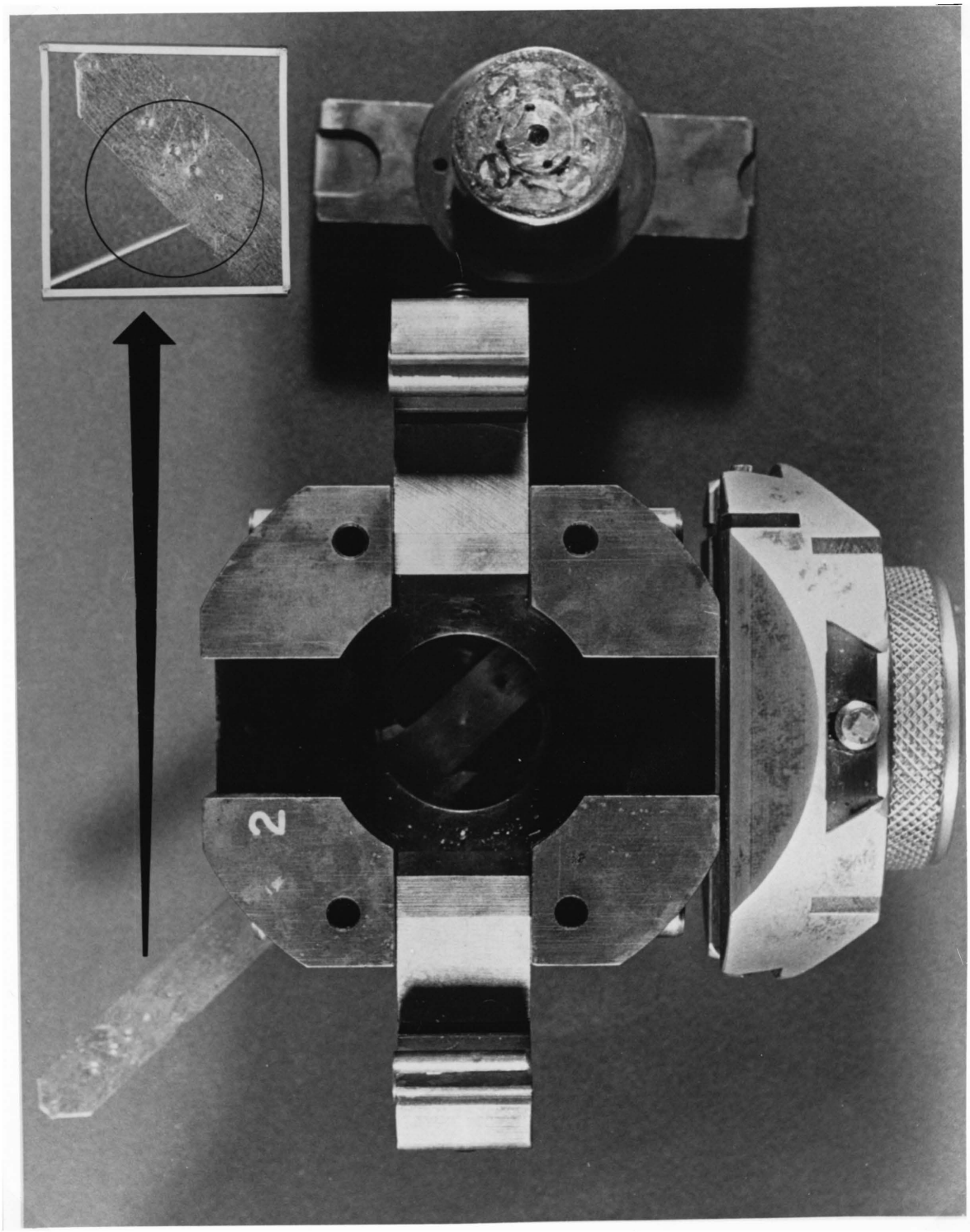

Figure 6.2:

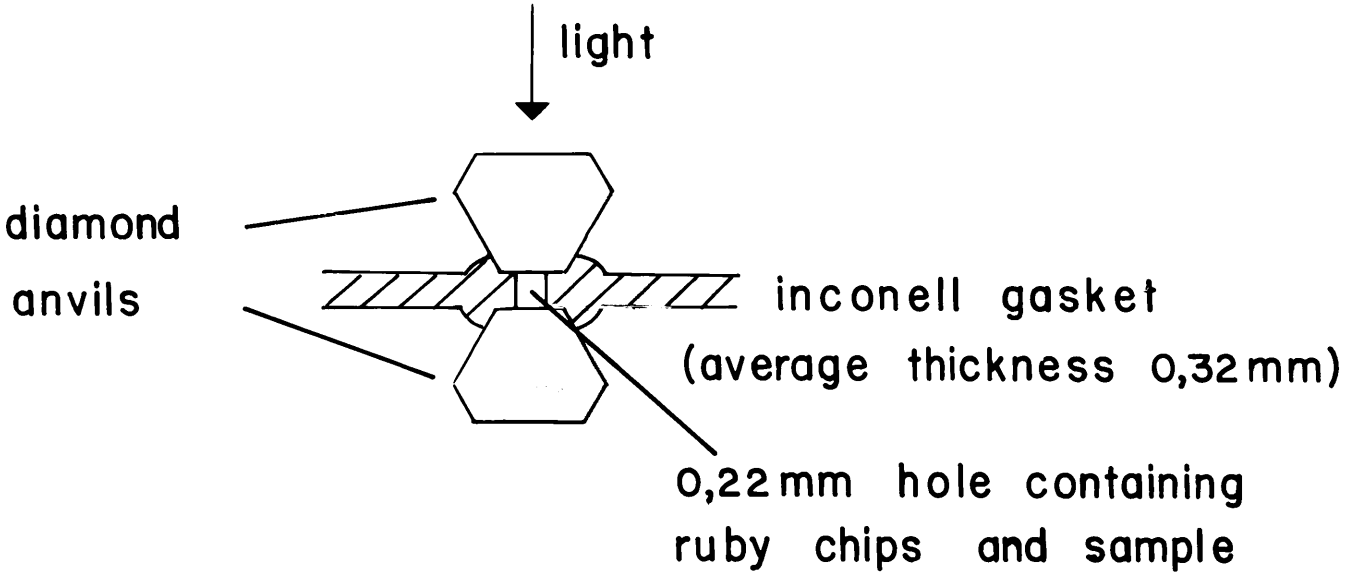

DIAMOND ANVIL CELL

The hardened gaskets were filled with sample and the pressure inside the hole was determined by measuring the R_1 and R_2 lines of the ruby chip added to the sample in the hole. These lines were also used to determine whether hydrostatic conditions prevailed inside the cell.

The optics used in the high pressure cell are given in figures 6.3 and 6.4.

The high temperature experiments were done on the Dilor Raman spectrometer, using a high temperature cell supplied by Dilor Industries, Lille, France. The temperatures quoted are correct within 5 K, and the spectral resolution used was 1 cm^{-1}.

Figure 6.3:

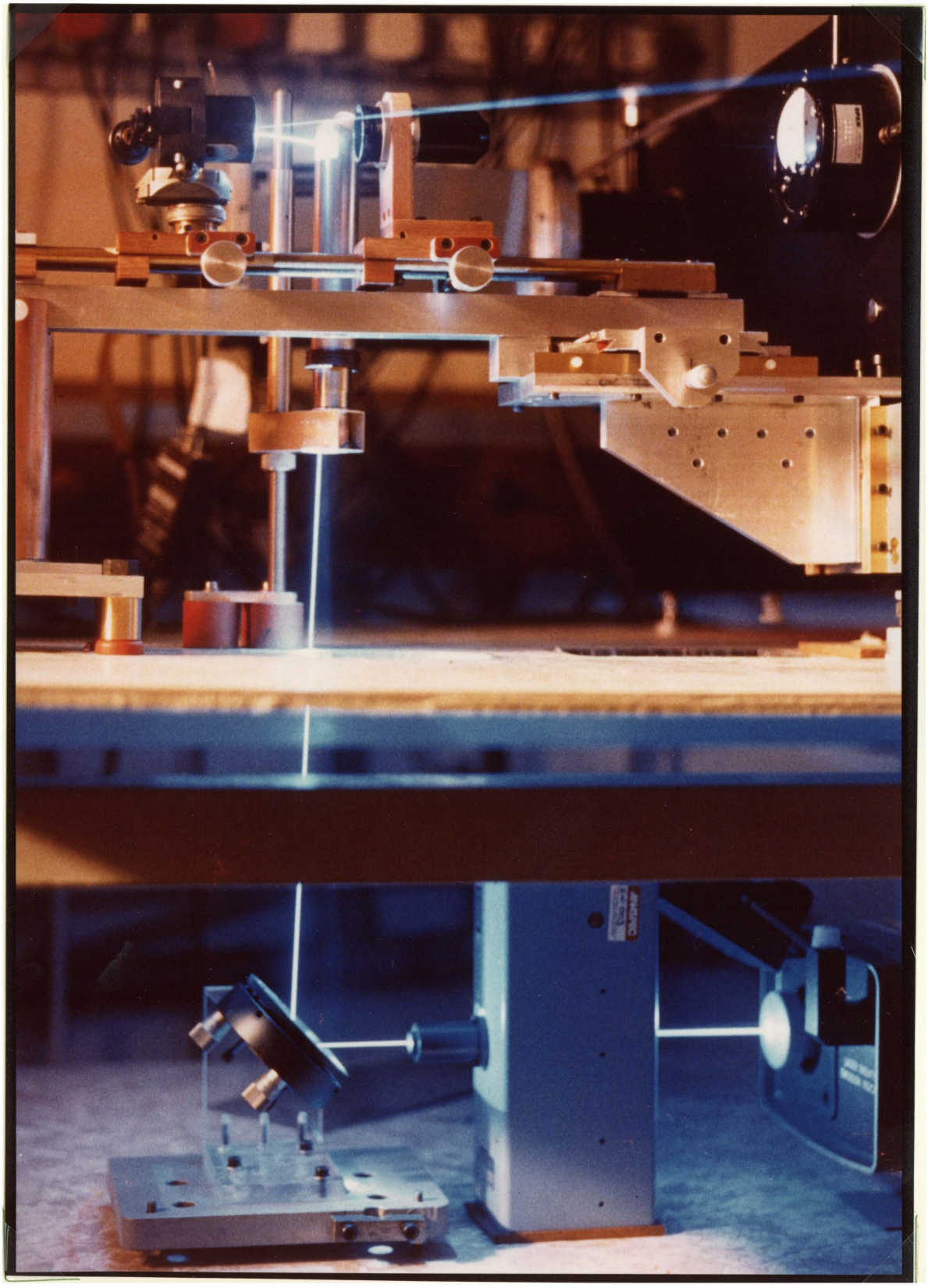

Figure 6.4:

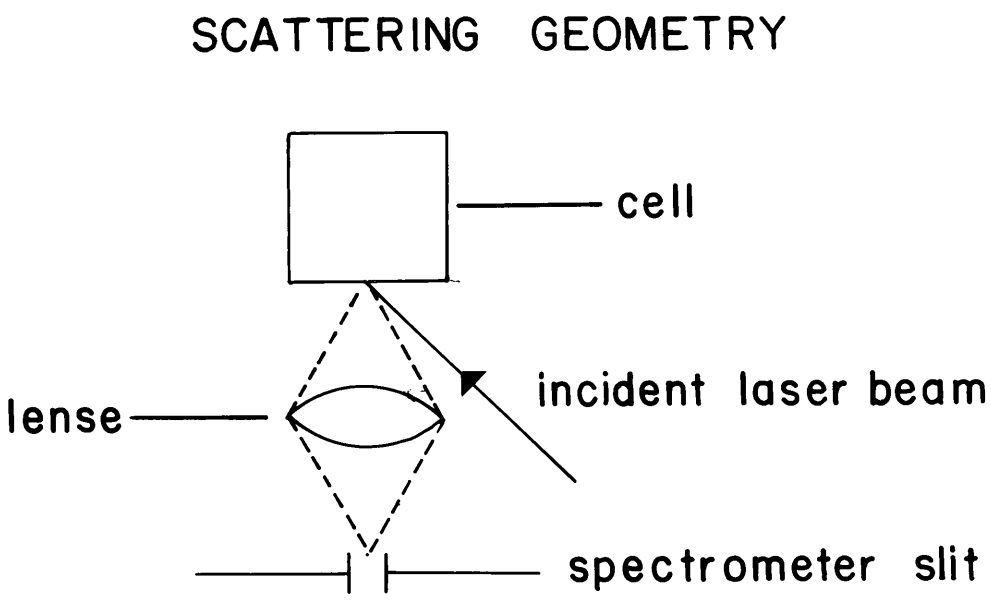

The infrared spectra were recorded on a Brucker 113 VFT-IR spectrometer. KBr discs were used for mid infrared experiments, while polyethylene discs were used for far infrared studies.

6.2 SAMPLE PREPARATION

6.2.1 Pyridine

The pyridine used in the high pressure cell was purified by refluxing over KOH for a minimum of 24 hours, and then fractionally distilled. Only the fraction obtained at 110°C was used. The cell was immediately loaded with the dry pyridine. The remaining fraction of the purified pyridine was stored in a dessicator over P_2O_5.

6.2.2 MCl_2py_2 complexes

All of the complexes used were isolated from ethanolic solutions of pyridine and MCl_2. The products were crystallized from ethanol, dried under vacuum, and stored in a dessicator over P_2O_5. The C, H, N and M analysis were all found to be satisfactory (metal analysis within 0.5%)[19].

6.2.3 Ammonium Metavanadate

The NH_4VO_3 samples used in the measurements were purified according to methods already published in the literature[110]. These samples were recrystallized from H_2O - D_2O mixtures in order to obtain the spectra of the isotopic diluted species. The ammonium hexavanadate was prepared by heating ammonium metavanadate to 180° C.

Appendix A

RULES FOR VARIATIONS OBTAINED UNDER PRESSURE

Generally, all materials undergo changes on the application of pressure. These changes in solids are dictated by the following rules[30,40]:

A.1 The Pressure-Coordination Rule

According to this rule, the coordination number in the crystal structure structure transformation is increased with pressure. However, exceptions to this rule have been reported[40].

A.2 The Pressure-Homology Rule

If one compares crystal structures within a homologous series of compounds, then this rule states that the application of pressure on a lower homologue will have the effect that the crystal structure will assume that of the heaviest homologue in the series.

A.3 The Pressure-Distance Paradox

In order to increase the density of a solid, the interatomic distances must be shorter. The paradox arises from the fact that not all interactomic distances become shorter. The intramolecular or intralayer bond lengths generally become shorter, while the interlayer distances in the crystal lattice are lengthened.

Appendix B

HYDROGEN BONDING

B.1 GENERAL[42,96]

Hydrogen bonding occurs between a proton donor group A-H and a proton acceptor group B, where A is an electronegative atom and B is a lone electron pair of an electronegative atom or a π-electron orbital of an unsaturated system. The distinctly directional nature of this weak interaction may conflict with the requirements of the molecular stereochemistry within a solid containing hydrogen bonds.

The conflict between crystal packing requirements and the linearity required for Hydrogen-bonding may lead to a compromise in which the proton donor group may occupy a position equidistant from two acceptor groups, thus forming a *bifurcated* hydrogen bond. Bifurcated hydrogen bonds are rare, but have been found to be present in a number of ammonium compounds. There have also been reports of trifurcated hydrogen bonding, otherwise known as fluxional bonds, in some ammonium compounds.

Consider the effects of Hydrogen bonding in the complex A-H—B on the vibrational spectra. The vibrations can generally be categorized as follows:[1]

1. A-H—B (antisymmetrical stretch)
2. A-H—B (bend)
3. A-H—B ("symmetrical" stretch)
4. torsional modes

Although vibrations (1) and (2) may already exist without any hydrogen bonding, the dramatic broadening in (1) and frequency shifts in both (1) and (2) obviates the need to depend solely on the detection of the symmetrical stretching frequency in order to characterize the H-bonding. The most characteristic effects may be summarized as

- A shift of the A-H stretching mode to lower frequencies.
- A shift of the A-H bending mode to higher frequencies.
- An increase in the breadth of the A-H stretching frequency, as well as an increase in intensity of the mode in the infrared.

When the hydrogen bonding is weak (which is often the case), the electron density is low, causing small polarizability changes during vibration. An increase in intensity in any of the Raman bands would thus not be expected. The significant broadening of the Raman lines, as well as the shifts which the vibrations undergo when hydrogen bonding occurs, while

[1] may not be descriptions of pure normal modes.

diagnostic of hydrogen bonding, facilitate Fermi coupling. The detection and interpretation by Raman methods of the vibrational spectra can often be exceedingly difficult.

B.2 HYDROGEN BONDING IN AMMONIUM COMPOUNDS

All factors which restrict rotation of the ion to torsonial oscillations will be included in the term hydrogen bonding, as applied to the ammonium ion. It has been recommended [69] that the following criteria be met before assuming the presence of hydrogen bonding in an ammonium compound:

- the presence of the combination bands $\nu_4 + \nu_6$ and $\nu_2 + \nu_6$ in the i.r. spectrum
- the broadening of lattice mode absorptions
- the presence of the anti-symmetrical $\nu_4(NH_4)$ bending mode at frequencies higher than 1400 cm^{-1}.

The presence of the $\nu_4 + \nu_6$ and $\nu_2 + \nu_6$ combination modes has been found to depend on the coordination number about the NH_4^+ ion, and the NH-B angle.

B.2.1 Low temperatures[53]

At low temperatures, the presence of broad bands, high i.r. intensity, and a rich fine structure are indicative of strong hydrogen bonding. This fine structure can be attributed to two main factors

- Dynamic coupling of the vibrations of different NH_4^+ ions in the crystal
- Fermi resonance with overtone and combination modes.

Another Fermi resonance phenomenon is Evan holes. These are found when there is a large difference in strength between two different hydrogen bonds in the crystal. Decoupling of the stretching modes of these hydrogen bonds may then occur. If one considers the interaction of H with three equidistant acceptor atoms, then at very low temperatures it would be expected that the hydrogen will remain close to the threefold axis. In such cases, the N-H bond must be viewed as forming a symmetrically trifurcated hydrogen bond. This however is not the case at higher temperatures.

B.2.2 High temperatures[53]

Under high temperatures, the strengthening of the interaction of the hydrogen with the 3 equidistant acceptor atoms can be qualitatively explained in terms of an increase in the amplitude of the motions of the ammonium ion. These vibrations are likely to be low-frequency i.e. librational and internal (bending) motions. An increase in amplitude brings the hydrogen closer to the acceptor atoms. This results in an increase in the N-H-B angle until a linear hydrogen bond is approached. It is thus unlikely that a trifurcated bond will exist under such conditions. It is possible to distinguish between symmetrically trifurcated and normal bonds by observing the behaviour of the ν_1 vibrations on variation of the temperature. The $d\nu_1/dT$ is negative for the trifurcated bond and positive for the normal N-H-B bond.

Another means of recognizing hydrogen bonds is the halfwidths of the ν_1 absorptions. These halfwidths increase with temperature and have been found to be invariant to the structure and chemistry of individual crystals.

In general therefore the $\nu_2 + \nu_6$ and $\nu_{4_1} + \nu_6$ combination bands of NH_4^+ are observed in the room-temperature spectra when normal hydrogen bonds are present, but not when the NH_4^+ ion is found in a trifurcated situation; but when the temperature is lowered, the bands may occur in the latter case. It must be noted that these combination bands only occur when there are relatively strong hydrogen bonds present.

B.2.3 Deuteration Studies[69]

In the hydrogen bond A-H-B, the effect of deuteration substitution depends on two factors:

- An increase in dipole moment which causes a contraction of the A—B length.
- An expansion of the A—B length may take place due to the difference in zero point energy.

For short hydrogen bonds the expansion term is larger, causing a weakening of the hydrogen bond. The longer hydrogen bonds, on the other hand, become stronger.

In the case of the ammonium ion, undeuterated or fully deuterated samples cannot be used to determine site symmetries of the ammonium ions in vibrational spectroscopy. The isotopically dilute NH_3D^+, on the other hand, has proved to be very useful even in cases of higher site

symmetry. Since the N-D stretching and H-N-D bending modes, i.e. ν_1 and ν_{4bc} of the isotopically dilute NH_3D^+ are not prone to vibrational coupling or Fermi resonance, correlations between the vibrational spectra and crystallographic parameters can be determined.

Appendix C

SURFACE ENHANCED RAMAN SPECTROSCOPY (SERS)

Molecules adsorbed on the surface of metals can exhibit anomolously intense Raman signals with enhancement factors in the range $10^4 \ldots 10^6$. This phenomenon is generally referred to as surface enhanced Raman scattering. The nature of the enhancement mechanism is not yet completely understood. It is generally believed that the surface plasmon resonance and the chemical interaction between the adsorbed molecule and the metal surface play important roles[31,17].

Bibliography

[1] D. M. Adams and D. C. Newton, **Tables for Factor Group and Point Group Analysis**, Beckman-RIIC Ltd, Croyden (England) 1970

[2] D. M. Adams and R. Appleby, *J. Chem. Soc. , Farad. Trans. II*, 73, 1896 (1977)

[3] J. Akella and G. C. Kennedy, *J. Chem. Phys.*, 55, 793 (1974)

[4] S. Akyuz, A. B. Dempster, J. E. D. Davies and K. T. Holmes, *J. C. S. Dalton*, 1746 (1976)

[5] S. Akyuz, J. E. D. Davies and K. T. Holmes, *J. Mol. Struct.*, 42, 59 (1977)

[6] J. R. Allkins, R. J. Obremski, C. W. Brown and E. R. Lippincott, *Inorg. Chem.*, 8, 1450 (1969)

[7] L. I. Antropov, N. F. Kuleshova, *Chem. Abs.*, 107, 100504p (1987)

[8] A. Bajorek, K. Parlinski and M. Sudnik-Hrynkiewicz, *Physica*, 35, 456 (1967)

[9] R. M. Barr, M. Goldstein and W. D. Unsworth,
J. Cryst. Mol. Struct., 4, 165 (1974)

[10] M. S. Barvinok and A. V. Panin, *Russ. J. Inorg. Chem.*,
22, 192 (1977)

[11] S. G. Biswas, *Ind. J. Phys.*, 32, 13 (1958)

[12] J. Bradbury, K. P. Forest, R. H. Nuttall and D. W. A. Sharp,
Spectrochim. Acta, 23A, 2701 (1967)

[13] M. E. Brown and B. V. Stewart, *J. Therm. Anal.*, 2, 287 (1970)

[14] M. E. Brown, L. Glasser and B. V. Stewart, *J. Therm. Anal.*,
6, 529 (1974)

[15] M. E. Brown, L. Glasser and B. V. Stewart, *J. Therm. Anal.*,
7, 125 (1975)

[16] E. Castelluci, G. Sbrana and F. D. Verderame, *J. Chem. Phys.*,
51, 3762 (1969)

[17] R. K. Chang and T. E. Furtak, (Eds.),
Surface Enhanced Raman Scattering, Plenum Press, New York,
(1982)

[18] R. J. H. Clark and C. S. Williams, *Chem. and Ind.*, 1317 (1964)

[19] R. J. H. Clark and C. S. Williams, *Inorg. Chem.*, 4(3), 350 (1965)
and references therein

[20] G. E. Coates and D. Ridley, *J. Chem. Soc.*, 166 (1964)

[21] Cotton and Wilkinson, **Advanced Inorganic Chemistry: A comprehensive text**, 3rd Ed, Interscience Publishers, 1972, 505

[22] E. G. Cox, D. W. A. Cruickshank and J. A. S. Smith, *Proc. Roy. Soc. Ser. A*, 247, 1 (1958)

[23] J. E. Demuth, P. N. Sandra, J. M. Warlaumont, J. C. Tsang and K. Christmann, in **Vibrations at Surfaces**, (edited by R. Caudano, J.-M. Gilles and A. A. Lucas), 391, Plenum Press, New York (1982)

[24] D. P. DiLella and H. D. Stidham, *J. Raman Spectr.*, 9, 90 (1980)

[25] D. P. DiLella, *J. Raman Spectr.*, 9, 239 (1980)

[26] J. D. Dunitz, *Acta. Cryst.*, 10, 307 (1957)

[27] W. D. Ellenson and M. Nicol, *J. Chem. Phys.*, 61, 1380 (1974)

[28] H. T. Evans, *Zeitschrift für Kristallographi*, 114, 257 (1960)

[29] J. R. Ferraro, *Coord. Chem. Rev.*, 29, 1 (1979)

[30] E. Ferroni and E. Bondi, *Inorg. Nucl. Chem.*, 8, 458 (1958)

[31] M. Fleischman, P. J. Hendra and A. J. Mcquillan, Chem. Phys. Lett., 26, 163 (1974)

[32] C. W. Frank and L. B. Rogers, *Inorg. Chem.*, 5, 615 (1966)

[33] A. Frignani, C. Monticelli, G. Brunoro, M. Zucchini, I. H. Omar, *Br. Corros. J.*, 22, 103 (1987)

[34] N. S. Gill, R. S. Nyholm, G. A. Barclay, T. I. Christie and P. J. Pauling, *J. Inorg. Nucl. Chem.*, 18, 88 (1961)

[35] M. Goldstein, *Inorg. Chim. Acta*, 31, L-425 (1978)

[36] M. Goldstein and W. D. Unsworth, *Inorg. Chim. Acta*, 4, 342 (1970)

[37] M. Goldstein and W. D. Unsworth, *Spectrochim. Acta*, 28A, 1107 (1972)

[38] M. Goldstein and W. D. Unsworth, *Spectrochim. Acta*, 28A, 1297 (1972)

[39] M. Goldstein and W. D. Unsworth, *J. Mol. Struct.*, 14, 4511 (1972)

[40] V. Gutmann and H. Mayer, *Structure and Bonding*, 31, 49 (1976)

[41] S. D. Hamann, *Aust. J. Chem.*,31, 11 (1978)

[42] W. C. Hamilton and J. A. Ibers, **Hydrogen Bonding in Solids**, W. A. Benjamin Inc., 1968 New York, New York 10016

[43] F. C. Hawthorne and C. Calvo, *J. Solid State Chem.*,22, 157 (1977)

[44] J. Heaviside, P. J. Hendra, S. O. Paul, J. J. Freeman and R. M. Friedman, *Appl. Spectrosc.*,35, 220 (1981)

[45] A. M. Heyns, *J. Raman Spectr.*, 7, 137 (1978)

[46] A. M. Heyns and M. W. Venter, *J. Phys. Chem.*, 89, 4546 (1985)

[47] A. M. Heyns and M. W. Venter, Unpublished results

[48] M. Ito, *J. Chem. Phys.*, 42, 2844 (1965)

[49] M. Ito and T. Shigeoka, *Spectrochim. Acta*, 22, 1029 (1966)

[50] K. C. Khulbe and R. S. Mann, *Can. J. Chem.*, 53, 2917, (1975)

[51] J. J. Kim, G. Salvador and W. F. Sherman, **Proceedings of the 1988 International Conference on Raman Spectroscopy**, Edited by R. J. H. Clark and D. A. Long, 481–482, John Wiley and Sons (New York) 1988

[52] O. Knop, I. A. Oxton and M. Falk, *Can. J. Chem.*, 57, 404 (1979)

[53] O. Knop, W. J. Westerhaus and M. Falk, *Can. J. Chem.*, 58, 270 (1980)

[54] M. Laing, N. Sparrows and P. Sommerville, *Acta Crystallogr. Sect. B*, 27, 1986 (1971)

[55] W. Libus, S. K. Hoffmann, M. Kluczkowski and H. Twardowska, *Inorg. Chem.*, 19, 1625 (1980)

[56] J. Loisel and V. Lorenzelli, *J. Mol. Struct.*, 1, 157 (1967)

[57] P. Lund, D. H. Christensen, *Proc. 7th Int. Conf. Raman Spectr.*, 47 (1980)

[58] C. Matignon, *Chemiker-Ztg.*, 29, 105, (1986)

[59] A. A. McConnell and R. H. Nuttall, *J. Mol. Struct.*, 49, 207 (1978)

[60] S. Montero, *Spectrochim. Acta*, 32A, 843 (1976)

[61] S. Montero, *Phys. Status Solidi B*, 65, 133 (1976)

[62] D. Mootz and H. G. Wussow, *J. Chem. Phys.*, 75, 1517 (1981)

[63] B. Morosin, *Acta. Cryst.*, B31, 632 (1975)

[64] M. Moskovits and D. P. DiLella, **Surface Enhanced Raman Scattering**, (edited by R. K. Chang and T. E. Furtak), 243, Plenum Press, New York (1982)

[65] K. Nakamoto, *Angew. Chem. Int. Ed.*, 11, 666 (1972)

[66] M. Nicol, M. Vernon and J. T. Woo, *J. Chem. Phys.*, 63, 1992 (1975)

[67] S. Onodera and Y. Ikegami, *Inorg. Chem.*, 18, 466, (1979)

[68] S. Onodera and Y. Ikegami, *Inorg. Chem.*, 19, 615, (1980)

[69] I. A. Oxton, O. Knop and M. Falk, *Can. J. Chem.*, 53, 3394 (1975)

[70] I. A. Oxton, O. Knop and M. Falk, *J. Phys. Chem.*, 80, 1212 (1976)

[71] V. H. Paulus, *Z. Anorg. Allg. Chem.*, 369, 38 (1969)

[72] J. Peternelj, M. I. Valic and M. M. Pintar, *Physica*, 54, 604 (1971)

[73] G. J. Piermarni, A. D. Mighell, C. E. Weir and S. Block, *Science*, 165, 1250 (1969)

[74] G. Pongor, P. Pulay, G. Fograsi and J. E. Boggs, *J. Am. Chem. Soc.*, 106, 2765 (1984)

[75] M. A. Porai-Koshits, L. O. Atovmyan and G. N. Tishchenko, *J. Struct. Chem.*, 1, 312 (1961)

[76] C. Postmus, J. R. Ferraro and W. Wozniak, *Inorg. Chem.*, 6, 2030 (1967)

[77] C. Postmus, J. R. Ferraro, A. Quattrochi, K. Shobatake and K. Nakamoto, *Inorg. Chem.*, 8, 1851 (1969)

[78] K. S. Purcell and J. C. Kotz **Inorganic Chemistry**, Holt-Saunders, 1977

[79] F. Romain, P. Tougard, B. Pasquier, N. Le Calve, A. Novak, A. Peneau, L. Guibe and J. Ramakrishna, *Phase Trans.*, 3 259 (1983)

[80] J. E. Ruede and D. A. Thorton, *J. Mol. Struct.*, 34, 75 (1976)

[81] T. M. Sas, V. A. Novozhilov, Yu. A. Velikodnyi, V. N. Suvorov and V. E. Sorokin *Russ. J. Inorg. Chem.*, 23, 1805, (1978)

[82] Y. Sato, *J. Phys. Soc. Japan*, 20, 275 (1965)

[83] Y. Saito, M. Cordes and K. Nakamoto, *Spectrochim. Acta*, 28A, 1459 (1972)

[84] S. A. Selim, Ch. A. Philip and R. Sh. Mikhail, *Therm. Acta*, 36, 287, (1980)

[85] W. F. Sherman, *Bull. Soc. Chim. Fr.*, I-297, I-347 (1982)

[86] Yu. A. Sokolova, L. O. Atovmyan and M. A. Porai-Koshits, *J. Stuct. Chem.*, 7, 794 (1965)

[87] W. L. Steffen and G. J. Palenik, *Acta. Cryst.*, B32, 298 (1976)

[88] W. L. Steffen and G. J. Palenik, *Inorg. Chem.*, 16, 1119 (1977)

[89] H. D. Stidham and D. P. DiLella, *J. Raman Spectr.*, 8, 180 (1979)

[90] H. D. Stidham and D. P. DiLella, *J. Raman Spectr.*, 9, 247 (1980)

[91] M. Suzuki and W. J. Orville-Thomas, *J. Mol. Struc.*, 37, 321 (1977)

[92] M. M. Thiéry et al, *Solid State Comm.*, 54, 95 (1985);
J. Chem. Phys., 39, 4255 (1988)

[93] K. R. Thompson and K. D. Carlson, *J. Chem. Phys.*, 49, 4379 (1968)

[94] S. N. Vaidya and G. C. Kennedy, *J. Chem. Phys.*, 55, 987 (1971)

[95] J. A. C. Van Ooijen and J. Reedijk, *Inorg. Chim. Acta*, 25, 131 (1977)

[96] S. N. Vinogradov and R. H. Linnell, **Hydrogen Bonding**,
Van Nostrand Reinhold Company, 1971

[97] V. A. Walters, D. L. Snavely, S. D. Colson, K. B. Wiberg and
K. N. Wong, *J. Phys. Chem.*, 90, 593 (1986)

[98] P. T. T. Wong, *Can. J. Chem.*, 52, 2005 (1974)

[99] P. T. T. Wong, *Inorg. Chem.*, 14, 2271 (1975)

[100] P. T. T. Wong, *J. Chem. Phys.*, 63, 5108 (1975)

[101] P. T. T. Wong, *J. Phys. Chem.*, 78, 4840 (1983)

[102] P. T. T. Wong and D. G. Brewer, *Can. J. Chem.*, 46, 131 (1968)

[103] P. T. T. Wong and D. G. Brewer, *Can. J. Chem.*, 46, 139 (1968)

[104] P. T. T. Wong and D. G. Brewer, *Can. J. Chem.*, 47, 4589 (1969)

[105] H. Yamada and Y. Yamamoto,
J. Chem. Soc., Faraday Trans.1,75, 1215 (1979)

[106] M. R. Zakin, S. G. Grubb, H. E. King, Jr., and D. R. Herschbach,
J. Chem. Phys., 84, 1080 (1986)

[107] M. R. Zakin and D. R. Herschbach, *J. Chem. Phys.*, 85, 2376 (1986)

[108] S. J. Zakvi, G. N. Mehta, *J. Electrochem. Soc. India*, 36, 143 (1987)

[109] R. Zannetti and R. Serra, *Gazz. Chim. Ital.*, 90, 328 (1960)

[110] R. Zintl, Dissertation, Universität Regensburg (1984)